DYMORE FINITE ELEMENT ANALYSIS OF THE PAIRED BLADE TILTROTOR CONCEPTUAL DESIGN AND A COMPARABLE CONVENTIONAL TILTROTOR DESIGN

by

DAVID ORION BRAZIEL

Presented to the Faculty of the Graduate School of
The University of Texas at Arlington in Partial Fulfillment
of the Requirements
for the Degree of

MASTER OF SCIENCE IN AEROSPACE ENGINEERING

THE UNIVERSITY OF TEXAS AT ARLINGTON
May 2009

ACKNOWLEDGEMENTS

I would like to thank Dr. Kent Lawrence and Dr. Mark Wasikowski for the advice and guidance which made the completion of this project possible, Dr. Wen Chan for serving on my thesis committee, and Debi Barton for her help with managing deadlines and requirements.

I would like to thank Prof. Olivier A. Bauchau at the Georgia Institute of Technology for his assistance with my early use of the Dymore finite element analysis code, and for developing and providing the code open-source.

Thanks to David Popelka for his guidance, his advice on the content of this work, and his help with the details of rotor dynamics, and to Thomas C. Parham Jr. for helping me with rotor dynamics issues associated with this work.

Thanks to Dr. Jason Choi, without whose help with Dymore modeling issues, this work would have taken much longer to complete.

I owe thanks to Dr. Mithat Yuce, Dr. Jorge Morillo, Rupinder Singh, and Jeff Newman for their willingness to share their expertise in dynamics and modeling methods.

I am grateful to Tom Wood for his support in matters associated with this project as it relates to work at Bell Helicopter, and to John Brunken for providing the design of the subject rotor for this project.

I am thankful to my brother, Josh, for his I.T. consulting on aspects of this project and to his family for their support of my academic pursuits.

I thank my parents for their life-long support in all things, their hard work, and their determination to give me the opportunity to get an education.

April 20, 2009

ABSTRACT

DYMORE FINITE ELEMENT ANALYSIS OF THE PAIRED BLADE
TILTROTOR CONCEPTUAL DESIGN AND A
COMPARABLE CONVENTIONAL
TILTROTOR DESIGN

David Orion Braziel, M.S.

The University of Texas at Arlington, 2009

Supervising Professor: Kent L. Lawrence

Increasing the solidity of tiltrotors above that of current designs presents challenges associated with control system packaging and control couplings. The paired blade rotor concept addresses these issues by placing two blades that share a pitch link, located for acceptable control coupling, on each of three hub arms.

Dymore finite element models of the paired blade rotor and a reference rotor of equal solidity with six evenly spaced blades were developed to identify any potential design flaws of the paired blade rotor associated with rotor frequency placement or control couplings. The finite element rotor models are documented, and the results of the analyses are presented here.

TABLE OF CONTENTS

LIST OF ILLUSTRATIONS

LIST OF TABLES

CHAPTER 1

INTRODUCTION

1.1 Purpose and Scope of This Work

The goal of this project is to determine by analysis the practicality of a concept rotor for use on tiltrotor aircraft based on rotor mode frequency placement, reasonability of component properties, realistic control couplings, and component packaging. The concept rotor is a gimbaled flexure hub with three arms and two blades per arm (paired blade rotor). Finite element models of the paired blade rotor and a more conventional six bladed, evenly spaced, gimbaled flexure hub rotor were built for the Dymore code, which was developed at Georgia Tech. The Dymore models were run in a vacuum, so no loads analysis can be performed at this stage. A significant portion of what is presented here is various comparisons of the paired blade rotor to the six bladed evenly spaced rotor.

The scope of this project is to compare rotor modes, identify tuning issues, interpret mode shapes, compare kinematic and elastic couplings, investigate the effects of blade spacing for the paired blade rotor, and identify any benefits of the paired blade rotor.

1.2 Rotor Tuning Background

When selecting rotor component properties and other rotor parameters, care must be taken to ensure that the resulting natural frequencies of the rotor are reasonably well separated from forcing frequencies to avoid oscillatory rotor loads that exceed fatigue limits of the rotor structure. The process of calculating rotor frequencies for a particular set of parameters, comparing them to forcing frequencies, and making changes to the parameters to change the rotor frequencies to better separated values, if necessary, is referred to as tuning a rotor. This section covers the basic factors and issues associated with tuning rotors.

1.2.1 Rotor Rotating Natural Frequencies

Rotor rotating natural frequencies are the frequencies of orthogonal, fully-coupled modes of usually complex rotor structures with centrifugal force effects accounted for. The modes are coupled in the flap (out of the plane of rotation), lag (in the plane of rotation), and pitch (motion about an axis that runs along the span of the blade) degrees of freedom. Many rotor designs, including the ones considered here, have multiple load paths through several rotor components, some of which are connected by elastomeric bearings with discrete foci of articulation. The flexibility of the control system also affects rotor modes, in the pitch degree of freedom in particular. The Dymore finite element analysis code was used to calculate rotor rotating natural frequencies for this project.

1.2.2 Forcing Frequencies of Various Mode Types

Each of the three types of rotor modes –collective, cyclic, and scissors or reactionless- has a set of forcing frequencies that are integer multiples of the rotor speed. Common nomenclature for the cycles-per-rotor-revolution unit of frequency is per rev, abbreviated /Rev.

1.2.2.1 Collective Modes

Collective rotor modes can be thought of as having a boundary condition at the center of rotation that is cantilevered out of the plane of rotation and pinned in the plane of rotation. For rotors with evenly spaced blades, collective modes have forcing frequencies that are integer multiples of the number of blades /Rev.

1.2.2.2 Cyclic Modes

Cyclic modes have a boundary condition at the center of rotation that is pinned out of the plane of rotation and cantilevered in the plane of rotation. The rotor speed, 1 /Rev, is always a cyclic mode. For rotors with evenly spaced blades, the remainder of the cyclic mode forcing frequencies are the collective mode forcing frequencies +/- 1 /Rev. For example, a four bladed rotor would have collective mode forcing frequencies of 4 /Rev and 8 /Rev, and would have cyclic mode forcing frequencies of 1 /Rev, 3 /Rev, 5 /Rev, and 7 /Rev.

1.2.2.3 Scissors Modes

Scissors modes have a boundary condition at the center of rotation that is cantilevered both out of the plane of rotation and in the plane of rotation. Scissors mode forcing frequencies are the integer multiples of the rotor speed that are neither collective mode forcing frequencies nor cyclic mode forcing frequencies.

1.2.3 Realistic Rotor Parameters

While many rotor parameters and combinations of rotor parameters can be selected to achieve a suitably tuned rotor, the favorable results are of little real use if the properties input to the analysis are associated with a component or arrangement that is impossible to manufacture or one that would fail in the loading environment for which it is intended. A driving tenant of the work for this thesis was to avoid using any rotor component structural or mass properties or any other rotor parameters that were obviously unrealistic.

1.2.4 Tuning Rotors in a Vacuum

Investigating the frequency placement of a rotor in a vacuum is an important and relatively inexpensive first check of a proposed rotor design. No loads, performance, or aeroelastic stability predictions can be made without aerodynamic forces included in the model, but a fundamental characteristic of the rotor, its tuning, can be checked in a vacuum reliably. Although the ultimate suitability of a design cannot be verified by this method, configurations having poor tuning can be identified as such and redesigned without further expense.

1.3 Coupling Parameters

Coupling parameters are a measure of how the modal displacement in a particular degree of freedom is related to the modal displacement in a different degree of freedom in the same mode. The coupling parameters considered here are pitch-flap coupling (δ_3), pitch-cone coupling (δ_0), and pitch-lag coupling (K_{pl}). The total coupling is calculated using the modal pitch displacement of the blade at ¾ rotor radius. The kinematic coupling is calculated using the portion of the modal pitch displacement of the blade at ¾ rotor radius not including the elastic

blade twist from the pitch horn to ¾ radius. The elastic coupling is calculated using only the elastic blade twist between the pitch horn and ¾ radius. No stability analysis is run here. The coupling parameters are extracted from the model results to check that they are reasonable, and for the purpose of comparison between the six bladed evenly spaced rotor and the paired blade rotor.

1.3.1 Pitch-Flap Coupling (δ_3)

Pitch-flap coupling (δ_3) is the amount of blade pitch deflection in the rigid body, first cyclic out of plane (flapping) mode. The geometric δ_3 is the angle between the flapping axis and a line from the intersection of the flapping axis and the pitch-change axis (PCA) to the pitch link. Negative geometric δ_3 is illustrated in Figure 1.1. For the configuration shown in Figure 1.1, when the blade flaps up (out of the plane of the sheet) about the flapping axis, the pitch link would move up, but the control system is stiff enough that it moves very little. The result is a pitch-up input for a flap-up deflection, which is negative δ_3.

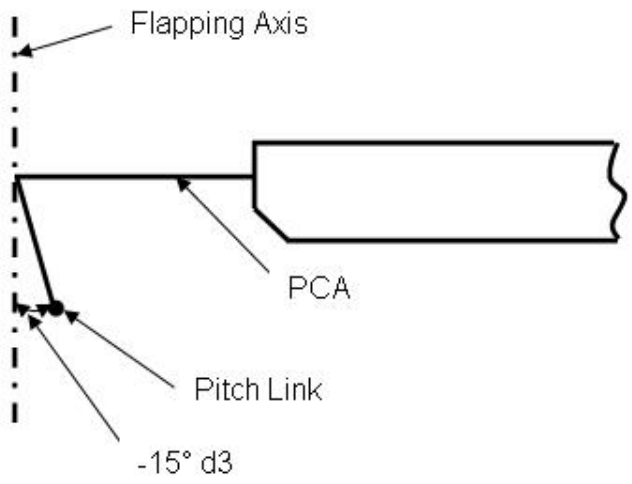

Figure 1.1 Illustration of negative geometric δ_3 for trailing edge pitch link

The δ_3 parameter is calculated from modal displacements as:

$$\delta_3 = \tan^{-1}\left(\frac{\theta}{\beta_{TPP}}\right) \tag{1.3.1.1}$$

where

$$\beta_{TPP} = \tan^{-1}\left(\frac{dz_{tip}}{R}\right) \tag{1.3.1.2}$$

The flapping mode is a rigid body mode so the tip-path-plane flapping (β_{TPP}) is used in the calculation of δ_3. The dz_{tip} parameter is the modal out of plane deflection at the blade tip, R is the rotor radius, and θ can be θ_k (the modal pitch deflection at the pitch horn) for kinematic δ_3, $\theta_{3/4}$ (the modal pitch deflection at the blade ¾ radius) for total δ_3, or $\theta_{3/4} - \theta_k$ (the elastic blade modal pitch deflection) for elastic δ_3. Negative geometric δ_3 was employed in both the six bladed even spacing rotor and the paired blade rotor.

Negative pitch-flap coupling has a stabilizing effect on flap-lag coupling of the rotor. A detailed discussion of the flap-lag rotor instability and the effect of δ_3 is available in Reference [1]. Positive δ_3 causes aerodynamic forces to reduce the frequency of the lead-lag mode and increase the frequency of the flapping mode. Positive δ_3 increases the frequency of the flapping mode because as the blade flaps up, it pitches down and a flap-down moment due to aerodynamics is created. The aerodynamic flap-down moment acts in a direction opposite the blade flapping motion that causes it, which increases the flapping frequency. Positive δ_3 reduces the frequency of the lead-lag mode because as the blade lags aft, the pitch-flap coupling reacts to the hub out of plane deflection and increases blade pitch. The aerodynamic loads associated with the increase in pitch further increase the inplane deflection of the blade, which reduces the inplane frequency. For stiff inplane rotors like the ones studied here, the inplane mode is tuned at a higher frequency than the flapping mode for low inflow ratios. The inflow ratio is the ratio of the component of the airspeed seen by a blade that is perpendicular to the plane of the rotor to the component of airspeed seen by a blade that is in the plane of the rotor. As the inflow ratio increases, the aerodynamic effects associated with positive δ_3 cause

the flapping mode frequency to increase and the inplane mode frequency to decrease to a point where the frequencies of these two modes are close to the same. When the flapping and inplane frequencies approach the same value, the response of the modes to small perturbations in aerodynamic loads will be in phase. As a result, the damping of the flapping mode will increase rapidly and the damping of the inplane mode will decrease rapidly to a negative value. This phenomenon is referred to as the flap-lag instability. This effect increases with airspeed for airplane mode forward flight. Designing stiff inplane tiltrotors with negative δ_3 prevents the flap-lag instability by causing aerodynamic forces to increase the frequency of the lead-lag mode and reduce the frequency of the flapping mode, separating the frequencies as forward flight velocity increases in airplane mode flight.

Gaffey also discusses the stabilizing effect of δ_3 on proprotor whirl flutter stability in Reference [1], but since no pylon structure is modeled in the analysis presented here, discussion of the details of whirl flutter is forgone in this work.

1.3.2 Control System Packaging and δ_3

Pitch-flap coupling is a parameter that must be monitored closely during the design phase of a stiff inplane tiltrotor for favorable aeroelastic stability characteristics. If the δ_3 value is not maintained at a reasonable negative value, the rotor will experience a flap-lag instability at high airspeeds in airplane mode.

Another concern affecting the location of the pitch link is the distance between the PCA and the pitch link. The pitch link reacts the pitching moment of the blade, and the pitch link loads would become excessive if the moment arm from the PCA to the pitch link was too small.

As the number of blades on an evenly spaced rotor increases, the space available to meet all of the requirements listed above decreases. The evenly spaced rotor modeled for reference in this document is not a candidate rotor because it has a fundamental design flaw by which the control system components present mechanical interferences with other rotor components. The Dymore post-processor screenshot in Figure 1.2 shows that for -15° δ_3, the

pitch horns of the evenly spaced rotor extend aft from the grip and well into the hub of the blade behind them.

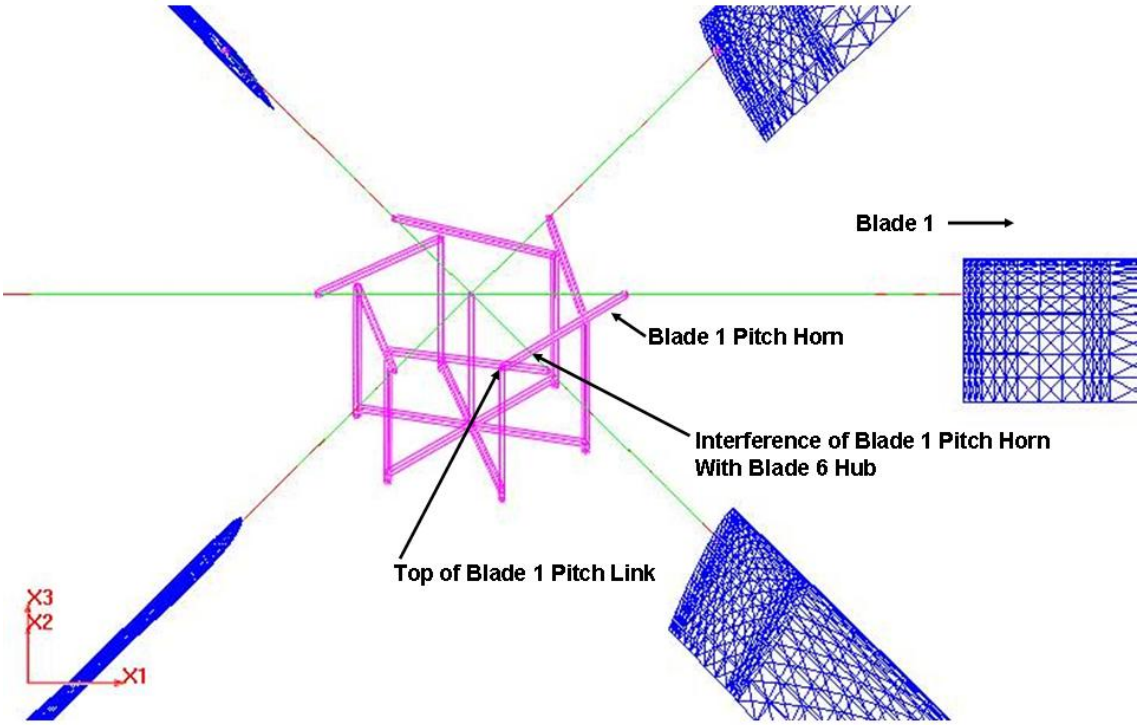

Figure 1.2 Evenly spaced six bladed rotor showing interference of pitch horn and adjacent blade

Even a 4-bladed evenly spaced rotor with -15° geom etric δ_3 does not have sufficient space between components of adjacent blades to avoid interferences for conventionally designed control systems.

1.3.3 Pitch-Cone Coupling δ_0

Pitch-cone coupling (δ_0) is a measure of the amount of blade modal pitch deflection in the first collective out of plane (coning) mode, which is cantilevered at the center of rotation. Cone-up, pitch-down δ_0 is positive. A rough analog to geometric δ_3 can be made for δ_0 using the coning hinge location and the pitch link location. For a trailing edge pitch horn, having the pitch link inboard of the coning hinge would result in positive δ_0 because the fixity of the control

system would input a pitch down moment to the blade when it coned up about this axis. This is the case for both rotors considered.

The δ_0 parameter is calculated from modal displacements as:

$$\delta_0 = \left(\frac{\theta}{\beta_{3/4}} \right) \tag{1.3.3.1}$$

As is the case for δ_3, θ can take on θ_k, $\theta_{3/4}$, or $(\theta_{3/4} - \theta_k)$ depending on the nature of the δ_0 value sought (kinematic, total or elastic respectively). The modal out of plane bending slope at the ¾ radius is $\beta_{3/4}$.

Positive pitch-cone coupling (cone-up, pitch down) was found to increase tiltrotor stability boundary airspeeds in Reference [2]. Positive pitch-cone coupling also provides a passive stabilizing response to vertical gusts in helicopter mode operation. When an upward vertical gust is encountered, the rotor blade coning angle is increased and the pitch down response associated with positive δ_0 provides a reduction in rotor thrust opposing a sudden, un-commanded increase in rotor thrust. The pitch-down response also acts to reduce the angle of attack of the blade, opposing the increase in angle of attack due to an upward gust and delaying blade stall. The effect of positive δ_0 is also favorable for downward vertical gusts because as the rotor coning angle is reduced by a downward gust, the blade pitch angle is increased, which causes an increase in rotor thrust opposing the reduction in rotor thrust due to the downward vertical gust. As the δ_0 coupling parameter becomes less positive or more negative, the pilot is charged with supplying larger, higher-rate control inputs to offset the effects of vertical gusts. More positive values of δ_0 improve ride quality since the rotor, and the aircraft, respond less rapidly to vertical gusts through the rotor.

1.3.4 Pitch-Lag Coupling K_{pl}

The pitch-lag coupling parameter (K_{pl}) is the ratio of the modal pitch deflection to the modal out of plane deflection of the blade in the first cyclic inplane (lead-lag) mode. Lag-aft, pitch-down K_{pl} is positive as defined by Johnson [3] and is the convention used here.

K_{pl} is calculated as:

$$K_{pl} = \left(\frac{\theta}{\zeta_{3/4}} \right) \tag{1.3.4.1}$$

Appropriate values of θ must be chosen for particular types of K_{pl} (kinematic, total, or elastic). The modal inplane bending slope at the ¾ radius is $\zeta_{3/4}$.

As Gaffey discusses in Reference [1], the pitch lag instability is caused by the coupling of the flapping and inplane deflections of the blade due to control system flexibility. The coupling of these motions changes the phasing angle between them such that the flapping motion generates forces that are in-phase with the inplane velocity vector, which is negative damping.

Control system flexibility allows a pitch-down blade motion when the blade moves inplane in the direction of rotation and is coned up above the pitch change axis. The associated flap-down moment causes the blade to flap up due to the phasing of flapping and inplane motions. For positive K_{pl}, the blade pitches up when it deflects inplane in the direction of rotation, which acts against the destabilizing pitch-down motion caused by the flexible control system for the same inplane deflection.

Negative pitch-lag coupling (lag-aft, pitch-up) has been shown analytically to have a destabilizing effect on whirl-flutter stability boundaries as discussed in References [4] and [5]. The presence of pre-cone in the rotor hub, which is a built in, steady coning angle that allows centrifugal force to offset large out of plane bending moments at the root of the yoke due to lift in hover, drives the total K_{pl} to a less positive or more negative value in airplane mode flight. This is because the aerodynamic loads acting to increase the coning angle are reduced by roughly an order of magnitude in airplane mode flight due to the large reduction in thrust compared to the hover condition, while the CF loads due to pre-cone are reduced by a much smaller amount due to the reduction in RPM from hover to airplane mode flight. The flap-down moment created by this dissimilarity applies a pitch-up moment to the root of the blade when the

tip of the blade lags aft, thus driving the K_{pl} parameter to a more negative or less positive value. No pre-cone was included in the rotor models presented here.

1.4 Dymore Finite Element Analysis Code

Dymore is an open-source finite element analysis tool for nonlinear elastic multibody systems developed by Prof. Olivier A. Bauchau at the Georgia Institute of Technology. The element library includes elastic bodies, rigid bodies, joint elements, constraint elements, and utility elements. A rigid body rotation option is used in the models presented here to represent centrifugal force. Centrifugal forces associated with the rigid rotation are computed and applied to the system in a quasi-steady manner. The static analysis capability of Dymore was used for these rotor models. In a static analysis Dymore solves the system equations resulting from setting all time derivatives to zero, and the deformed configuration of the system under the applied static loads is computed. Once the static solution has been calculated, eigenvalues and eigenvectors can be extracted from the system resulting from the linearization of the dynamic equations of motion. Dymore writes the equations of equilibrium in a Cartesian inertial frame.

1.4.1 Constraint Conditions in Multibody Systems

A distinguishing feature of multibody finite element analysis is the use of multiple joints at which various types of structural elements connect and are restrained from motion relative to one another in selected degrees of freedom with or without finite springrates associated with motion in some or all degrees of freedom. Reference [6] provides a detailed discussion of constraint conditions in multibody finite element analysis. The revolute joint in Dymore is a junction between two bodies that does not allow any relative displacement between the bodies and allows relative rotation between the bodies about only one axis. The prismatic joint restricts to zero any relative rotation between two bodies and allows prescribed-time-dependent relative displacement along only one axis between the bodies. A spherical joint is a constraint element (joint) that constrains two bodies connected by the joint from any displacement relative to one another while allowing relative rotations between the bodies about any of the three possible

axes. A universal joint is a constraint element that prevents the relative displacement of two bodies and allows relative rotations of the bodies about two axes only. Details related to all Dymore elements and Dymore input syntax are provided in the Dymore 2.0 User's Manual, Reference [7].

1.4.2 Lagrange Multiplier Technique for Enforcing Constraints in Static Problems

As discussed in References [6] and [8], Dymore uses the Lagrange multiplier technique to formulate constraint conditions. Consider a stationary point of a function of multiple variables $F = F(u_1,u_2,\ldots,u_n)$ with the variables subject to a constraint of the form $C(u_1,u_2,\ldots,u_n) = 0$. At a stationary point in F, the variation (δ) in F is 0.

$$\delta F = \frac{\partial F}{\partial u_1}\delta u_1 + \frac{\partial F}{\partial u_2}\delta u_2 + ... + \frac{\partial F}{\partial u_n}\delta u_n = 0$$

Taking a variation of the constraint yields:

$$\delta C = \frac{\partial C}{\partial u_1}\delta u_1 + \frac{\partial C}{\partial u_2}\delta u_2 + ... + \frac{\partial C}{\partial u_n}\delta u_n = 0\,.$$

Combining these two equations yields:

$$\sum_{i=1}^{n}\left[\frac{\partial F}{\partial u_i} + \lambda\frac{\partial C}{\partial u_i}\right]\delta u_i = 0$$

where λ is an arbitrary function of the variables u_i called the Lagrange multiplier. Careful selection of the Lagrange Multiplier leads to the condition

$$\delta F + \delta\lambda C = 0\,.$$

where all δu_i are independent. Due to the constraint, the stationary condition is rewritten as

$$\delta(F + \lambda C) = 0\,.$$

A modified function is introduced whereby $F^+ = F + \lambda C$, which has no variation in F^+ for all arbitrary variations δu_i and $\delta\lambda$. The result is that the initial constrained problem is replaced by an unconstrained problem stated as

$$\delta F^{+} = 0, \quad F^{+} = F\ \lambda C .$$

The absence of variation in F^{+} implies

$$\sum_{i=1}^{n}\left[\frac{\partial F}{\partial u_i} + \lambda \frac{\partial C}{\partial u_i}\right]\delta u_i + C\delta\lambda = 0 .$$

Since δu_i and $\delta\lambda$ are independent and arbitrary, the above relation leads to

$$\frac{\partial F}{\partial u_i} + \lambda\frac{\partial C}{\partial u_i} = 0, \quad i = 1, 2, \ldots, n; \text{ and } C = 0$$

The Lagrange multiplier technique yields an unconstrained problem, but leads to n + 1 unknowns by introducing λ. The constraint can be used to eliminate one of the unknowns, resulting in an unconstrained problem with n – 1 unknowns. The Lagrange multiplier technique is easily modified to multiple constraints by introducing multiple Lagrange multipliers. Use of an augmented Lagrangian approach, as discussed in Reference [6], improves the conditioning of the effective stiffness matrix and allows the safe use algorithms without pivoting like the skyline solver.

1.4.3 General Formulation of Structural Elements

As stated in Reference [6], the formulation of structural elements in Dymore is performed based on the principle of virtual work, which states that a particle is in equilibrium if and only if the variation in potential of the conservative forces equals the virtual work done by the non conservative and inertial forces for all arbitrary virtual displacements. Extension of this principle to a system of particles is trivial. The introduction of constraints modifies the statement of the principle of virtual work to include the caveat “kinematically admissible virtual displacements.” It is noted that the constraint forces are conservative in nature. For the elastic beam elements used in the rotor models presented here, the non conservative force is the centrifugal force caused by the rigid body rotation of the rotor, and the conservative forces not associated with constraints are the restoring loads due to the bending of the beam.

Beam elements in Dymore account for arbitrarily large displacements and finite rotations, but are limited to small strains. Dymore assumes that a cross-section of a beam does not deform in its own plane and that the cross-section remains planar after deformation.

While it is of great importance to identify the exact physical meaning of the Lagrange multipliers to characterize the equations derived from the principle of virtual work, Lagrange multipliers can be interpreted as constraint forces.

CHAPTER 2

THE PAIRED BLADE ROTOR

2.1 Paired Blade Rotor Overview

The paired blade rotor is a proposed configuration for tiltrotor aircraft in which each of the three arms of a gimbaled yoke connects to two blades. A general sketch of the paired blade rotor disk is shown in Figure 2.1. This configuration addresses the δ_3 and control system packaging problems discussed above while increasing rotor solidity, the fraction of the total rotor disk area made up of blade planform area, for improved performance. Each pair of blades on a yoke arm is controlled by one trailing edge pitch link positioned for desired geometric δ_3. A four-link mechanism with a horizontal link (long axis in the plane of rotation) connecting the grips of the blades in a pair to transmit the pitch control input from the trailing-edge grip to the leading-edge grip. The four link pitch control mechanism is shown as a section cutaway from the rough layout planform hub view in Figure 2.2.

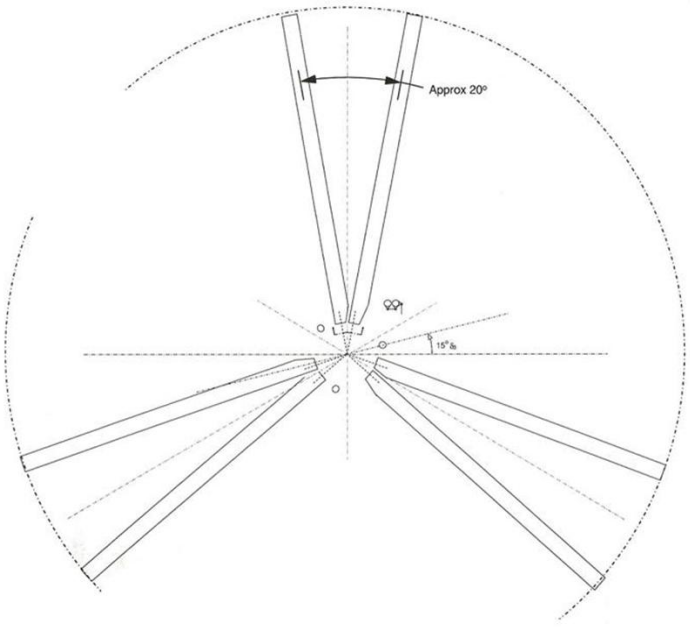

Figure 2.1 Sketch of paired blade rotor disk

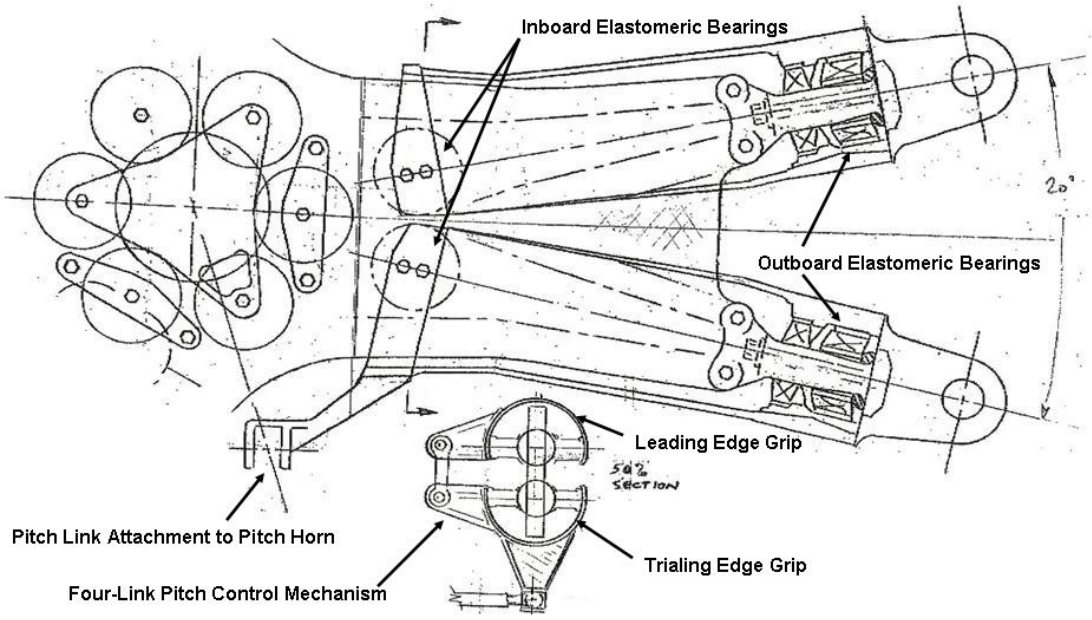

Figure 2.2 Rough layout planform hub view with four link mechanism cutaway

2.2 Paired Blade Rotor Configuration

The paired blade rotor is a gimbaled flexure rotor hub with elastomeric feathering bearings. The gimbal at the center of rotation accommodates rotor flapping and is connected to the flexure (yoke). The yoke is a composite structure that accommodates rotor coning and the lead-lag motion of one rotor arm relative to adjacent arms. The yoke is connected to inboard elastomeric feathering bearings with rigid structures called bearing beams, and to outboard elastomeric feathering bearings via the structurally rigid spindles. The yoke is a non feathering component, stated alternatively: the yoke does not experience deflections in the pitch degree of freedom when pitch inputs are imparted by the control system. Feathering structures called the grips connect the inboard elastomeric bearing beams to the outboard elastomeric feathering bearings and act parallel in bending to the non-feathering yoke over this radial range. The rotor blade is connected rigidly to the grip. A schematic of the configuration of a single blade of the paired blade rotor viewed from the trailing-edge looking forward is shown in Figure 2.3.

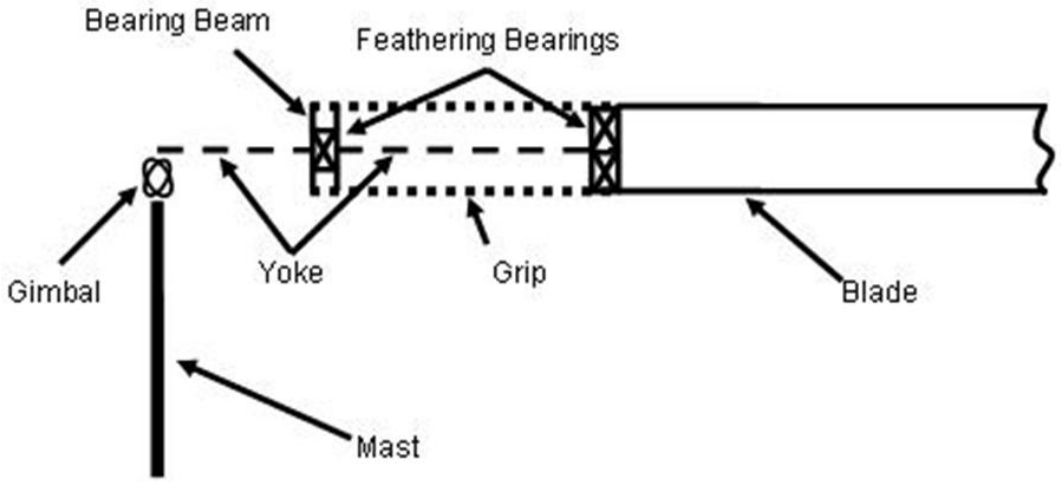

Figure 2.3 Schematic of the configuration of a single blade of the paired blade rotor viewed from the trailing-edge looking forward

CHAPTER 3

DYMORE MODEL DOCUMENTATION

This chapter documents the Dymore model input parameters for the six bladed evenly spaced (6BES) rotor and the paired blade rotor (PBR) with 20° spacing between blades in a pair. A later chapter presents results of PBR models with various blade spacings. All input parameters to the PBR models with blade spacing not equal to 20° except for the blade spacing angle are identical to those presented in this chapter. The first section of this chapter documents the model parameters common to both the 6BES rotor and the PBR. The second and third sections document input parameters unique to the 6BES and PBR rotor models, respectively.

3.1 Dymore Model Input Parameters Common to The 6BES and PBR Models

3.1.1. Common General Rotor Parameters

Many of the parameters fundamental to the character of a rotor are common between the 6BES and PBR rotor models. For instance, the rotor radius, operating RPM, blade collective pitch angles analyzed, and feathering bearing radial stations are common to the two rotor models. These Parameters are listed in Table 3.1.

Table 3.1 General Rotor Parameters Common to 6BES and PBR Rotor Models

Parameter	Value	Units
Rotor Radius	423.64	in
Helicopter Mode Rotor Speed	209.6	RPM
Helicopter Mode Rotor Speed	100	% Nr
Airplane Mode Rotor Speed	157.2	RPM
Airplane Mode Rotor Speed	75	% Nr
Helicopter Mode Low Blade Coll	38	deg
Helicopter Mode Mid Blade Coll	75	deg
Helicopter Mode High Blade Coll	78.6	deg
Airplane Mode Low Blade Coll	67.4	deg
Airplane Mode Mid Blade Coll	87.77	deg
Airplane Mode High Blade Coll	95.36	deg
Inboard Feathering Bearing Radial Station	25.83	in
Outboard Feathering Bearing Radial Station	82.22	in

Neither of the rotor models contains any pre-cone, pre-lag, torque offset, or underslinging.

3.1.2. Common Configuration and Selected Finite Element Parameters

The root end of the inboard yoke beam element connects to a flexible joint element (6-axis spring) used to model the gimbal at the center of rotation. The PBR model has two yoke beams per arm, which are coincident at the gimbal spring. The gimbal flexible joint element is connected to the top of the rigid mast element. The rigid mast element connects the gimbal spring at the top of the mast to the rigid rotating swashplate element at the bottom of the mast. The rigid swashplate element connects the mast to a revolute joint, which is connected to a rigid non-rotating swashplate element. The non-rotating swashplate element is connected to the boundary condition, which does not allow translation in any direction or rotation about any axis.

An auxiliary rigid element connects the rotating swashplate to a prismatic joint (used for blade collective input specification) at the bottom of the pitch link. The prismatic joint is connected to the bottom of the rigid pitch link element through a universal joint that is used to model the rod-end connection at the bottom of the pitch link. The rigid pitch link element has a flexible joint embedded close to the bottom of the pitch link that is set up to model the flexibility of the control system along the pitch link axis. The top of the pitch link rigid element is connected to the rigid pitch horn through a spherical joint that allows unrestrained rotation in three axes. The rigid pitch horn element connects the spherical joint at the top of the pitch link to the root end of the inboard grip beam element at the inboard feathering bearing radial station. Rigid elements, flexible, universal, spherical, and prismatic joints discussed in this section were modeled as massless. The coordinates of points of connection discussed in this section are listed in Table 3.2.

Table 3.2 Configuration Connection Point Coordinates Common to 6BES and PBR

Point*	**Span Coordinate (in)**	**Inplane Coord. (in)**	**Out of Plane Coord. (in)**
Center of Rotation	0	0	0
Mast Bottom	0	0	-26.74

* All points defined in global coordinate system

The global coordinate system has its origin at the intersection of the mast axis and the blade pitch change axis (PCA). The e_1 or span axis extends radially outward coincident with the blade 1 PCA for the 6BES model and bisecting the angle between the blade 1 PCA and blade 2 PCA for the PBR model. The e_2 or inplane axis extends from the origin perpendicular to the span axis in a direction from blade trailing edge to blade leading edge. The e_3 or out of plane axis extends in a direction consistent with the right hand rule in the direction of positive blade flapping. A Dymore post-processor screen shot of a single blade of the 6BES rotor model connected to the hub, which is common to both rotor models, is shown in Figure 3.1.

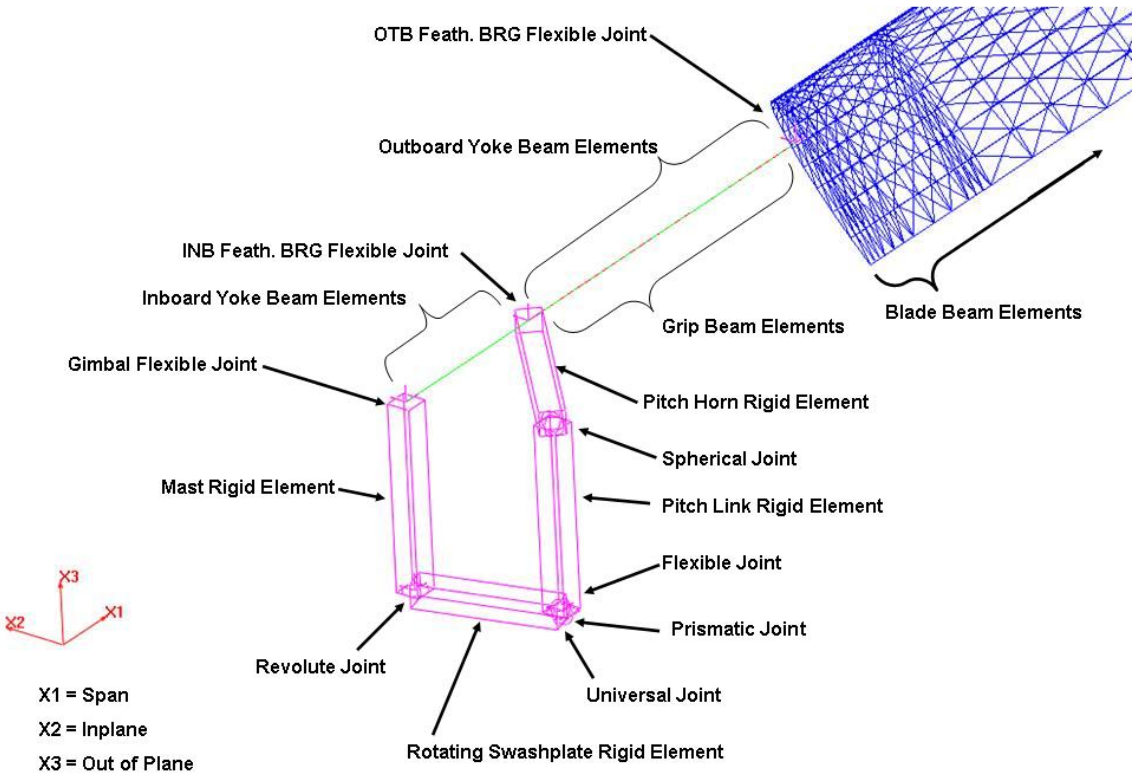

Figure 3.1 Dymore post-processor screenshot of 6BES model single blade connected to hub.

3.1.3. Beam Finite Element Parameters Common to 6BES and PBR

Beam finite element parameters such as the number of beam elements per component and the shape functions of beam elements that are common to both rotor models are

documented in this section. All beam elements used in both rotor models have cubic shape functions. The blades in both rotor models are represented by 27 beam elements. The unequal lengths of the blade beam elements are identical between the two rotor models. The blade beam element endpoint radial stations are listed in Table 3.3. These spanwise coordinates are input in different coordinate systems in the 6BES rotor model and the PBR model.

Table 3.3 Blade Beam Element Endpoint Spanwise Stations Common to 6BES and PBR

Span Coord. (in)	Continued	Continued	Continued
82.22	154.07	311.22	401.92
85.28	164.27	317.74	406.43
85.29	191.89	348.97	410.97
91.28	211.82	380.20	415.50
102.34	233.55	386.99	416.59
106.60	255.27	393.78	422.02
129.78	281.88	397.17	423.64

3.1.4. Common Finite Element Structural and Mass Properties

The element properties common to the 6BES and PBR rotor models are documented in this section. Common blade beam element spanwise property distributions are listed in Tables 3.4 and 3.5.

Table 3.4 Blade Beam Element Property Distributions Common to 6BES and PBR Set 1

Radial Station (in)	Twist (deg)	Beamwise CG (in)	Chordwise CG (in)	Beamwise Mom. of Inert. (in-lb-s^2/in)	Chordwise Mom. of Inert. (in-lb-s^2/in)
82.23	53.06	-0.181	0.422	16.17	22.17
85.29	53.06	-0.181	0.422	16.17	22.17
85.30	53.06	-0.181	0.422	0.150	0.894
91.28	53.06	-0.181	0.422	0.150	0.894
91.29	51	-0.217	0.685	0.110	0.789
102.34	51	-0.217	0.685	0.110	0.789
102.35	50.5	-0.232	0.980	0.0874	0.679
106.60	50.5	-0.232	0.980	0.0874	0.679
106.61	46.4	-0.265	1.37	0.0660	0.524
129.78	46.4	-0.265	1.37	0.0660	0.524
129.79	42.5	-0.314	1.32	0.0471	0.439
154.07	42.5	-0.314	1.32	0.0471	0.439

Table 3.4 – *Continued*

154.08	40.3	-0.314	1.19	0.0334	0.398
164.27	40.3	-0.314	1.19	0.0334	0.398
164.28	36.7	-0.275	0.936	0.0210	0.350
191.89	36.7	-0.275	0.936	0.0210	0.350
191.90	34.94	-0.213	0.973	0.0123	0.295
211.82	34.94	-0.213	0.973	0.0123	0.295
211.84	33.39	-0.209	1.14	0.00887	0.307
233.55	33.39	-0.209	1.14	0.00887	0.307
233.56	31.86	-0.185	1.09	0.00592	0.272
255.27	31.86	-0.185	1.09	0.00592	0.272
255.28	30.26	-0.201	0.059	0.00349	0.202
281.88	30.26	-0.201	0.059	0.00349	0.202
281.89	28.38	-0.176	-0.184	0.00228	0.155
311.21	28.38	-0.176	-0.184	0.00228	0.155
311.22	28.01	-0.167	-0.066	0.00176	0.141
317.73	28.01	-0.167	-0.066	0.00176	0.141
317.74	26.05	-0.158	0.110	0.00166	0.140
348.96	26.05	-0.158	0.110	0.00166	0.140
348.97	24.07	-0.130	-0.238	0.00146	0.124
380.19	24.07	-0.130	-0.238	0.00146	0.124
380.20	23.68	-0.114	-0.435	0.00134	0.117
386.98	23.68	-0.114	-0.435	0.00134	0.117
386.99	23.30	-0.102	0.097	0.00136	0.127
393.77	23.30	-0.102	0.097	0.00136	0.127
393.78	23.12	-0.094	0.349	0.00137	0.132
397.16	23.12	-0.094	0.349	0.00137	0.132
397.18	22.84	0.100	0.395	0.00160	0.132
401.91	22.84	0.100	0.395	0.00160	0.132
401.92	22.56	0.106	0.302	0.00158	0.130
406.42	22.56	0.106	0.302	0.00158	0.130
406.43	22.28	0.113	0.213	0.00157	0.128
410.96	22.28	0.113	0.213	0.00157	0.128
410.98	22.00	0.119	0.122	0.00155	0.125
415.49	22.00	0.119	0.122	0.00155	0.125
415.50	21.93	-0.0683	0.099	0.00132	0.124
416.58	21.93	-0.0683	0.099	0.00132	0.124
416.59	21.60	0.0914	-0.182	0.00137	0.116
422.01	21.60	0.0914	-0.182	0.00137	0.116
422.02	21.5	-0.0837	-4.00	0.00119	0.177
423.64	21.5	-0.0837	-4.00	0.00119	0.177

Table 3.5 Blade Beam Element Property Distributions Common to 6BES and PBR Set 2

Radial Station (in)	Torsion Stiffness (e-6 lb-in^2)	Beamwise SC (in)	Chordwise SC (in)	Beamwise NA (in)	Chordwise NA (in)
82.23	6508	-0.0109	0.362	-0.151	0.272
85.29	6508	-0.0109	0.362	-0.151	0.272
85.30	6508	-0.0109	0.362	-0.151	0.272
91.28	6508	-0.0109	0.362	-0.151	0.272
91.29	4834	-0.0380	0.634	-0.195	0.869
102.34	4834	-0.0380	0.634	-0.195	0.869
102.35	3888	-0.0597	0.996	-0.213	1.45
106.60	3888	-0.0597	0.996	-0.213	1.45
106.61	2880	-0.156	2.17	-0.253	1.92
129.78	2880	-0.156	2.17	-0.253	1.92
129.79	1856	-0.204	3.23	-0.309	2.32
154.07	1856	-0.204	3.23	-0.309	2.32
154.08	1286	-0.167	3.26	-0.315	2.38
164.27	1286	-0.167	3.26	-0.315	2.38
164.28	776.6	-0.0993	3.89	-0.281	2.29
191.89	776.6	-0.0993	3.89	-0.281	2.29
191.90	471.2	-0.0887	4.12	-0.212	2.31
211.82	471.2	-0.0887	4.12	-0.212	2.31
211.84	301.3	-0.102	4.22	-0.204	2.31
233.55	301.3	-0.102	4.22	-0.204	2.31
233.56	210.8	-0.144	3.56	-0.184	1.90
255.27	210.8	-0.144	3.56	-0.184	1.90
255.28	118.8	-0.158	2.86	-0.167	1.85
281.88	118.8	-0.158	2.86	-0.167	1.85
281.89	70.94	-0.144	2.27	-0.137	1.77
311.21	70.94	-0.144	2.27	-0.137	1.77
311.22	51.73	-0.110	1.88	-0.114	1.66
317.73	51.73	-0.110	1.88	-0.114	1.66
317.74	49.60	-0.0595	1.63	-0.0987	1.40
348.96	49.60	-0.0595	1.63	-0.0987	1.40
348.97	45.18	-0.0158	1.00	-0.0765	0.922
380.19	45.18	-0.0158	1.00	-0.0765	0.922
380.20	41.32	0.00317	0.634	-0.0647	0.526
386.98	41.32	0.00317	0.634	-0.0647	0.526
386.99	39.70	0.0201	0.083	-0.0575	0.185
393.77	39.70	0.0201	0.083	-0.0575	0.185
393.78	38.74	0.0301	-0.242	-0.0521	-0.0255
397.16	38.74	0.0301	-0.242	-0.0521	-0.0255
397.18	38.34	0.0326	-0.313	-0.0475	-0.0994
401.91	38.34	0.0326	-0.313	-0.0475	-0.0994
401.92	37.89	0.0353	-0.394	-0.0423	-0.183

Table 3.5 – *Continued*

406.42	37.89	0.0353	-0.394	-0.0423	-0.183
406.43	37.45	0.0380	-0.473	-0.0371	-0.265
410.96	37.45	0.0380	-0.473	-0.0371	-0.265
410.98	37.01	0.0407	-0.552	-0.0324	-0.347
415.49	37.01	0.0407	-0.552	-0.0324	-0.347
415.50	36.74	0.0423	-0.600	-0.0290	-0.398
416.58	36.74	0.0423	-0.600	-0.0290	-0.398
416.59	36.14	0.0287	-0.487	-0.0276	-0.349
422.01	36.14	0.0287	-0.487	-0.0276	-0.349
422.02	35.30	0.00362	-0.243	-0.0281	-0.218
423.64	35.30	0.00362	-0.243	-0.0281	-0.218

Properties labeled beamwise and chordwise in Tables 3.4 and 3.5 refer to local blade cross-section axes which have an origin at the PCA and are normal to the chord line for beamwise properties and parallel to the chord line for chordwise properties. Mass moments of inertia are taken about the local blade center of gravity. Chordwise offsets are positive aft.

Common yoke beam element spanwise property distributions are listed in Table 3.6. The yoke is an un-twisted component and all cg, shear center, and neutral axis offsets are 0. The twist and offset parameters listed for the blade in Tables 3.4 and 3.5 are omitted from the yoke properties in Table 3.6

Table 3.6 Yoke Beam Element Property Distributions Common to 6BES and PBR

Radial Station (in)	**Weight per Length (lb/in)**	**Beamwise Stiffness (e-6 lb-in^2)**	**Beamwise Mom of Inert. (in-lb-s^2/in)**	**Chordwise Mom of Inert. (in-lb-s^2/in)**	**Torsion Stiffness (e-6 lb-in^2)**
0	25.44	966.9	0.00736	0.1231	298.3
6.76	25.44	966.9	0.00736	0.1231	298.3
6.77	25.06	966.9	0.00736	0.1231	298.3
13.5	25.06	966.9	0.00736	0.1231	298.3
13.51	29.13	966.9	0.00736	0.1231	298.3
22.89	29.13	966.9	0.00736	0.1231	298.3
22.90	138.0	966.9	0.00736	0.1231	226.5
25.83	138.0	966.9	0.00736	0.1231	226.5
25.84	23.75	122.8	0.00736	0.1231	112.6
31.5	23.75	122.8	0.00736	0.1231	112.6
31.51	2.245	90.54	0.00736	0.1231	128.6
36.34	2.245	90.54	0.00736	0.1231	128.6
36.35	1.826	44.59	0.00736	0.1231	102.6

Table 3.6 – *Continued*

40.82	1.826	44.59	0.00736	0.1231	102.6
40.83	1.566	27.53	0.00736	0.1231	117.7
45.65	1.566	27.53	0.00736	0.1231	117.7
45.66	1.442	24.60	0.00736	0.1231	85.87
56.57	1.442	24.60	0.00736	0.1231	85.87
56.58	1.557	36.08	0.00736	0.1231	169.1
62.05	1.557	36.08	0.00736	0.1231	169.1
62.06	1.297	55.75	0.00736	0.1231	318.6
68.15	1.297	55.75	0.00736	0.1231	318.6
68.16	1.297	55.75	0.00736	0.1231	318.6
74.50	1.297	55.75	0.00736	0.1231	318.6
74.51	27.24	55.75	0.1041	0.2198	730.2
82.22	27.24	55.75	0.1041	0.2198	730.2

Grip beam element properties common to both rotor models are listed in Table 3.7. The grip was modeled as virtually massless in both rotor models, and weight is omitted from Table 3.7. The grip is an untwisted component, and all cg, shear center, and neutral axis offsets are 0. Twist and all offsets are omitted from Table 3.7. The grip is the feathering structure that surrounds the non-feathering yoke between the inboard elastomeric feathering bearing flexible joint element and the outboard elastomeric bearing flexible joint element.

Table 3.7 Grip Beam Element Property Distributions Common to 6BES and PBR

Radial Station (in)	**Beamwise Stiffness (e-6 lb-in^2)**	**Chordwise Stiffness (e-6 lb-in^2)**	**Torsion Stiffness (e-6 lb-in^2)**
25.83	9485	21194	21717
82.22	9485	21194	21717

The flexible joint element properties used to model the inboard and outboard feathering bearings and the gimbal joint for collective and cyclic mode boundary conditions were common between the 6BES rotor model and the PBR model. Table 3.8 contains these flexible joint element properties.

Table 3.8 Flexible Joint Element Properties Common to 6BES and PBR

Flexible Joint	Spanwise Linear K (lb/in)	Inplane Linear K (lb/in)	Out of Plane Linear K (lb/in)	Rotation About Span Axis Angular K (in-lb / deg)	Rotation About Inplane Axis Angular K (in-lb / deg)	Rotation About Out of Plane Axis Angular K (in-lb / deg)
INB Feath BRG	8.33E+06	46,165,917	80,111,417	20.03	20.03	20.03
OTB Feath BRG	8.33E+06	19,009,500	19,009,500	1602.2	20.03	20.03
Gimbal COL BC	8.33E+12	8.33E+12	8.33E+12	2.09E+13	2.09E+13	1,049,187
Gimbal CYC BC	8.33E+12	8.33E+12	8.33E+12	2.09E+13	40392	2.09E+13

Properties of other Dymore joint elements used in both the 6BES rotor model and the PBR rotor model are shown in Table 3.9.

Table 3.9 Joint Element Properties Common to 6BES and PBR

Joint Type	Location	Span Translation	Inplane Translation	Out of Plane Translation	Span Rotation	Inplane Rotation	OOP Rotation
Revolute	Mast Bottom	NO	NO	NO	NO	NO	Free

3.2 Dymore Model Input Parameters Unique to The 6BES Rotor

3.2.1. 6BES-Particular General Rotor Parameters

The general rotor parameters that are used in the Dymore rotor model of the 6BES rotor and not in the model of the PBR are presented in this section. The geometric δ_3 used for the 6BES rotor model is -15°. Each blade is separated 60° in the plane of rotation from either adjacent blade. There is one pitch link per blade in the 6BES rotor model.

3.2.2. 6BES-Particular General Configuration and Selected Finite Element Parameters

In the 6BES rotor model, a set of inboard yoke beam elements connects the gimbal flexible joint element to the inboard feathering bearing flexible joint. The inboard bearing joint connects the root end of the grip beam element, the outboard end of the inboard set of yoke beam elements, and the inboard end of the outboard set of yoke beam elements. The root end of the grip beam element is also connected to top of the pitch link by a rigid pitch horn element as described in section 3.1.2. A set of outboard yoke beam elements connect the inboard feathering bearing flexible joint element to the outboard feathering bearing flexible joint element.

The outboard feathering bearing connects the outboard yoke beam elements, the outboard end of the grip beam element, and the root end of the inboard blade beam element. The blade beam elements extent from the outboard feathering bearing to the blade tip with no connections to anything but each other along the span. The coordinates and descriptive names of salient points discussed in this section are listed in Table 3.10.

Table 3.10 Configuration Connection Point Coordinates of 6BES Model

Point*	Span Coordinate (in)	Inplane Coord. (in)	Out of Plane Coord. (in)
Pitch Link Top	5.12	-19.1	0
FJ Control Sys	5.12	-19.1	-26.52
Pitch Link Bottom	5.12	-19.1	-26.74
INB Feath BRG	25.83	0	0
OTB Feath BRG	82.22	0	0

* All points defined in global coordinate system
Pitch link coordinates for level pitch horn, 69° blade root collective pitch angle

3.2.3. 6BES-Particular Beam Finite Element Parameters

Beam element parameters associated with the 6BES rotor model and not with the PBR model are documented in this section. The 6BES yoke is represented by a set of 4 inboard beam elements and a set of 9 outboard beam elements. The 6BES yoke beam element endpoints are listed in Table 3.11.

Table 3.11 Yoke Beam Element Endpoint Spanwise Stations of 6BES Model

Inboard Elements Span Coord. (in)*	Outboard Elements Span Coord. (in)*
0	25.83
6.77	31.50
13.51	36.34
22.90	40.82
25.83	45.65
	56.57
	62.05
	68.15
	74.50
	82.22

* All coordinates defined in global system

The 6BES grip is modeled with 1 beam element.

3.2.4. 6BES-Particular Finite Element Structural and Mass Properties

Element properties used in the 6BES Dymore rotor model are documented in this section. The blade beam element property distribution of the 6BES rotor is listed in Table 3.12 and the yoke beam element property distribution of the 6BES rotor is listed in Table 3.13.

Table 3.12 Blade Beam Element Property Distributions of the 6BES Model Not Presented in Section 3.1

Radial Station (in)	Weight per Length (lb/in)	Beamwise Stiffness (e-6 lb-in^2)	Chordwise Stiffness (e-6 lb-in^2)
82.23	49.61	12996	9950
85.29	49.61	12996	9950
85.30	2.562	9950	9950
91.28	2.562	9950	9950
91.29	2.390	6654	9981
102.34	2.390	6654	9981
102.35	2.167	5073	6523
106.60	2.167	5073	6523
106.61	1.830	4411	6096
129.78	1.830	4411	6096
129.79	1.547	3003	6007
154.07	1.547	3003	6007
154.08	1.386	3899	5199
164.27	1.386	3899	5199
164.28	1.130	3325	4433
191.89	1.130	3325	4433
191.90	0.9816	3123	4164
211.82	0.9816	3123	4164
211.84	1.228	2180	2907
233.55	1.228	2180	2907
233.56	1.134	1736	2315
255.27	1.134	1736	2315
255.28	0.9193	1197	1596
281.88	0.9193	1197	1596
281.89	0.7912	760.1	1013
311.21	0.7912	760.1	1013
311.22	0.7853	558.2	744.2
317.73	0.7853	558.2	744.2
317.74	0.8054	448.6	598.1
348.96	0.8054	448.6	598.1
348.97	0.7399	376.2	501.6

Table 3.12 – *Continued*

380.19	0.7399	376.2	501.6
380.20	0.7608	334.4	445.9
386.98	0.7608	334.4	445.9
386.99	0.9300	302.5	403.3
393.77	0.9300	302.5	403.3
393.78	1.020	281.4	375.1
397.16	1.020	281.4	375.1
397.18	1.422	268.7	358.3
401.91	1.422	268.7	358.3
401.92	1.412	256.0	341.3
406.42	1.412	256.0	341.3
406.43	2.403	243.7	324.9
410.96	2.403	243.7	324.9
410.98	2.393	231.7	308.9
415.49	2.393	231.7	308.9
415.50	1.972	222.4	296.6
416.58	1.972	222.4	296.6
416.59	2.326	214.8	286.5
422.01	2.326	214.8	286.5
422.02	2.603	210.2	280.2
423.65	2.603	210.2	280.2

Table 3.13 Yoke Beam Element Property Distributions of The 6BES Model Not Presented in Section 3.1

Radial Station (in)	**Chordwise Stiffness (e-6 lb-in^2)**	**RSTA Continued (in)**	**Chord EI Continued (e-6 lb-in^2)**
0	10349	40.82	5217
6.76	10349	40.83	3856
6.77	15525	45.65	3856
13.5	15525	45.66	2540
13.51	15525	56.57	2540
22.89	15525	56.58	2294
22.90	15525	62.05	2294
25.83	15525	62.06	5957
25.84	11474	68.15	5957
31.5	11474	68.16	5957
31.51	7302	74.50	5957
36.34	7302	74.51	5957
36.35	5217	82.22	5957

The properties of the flexible joint element close to the bottom of the pitch link and the flexible joint used to model the gimbal with scissors mode boundary conditions for the 6BES rotor model are listed in Table 3.14.

Table 3.14 Flexible Joint Element Properties of The 6BES Model

Flexible Joint	Spanwise Linear K (lb/in)	Inplane Linear K (lb/in)	Out of Plane Linear K (lb/in)	Rotation About Span Axis Angular K (in-lb / deg)	Rotation About Inplane Axis Angular K (in-lb / deg)	Rotation About Out of Plane Axis Angular K (in-lb / deg)
Gimbal SCI BC	8.33E+12	8.33E+12	8.33E+12	2.09E+13	2.09E+13	2.09E+13
FJ PL 38°Coll	8.33E+07	8.33E+07	31,325	2.09E+08	2.09E+08	2.09E+08
FJ PL 67.4°Coll	8.33E+07	8.33E+07	36,359	2.09E+08	2.09E+08	2.09E+08
FJ PL 75°Coll	8.33E+07	8.33E+07	36,973	2.09E+08	2.09E+08	2.09E+08
FJ PL 78.6°Coll	8.33E+07	8.33E+07	31,163	2.09E+08	2.09E+08	2.09E+08
FJ PL 87.77°Coll	8.33E+07	8.33E+07	36,610	2.09E+08	2.09E+08	2.09E+08
FJ PL 95.36°Coll	8.33E+07	8.33E+07	35,859	2.09E+08	2.09E+08	2.09E+08

Properties of other 6BES rotor model joint elements are listed in Table 3.15.

Table 3.15 Joint Element Properties of The 6BES Model

Joint Type	Location	Span Linear	Inplane Linear	Out of Plane Linear	Span Rotation	Inplane Rotation	Out of Plane Rotation
Spherical	PL Top	NO	NO	NO	Free	Free	Free
Universal	PL Bottom	NO	NO	NO	Free	Free	NO
Prismatic	PL Bottom	NO	NO	Prescribed	NO	NO	NO

Axes are referenced to global coordinate system

3.3 Dymore Model Input Parameters Unique to The PBR Rotor

Rotor model parameters that are used in the PBR model and not in the 6BES model are documented in this section. The parameters discussed in section 3.1 and parameters presented in this section represent enough information to build an identical model of the PBR in another multi-body finite element analysis code.

3.3.1. PBR-Particular General Rotor Parameters

The general rotor parameters that are used in the Dymore rotor model of the PBR rotor or and not in the model of the 6BES rotor are presented in this section. The paired blade rotor

model has a geometric δ_3 of -5°. The spacing between blades in a pair for the baseline PBR rotor model is 20°. One pitch link per rotor arm provides blade pitch control inputs to blades in a pair via a trailing edge pitch horn and a four-link pitch control mechanism.

3.3.2. PBR-Particular Configuration and Selected Finite Element Parameters

Rotor model parameters particular to the PBR rotor model that are related to the model configuration and some of the finite elements used are presented in this section. Coordinates of salient points in the PBR rotor model configuration that are not included in Table 3.2 are listed in Table 3.16.

Table 3.16 Configuration Connection Point Coordinates of the PBR Model

Point*	Span Coordinate (in)	Inplane Coord. (in)	Out of Plane Coord. (in)	Coordinate System
Pitch Link Top	1.723	-19.6986	0	Global
FJ Control Sys	1.723	-19.6986	-26.52	Global
Pitch Link Bottom	1.723	-19.6986	-26.74	Global
Leading Edge INB Yoke Lock	12.84	0	0	Leading Edge Blade
Leading Edge INB Feath BRG	25.83	0	0	Leading Edge Blade
Leading Edge OTB Yoke Lock	54.02	0	0	Leading Edge Blade
Leading Edge OTB Feath BRG	82.22	0	0	Leading Edge Blade
Trailing Edge INB Yoke Lock	12.84	0	0	Trailing Edge Blade
Trailing Edge INB Feath BRG	25.83	0	0	Trailing Edge Blade
Trailing Edge OTB Yoke Lock	54.02	0	0	Trailing Edge Blade
Trailing Edge OTB Feath BRG	82.22	0	0	Trailing Edge Blade
4 Link Leading Edge Connection	25.83	0	-4.8	Leading Edge Blade
4 Link Trailing Edge Connection	25.83	0	-4.8	Trailing Edge Blade

The leading edge blade coordinate system is the global coordinate system rotated + 10° about the out of plane axis.

The trailing edge blade coordinate system is the global coordinate system rotated - 10° about the out of plane axis.

3.3.2.1 PBR Configuration Parameters Common to Leading and Trailing Edge Blades

For ease of discussion and brevity, the configuration parameters that are duplicated from the trailing edge (TE) blade to the leading edge (LE) blade of the blades that share a rotor arm and four-link control mechanism are presented at once as common parameters in this section. For LE blades and TE blades, the yoke is comprised of four segments. The segments are referred to here as segments 1, 2, 3, and 4. The yoke segment numbers increase with

radial station from the yoke root at station 0.0 to the outboard feathering bearing at station 82.22 (in).

A set of beam elements used to model yoke segment 1 connects the gimbal flexible joint element to yoke segment 2. One of two rigid elements that connect the LE and TE yokes attaches at this junction of yoke segment 1 and yoke segment 2. Beam elements used to model yoke segment 2 connect yoke segment 1 to the inboard feathering bearing flexible joint element. The inboard feathering bearing flexible joint element connects yoke segment 2, yoke segment 3, and the root end of the grip beam elements. Yoke segment 3 beam elements connect the inboard feathering bearing flexible joint element to yoke segment 4 beam elements. The second of two rigid elements that connect the LE and TE yokes attaches at this junction of yoke segments 3 and 4. Yoke segment 4 beam elements connect yoke segment 3 beam elements and the outboard feathering bearing flexible joint. The outboard feathering bearing flexible joint element connects yoke segment 4 to the outboard end of the grip and the inboard end of the blade.

3.3.2.2 PBR Configuration Parameters Unique to the Trailing Edge Blade

The trailing edge blade has one configuration feature that the leading edge blade does not. A rigid pitch horn element connects the inboard grip beam element of the TE blade to the spherical joint at the top of the pitch link as discussed in section 3.1.2

3.3.2.3 Four-Link Pitch Control Mechanism Configuration Parameters

The mechanism used to transmit blade pitch control inputs from the trailing edge blade to the leading edge blade is referred to as the four-link pitch control mechanism. A rigid element connects the inboard feathering bearing flexible joint of the TE blade to a universal joint located some distance directly below (negative out of plane offset) the TE inboard feathering bearing. The TE four link universal joint is connected to and coincident with the four link TE revolute joint. The TE four link revolute joint is connected to the LE four link revolute joint by a rigid element, the four link inplane link, with mass properties for four-link configuration checkout purposes only. The four link revolute joints have a finite springrate to prevent numerical failures

of Dymore for this configuration related to the unrestrained motion of the four-link inplane link spinning about its long axis. The LE four-link revolute joint is connected to and coincident with a universal joint located some distance directly below the LE inboard feathering bearing. The LE four-link universal joint is connected to the LE inboard feathering bearing some distance directly above it with a rigid element, completing the modeling of the four-link mechanism. Dymore post-processor screenshots of the PBR with labels to aid in the visualization of the configuration discussed here are shown in Figures 3.2 and 3.3.

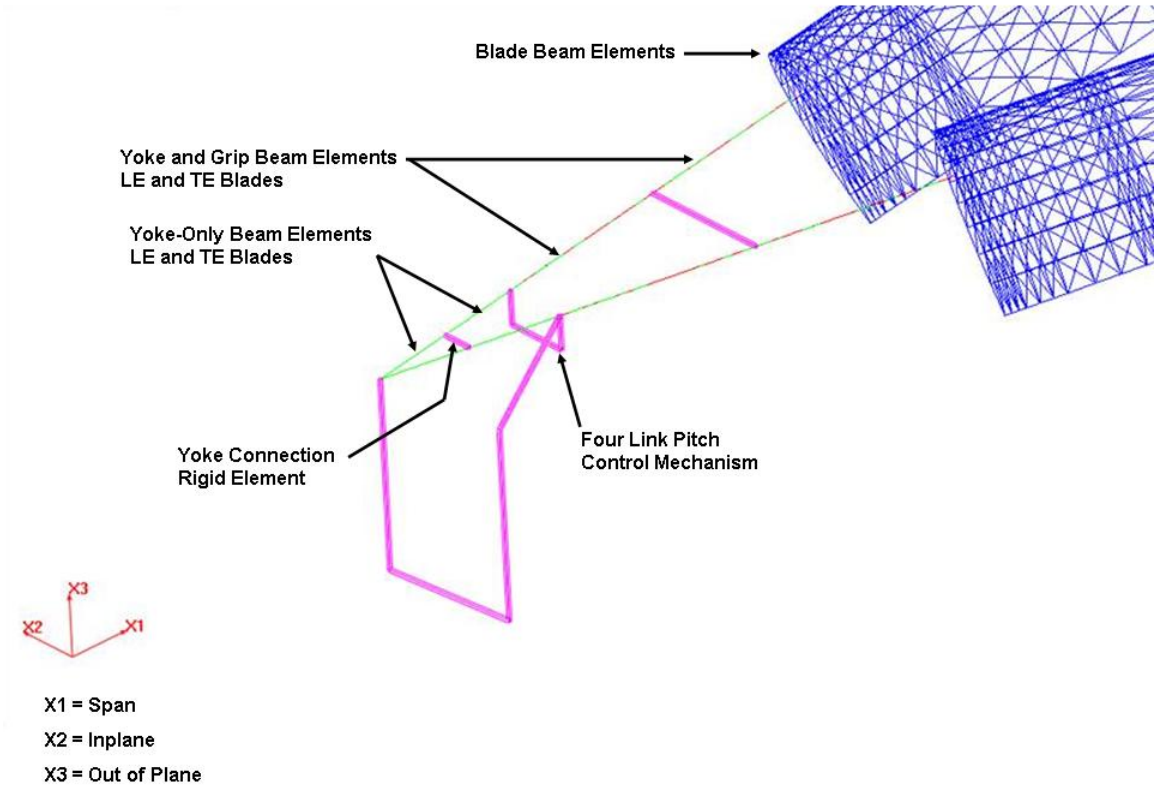

Figure 3.2 Dymput image of PBR rotor model configuration with rotor component label set 1.

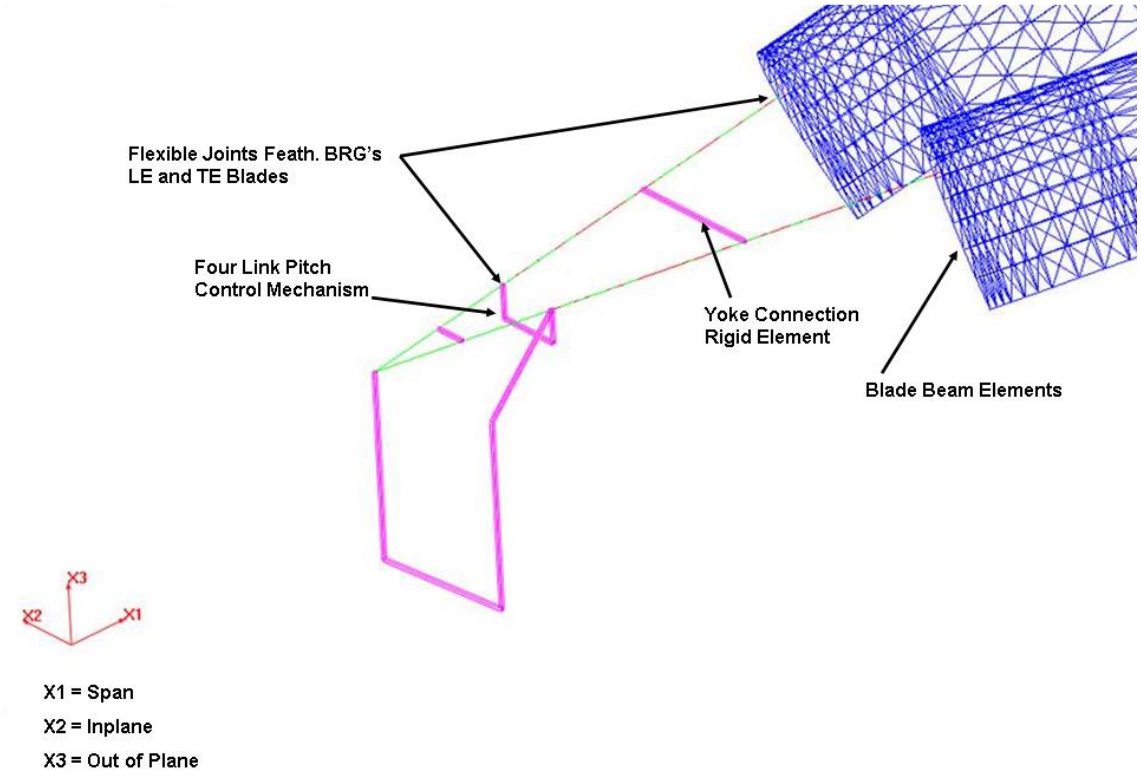

Figure 3.3 Dymput image of PBR rotor model configuration with rotor component label set 2.

3.3.3. PBR-Particular Finite Element Beam Parameters

Beam element parameters that are included only in the PBR Dymore model are documented in this section. The PBR yoke is modeled in 4 segments as discussed in section 3.3.2.1. Yoke segments 1 and 2 modeled with four beam elements each, and yoke segments 3 and 4 are modeled with 9 beam elements each. The PBR yoke beam element endpoints are listed in Table 3.17. The PBR grip is represented in Dymore as 4 beam elements with equal length.

Table 3.17 Yoke Beam Element Endpoints of the PBR Model

Yoke Seg. 1 Span Coord. (in)	Yoke Seg. 2 Span Coord. (in)	Yoke Seg. 3 Span Coord. (in)	Yoke Seg. 4 Span Coord. (in)
0	12.84	25.83	54.02
3.37	16.24	28.66	56.86
6.72	19.63	31.08	59.28
11.38	24.35	33.32	61.52
12.84	25.83	35.74	63.93
		41.20	69.39
		43.94	72.13
		46.99	75.18
		50.16	78.36
		54.02	82.22

The spanwise coordinates of the beam element endpoints of the PBR model are defined in either a coordinate system whose span axis is aligned with the TE blade PCA or a coordinate system whose span axis is aligned with the leading edge blade PCA, which are rotated + 10° about the out of plane axis or -10° about the out of plane axis respectively, for the 20° blade spacing baseline case.

3.3.4. PBR-Particular Finite Element Structural and Mass Properties

Element properties that are unique to the PBR rotor model are documented in this section. Blade beam element property distributions used in the PBR rotor that are not shared with the 6BES blade rotor model properties are presented in Table 3.18.

Table 3.18 Blade Beam Element Property Distributions of the PBR Model Not Presented in Section 3.1

Radial Station (in)	Weight per Length (lb/in)	Beamwise Stiffness (e-6 lb-in^2)	Chordwise Stiffness (e-6 lb-in^2)
82.23	49.61	13266	13266
85.29	49.61	13266	13266
85.30	2.562	13266	13266
91.28	2.562	13266	13266
91.29	2.390	12099	12099
102.34	2.390	12099	12099
102.35	2.167	7247	7247

Table 3.18 – *Continued*

106.60	2.167	7247	7247
106.61	1.830	7389	7389
129.78	1.830	7389	7389
129.79	1.547	6674	6674
154.07	1.547	6674	6674
154.08	1.386	5199	5199
164.27	1.386	5199	5199
164.28	1.130	4433	4433
191.89	1.130	4433	4433
191.90	1.0455	3785	3785
211.82	1.0455	3785	3785
211.84	0.991	2568	3424
233.55	0.991	2568	3424
233.56	1.572	2310	3080
255.27	1.572	2310	3080
255.28	1.5262	1920	2560
281.88	1.5262	1920	2560
281.89	1.3981	1502.1	2003
311.21	1.3981	1502.1	2003
311.22	1.3922	1127.6	1503.5
317.73	1.3922	1127.6	1503.5
317.74	3.3351	1019.5	1359.4
348.96	3.3351	1019.5	1359.4
348.97	0.7399	874.8	1166.4
380.19	0.7399	874.8	1166.4
380.20	0.7608	796.2	1061.6
386.98	0.7608	796.2	1061.6
386.99	0.9300	737.8	983.7
393.77	0.9300	737.8	983.7
393.78	1.020	703.4	937.9
397.16	1.020	703.4	937.9
397.18	1.422	689.1	918.8
401.91	1.422	689.1	918.8
401.92	3.255	673.6	898.2
406.42	3.255	673.6	898.2
406.43	3.245	658.6	878.1
410.96	3.245	658.6	878.1
410.98	3.235	643.6	858.1
415.49	3.235	643.6	858.1
415.50	2.814	635.5	847.3
416.58	2.814	635.5	847.3
416.59	3.168	631.9	842.6
422.01	3.168	631.9	842.6
422.02	3.445	636.9	849.1
423.65	3.445	636.9	849.1

Yoke beam element property distributions used in the PBR rotor that are not shared with the 6BES blade rotor model properties are presented in Table 3.19.

Table 3.19 Yoke Beam Element Property Distributions of the PBR Model Not Presented in Section 3.1

Radial Station (in)	Chordwise Stiffness (e-6 lb-in^2)	RSTA Continued (in)	Chord EI Continued (e-6 lb-in^2)
0	3415	40.82	1722
6.76	3415	40.83	1272
6.77	5123	45.65	1272
13.5	5123	45.66	838
13.51	5123	56.57	838
22.89	5123	56.58	757
22.90	5123	62.05	757
25.83	5123	62.06	1966
25.84	3786	68.15	1966
31.5	3786	68.16	1966
31.51	2410	74.50	1966
36.34	2410	74.51	1966
36.35	1722	82.22	1966

The properties of the flexible joint element in the pitch link load path are listed in Table 3.20.

Table 3.20 PBR Control System Stiffness Flexible Joint Springrates

Flexible Joint	Spanwise Linear K (lb/in)	Inplane Linear K (lb/in)	Out of Plane Linear K (lb/in)	Rotation About Span Axis Angular K (in-lb / deg)	Rotation About Inplane Axis Angular K (in-lb / deg)	Rotation About Out of Plane Axis Angular K (in-lb / deg)
FJ PL 38°Coll	8.33E+07	8.33E+07	46,092	2.09E+08	2.09E+08	2.09E+08
FJ PL 67.4°Coll	8.33E+07	8.33E+07	53,646	2.09E+08	2.09E+08	2.09E+08
FJ PL 75°Coll	8.33E+07	8.33E+07	54,573	2.09E+08	2.09E+08	2.09E+08
FJ PL 78.6°Coll	8.33E+07	8.33E+07	45,997	2.09E+08	2.09E+08	2.09E+08
FJ PL 87.77°Coll	8.33E+07	8.33E+07	54,009	2.09E+08	2.09E+08	2.09E+08
FJ PL 95.36°Coll	8.33E+07	8.33E+07	53,199	2.09E+08	2.09E+08	2.09E+08

The axes of articulation of the universal, spherical, and revolute joints used in the PBR model only are listed in Table 3.21.

Table 3.21 Joint Element Properties of PBR Model

Flexible Joint	Spanwise Linear K (lb/in)	Inplane Linear K (lb/in)	Out of Plane Linear K (lb/in)
FJ PL 38°Coll	8.33E+07	8.33E+07	46092
FJ PL 67.4°Coll	8.33E+07	8.33E+07	53646
FJ PL 75°Coll	8.33E+07	8.33E+07	54573
FJ PL 78.6°Coll	8.33E+07	8.33E+07	45997
FJ PL 87.77°Coll	8.33E+07	8.33E+07	54009
FJ PL 95.36°Coll	8.33E+07	8.33E+07	53199

Flexible Joint	Rotation About Span Axis Angular K (in-lb / deg)	Rotation About Inplane Axis Angular K (in-lb / deg)	Rotation About Out of Plane Axis Angular K (in-lb / deg)
FJ PL 38°Coll	2.09E+08	2.09E+08	2.09E+08
FJ PL 67.4°Coll	2.09E+08	2.09E+08	2.09E+08
FJ PL 75°Coll	2.09E+08	2.09E+08	2.09E+08
FJ PL 78.6°Coll	2.09E+08	2.09E+08	2.09E+08
FJ PL 87.77°Coll	2.09E+08	2.09E+08	2.09E+08
FJ PL 95.36°Coll	2.09E+08	2.09E+08	2.09E+08

The mass properties of the four-link inplane link were included as part of a diagnostic setup during mode type identification. These mass properties are listed in Table 3.22. Center of mass coordinates are listed in the global coordinate system.

Table 3.22 PBR Model Four-Link Inplane Link Mass Properties

Total Mass lb-s^2/in	Center of Mass Spanwise Coordinate (in)	Center of Mass Inplane Coordinate (in)	Center of Mass Out of Plane Coordinate (in)	Inertia About Span Axis wrt Center Mass (in-lb-s^2/in)	Inertia About Inplane Axis wrt Center Mass (in-lb-s^2/in)	Inertia About Out of Plane Axis wrt Center Mass (in-lb-s^2/in)
8.33E-08	25.43	0	-4.8	1.00E-06	0.1	1.00E-06

CHAPTER 4

METHOD FOR DETERMINING MODE TYPES AND FORCING FREQUENCIES

It is not necessary to perform a Coleman coordinate transformation to determine the forcing frequencies and mode types of rotor modes returned by analysis. An alternative method that employs hub reaction and blade tip modal displacement data from Dymore output files is used for this project and discussed in this chapter.

4.1 Mode Type Identification

The method used for determining collective, cyclic, and scissors mode types of the rotor modes generated by Dymore analysis is based on modal loads at the rotor hub.

The baseline rotor model gimbal flexible joint properties were selected to match particular boundary conditions and do not lend to mode type identification. For the rotor model configurations of the 6BES and PBR rotors, a utility model was built for each with gimbal flexible joint properties selected solely to facilitate mode type identification. Outputs were read from sensor elements in Dymore measuring the displacements of the gimbal in 6 degrees of freedom for each rotor mode.

Each mode generated by the utility models was assigned a mode type name based on the criteria below.

$$F_z \text{ or } M_z \neq 0, \quad \text{Collective Mode}$$

$$F_x, F_y, M_x \text{ or } M_y \neq 0, \quad \text{Cyclic Mode}$$

$$\text{All Modal Loads} = 0, \quad \text{Scissors Mode}$$

where x, y, and z are span, inplane, and out of plane axes, respectively, F is a force along the axis, and M is a moment about the axis.

This method was also used for mode type identification during fanplot generation for the baseline models.

4.2 Forcing Frequency Determination

The method for determining the forcing frequencies that excite each rotor mode uses the blade tip modal displacements from the utility models. An n /Rev frequency is determined to excite a rotor mode if the frequency performs nonzero virtual work on the mode. From Bramwell [9], the work done on each mode by a forcing frequency is calculated as:

$$W_{\phi} = \sum_{k=1}^{b} \phi_k \cos n(\psi_k)$$

where

n is an integer representing the integer multiple of the rotor speed

k is the blade number index

ϕ_k is the modal tip displacement for the k^{th} blade

ψ_k is the azimuthal position of the k^{th} blade (blade 1 is set at $\psi_k = 0$)

W_{ϕ} is the work done by n /Rev forcing frequency in modal displacements ϕ_k

Figure 4.1 illustrates that for the 6BES rotor, a collective mode, whose blade tips are all deflected to the same modal displacement value, is excited by a 6 /Rev forcing frequency and that the sum of the virtual work done by a 5 /Rev forcing frequency is zero.

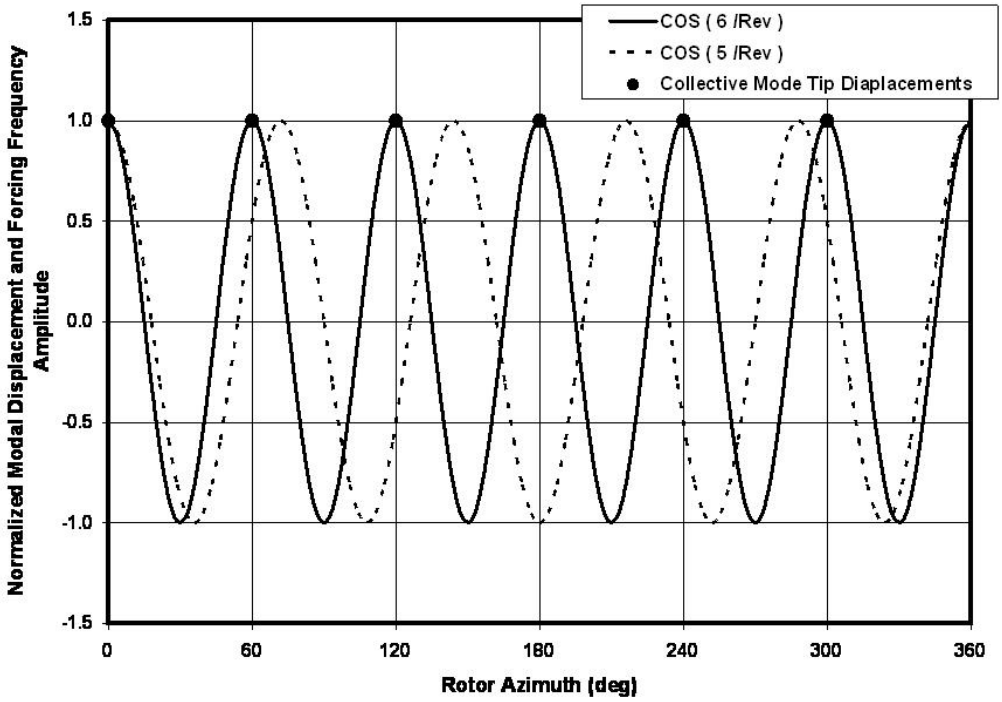

Figure 4.1 6 Bladed evenly spaced rotor collective mode tip deflections overlaid with 5/ Rev and 6 /Rev forcing frequencies.

Using the modes from the utility models for mode type identification and forcing frequency calculation allows for the determination of which mode types are excited by which forcing frequencies. This is an integral step in the fanplot generation process. The only difference between the utility models and the baseline models is the gimbal flexible joint springrates, meaning the utility model component stiffness distribution, mass property distribution, and rotor configuration are identical to those of the baseline models. Therefore, the forcing frequencies determined to excite certain mode types for the utility models will excite the same mode types for the baseline models.

4.3 Results of Mode Type Identification and Forcing Frequency Determination

The process for mode type identification and forcing frequency determination discussed above was run on the 6BES and PBR Dymore rotor models.

4.3.1. 6BES Mode Type Identification and Forcing Frequency Determination

The forcing frequencies for various mode types of evenly spaced rotors are well known and discussed in section 1.2.2. The process described in this chapter confirmed the familiar result that for a 6 bladed evenly spaced rotor, 6 and 12 /Rev are collective mode forcing frequencies, 1, 5, 7, and 11 /Rev are cyclic mode forcing frequencies, and that 2, 3, 4, 8, 9, and 10 /Rev are scissors mode forcing frequencies.

4.3.2. PBR Mode Type Identification and Forcing Frequency Determination

The PBR baseline model with 20° separation between blades in a pair was determined to have collective modes excited by 3, 6, 9, and 12 /Rev forcing frequencies, to have cyclic modes excited by 1, 2, 4, 5, 7, 8, 10, and 11 /Rev forcing frequencies, and to have no scissors modes.

The absence of scissors modes in the PBR model is counter-intuitive for a 6 bladed rotor of any blade spacing. Several models of side cases were run to determine whether the removal of any single design feature would result in a rotor model that had scissors modes. It was determined that the removal of the rigid body elements connecting the LE and TE yokes resulted in a model with scissors modes. The purpose of these links is to approximate the LE and TE yokes as a single yoke to a certain radial station as the design specifies. The rigid yoke links were left in the final PBR model configuration for this project.

CHAPTER 5

DYMORE MODEL RESULTS

The post-processed data of the Dymore model outputs is organized in this chapter. Section 5.1 is a brief discussion of the rotor frequency correlation of the 6BES Dymore model to a Bell Helicopter Textron (Bell) in-house rotating rotor frequency code. Sections 5.2 - 5.5 are comparisons of the Dymore results of the PBR model to those of the 6BES model. Section 5.6 presents the results of a series of Dymore models of the PBR with various spacing angles between blades in a pair.

5.1 Validation of Dymore Modeling Process With Bell In-House Rotor Freq Code For 6BES

Before the PBR Dymore model was built or the 6BES rotor model was tuned, a check of the Dymore modeling process used to model an early version of the 6BES rotor was conducted by comparing the Dymore generated frequencies to those generated by a Bell in-house code for the same input parameters.

The average of the absolute values of the differences in frequencies of corresponding modes between the two codes was 0.815%. The maximum absolute value of difference in frequency of corresponding modes was 3.90% for a high collective, airplane mode RPM scissors mode at around 8 /Rev. This correlation was determined to be sufficiently close to validate the Dymore modeling process.

5.2 Comparison of 6BES and PBR Rotor Modes

A plot of rotor natural frequencies (in units of cycles per minute) versus rotor speed (in units of revolutions per minute) with forcing frequency lines overlaid is referred to as a fanplot. The frequencies of the 6BES and PBR Dymore rotor models are presented in fanplots in this section.

5.2.1. 6BES Rotor Dymore Fanplots

Fanplots of the 6BES rotor model output data are shown below. The 6BES rotor collective mode fanplot is shown in Figure 5.1.

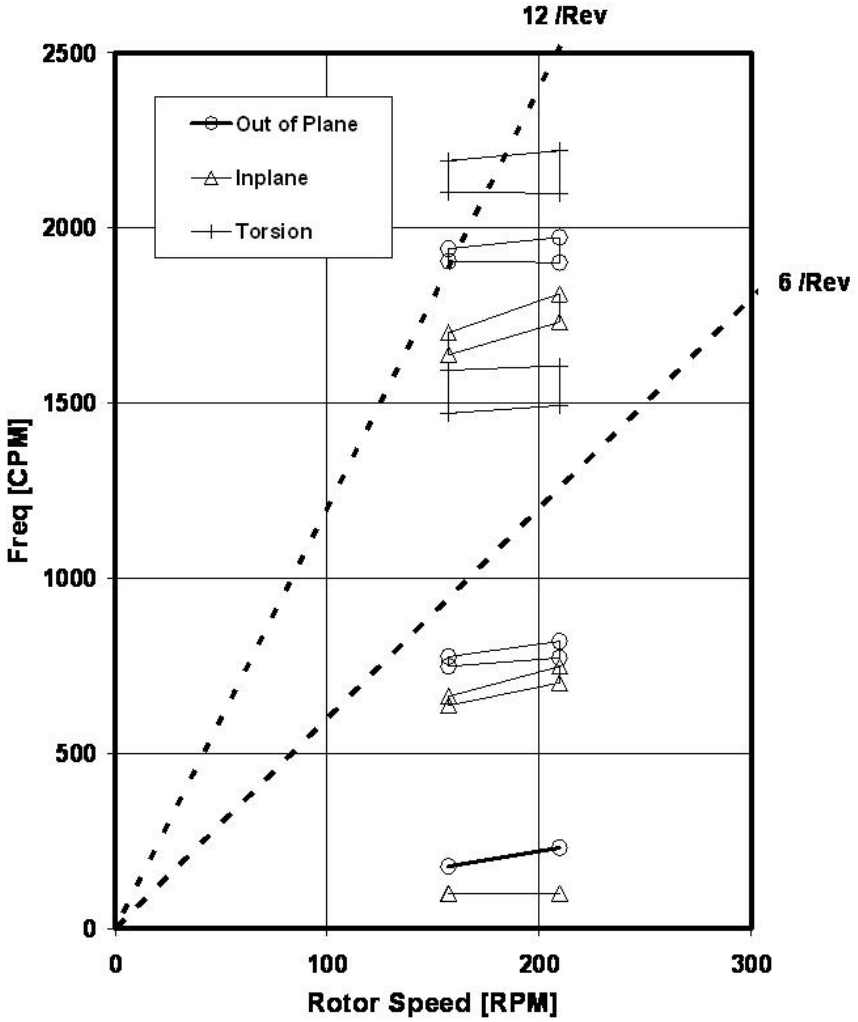

Figure 5.1 6BES Collective mode fanplot.

The 6BES rotor collective modes are well tuned. The proximity of the third collective out of plane mode to 12 /Rev is of little concern since frequencies that high generate negligible loads.

The 6BES rotor cyclic mode fanplot is shown in Figure 5.2.

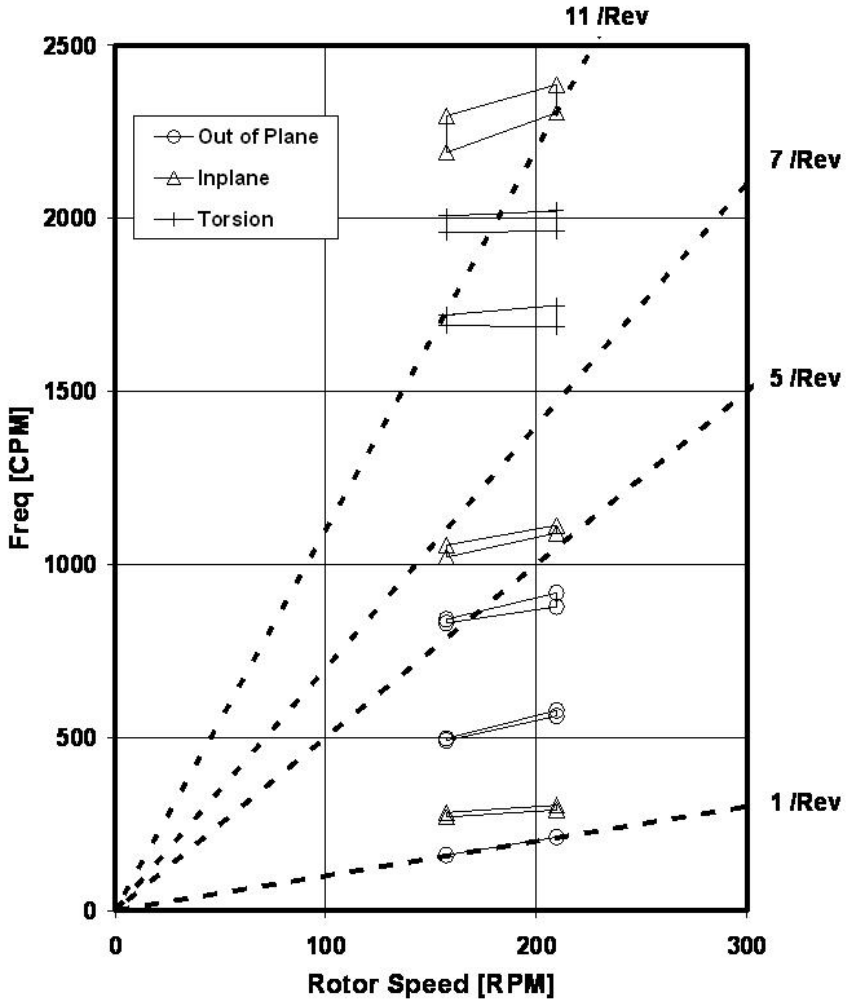

Figure 5.2 6BES Cyclic mode fanplot.

The 6BES rotor cyclic modes are reasonably well tuned. The flapping mode is very close to 1/Rev, as is expected for a gimbaled rotor with modest δ_3 magnitude. The third cyclic out of plane mode straddles 5 /Rev. That is, the airplane mode (low) RPM frequencies are tuned above 5 /Rev and the helicopter mode (high) RPM frequencies are tuned below 5 /Rev. Provided a rapid transition from helicopter mode RPM to airplane mode RPM, and vice versa, the rotor will spend very little time at the resonant frequency of this mode, making the tuning acceptable. The tuning of the higher modes around 11 /Rev is of little significance.

The 6BES rotor scissors mode fanplot is shown in Figure 5.3.

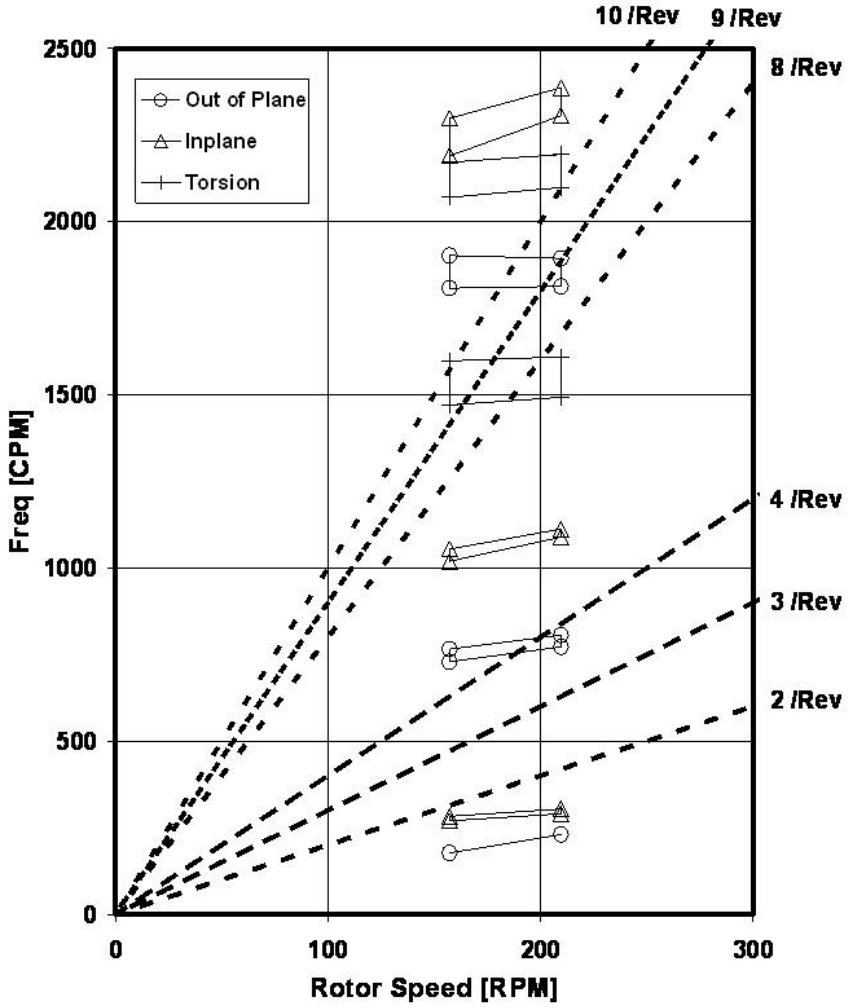

Figure 5.3 6BES Scissors mode fanplot.

The 6BES rotor scissors modes are reasonably well tuned. The first scissors inplane mode at low RPM and low blade collective pitch angle is separated from 2/Rev by 0.2 /Rev, an acceptable placement. The second scissors out of plane mode at high RPM and high blade collective is separated from 4 /Rev by 0.15 /Rev. The tuning of this mode is marginal.

5.2.2. PBR Rotor Dymore Fanplots

Fanplots of the PBR rotor model output data are shown below. PBR fanplots have several cases of separate modes being tuned closely together. Some modes in the fanplots

have been colored solely to aid in differentiating them from other closely tuned modes. The PBR rotor collective mode fanplot is shown in Figure 5.4.

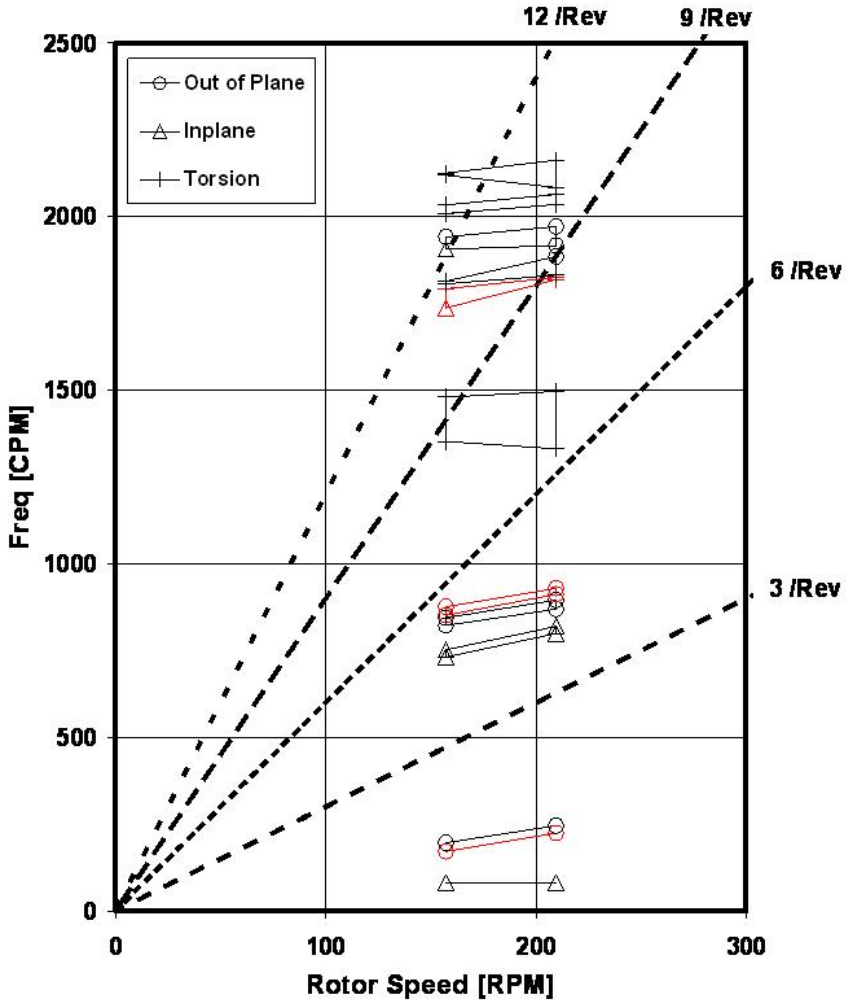

Figure 5.4 PBR Collective mode fanplot.

The PBR rotor collective modes are well tuned. The PBR cyclic mode fanplot is shown in Figure 5.5.

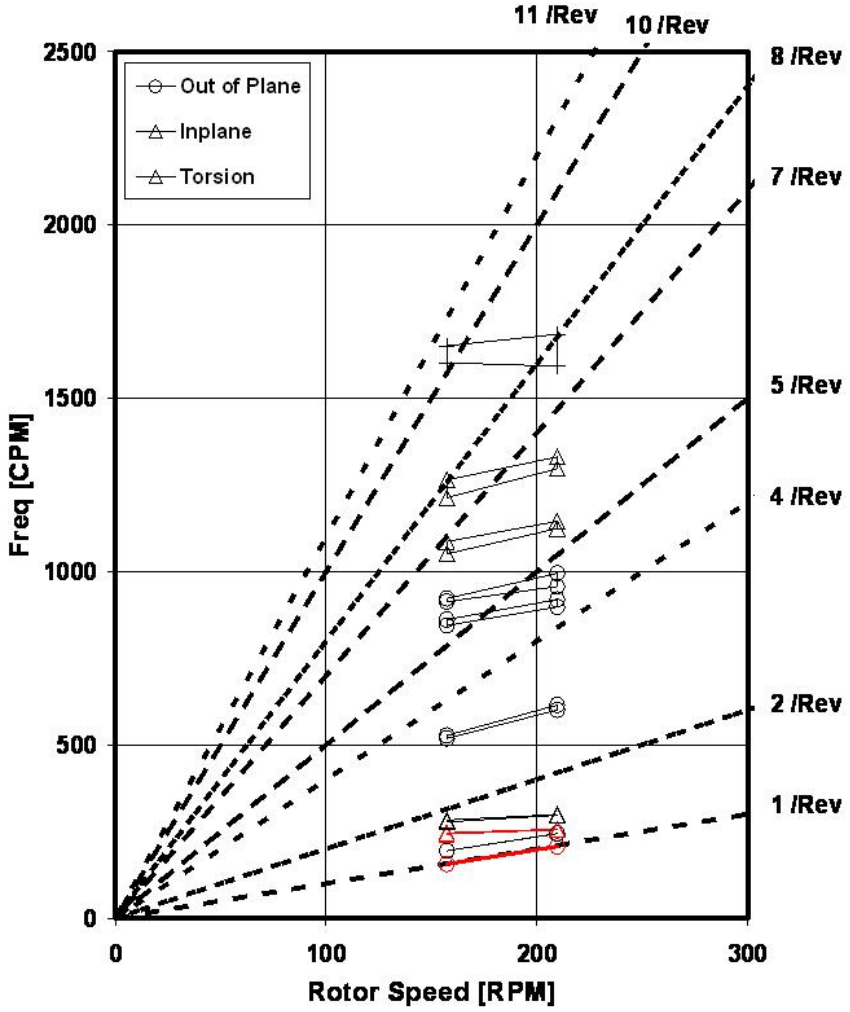

Figure 5.5 PBR Cyclic mode fanplot.

The PBR rotor cyclic modes are tuned reasonably well. The 6th and 7th cyclic modes straddle 5 /Rev, but are well separated from 5 /Rev at the operating RPM's. The 8th and 9th cyclic modes would need to be tuned away from 7 /Rev and 8 /Rev respectively for airplane mode RPM and low blade collective pitch in the event that loads analysis predicts high loads generated by these modes. In any event, the low blade collective angle in airplane mode is associated with forward flight near the stall speed, and time spent at this condition would be limited.

5.2.3. 6BES and PBR Fanplot Comparison

Fundamental differences in the 6BES and PBR fanplots are the forcing frequencies, the presence of distinct but very similarly shaped modes tuned closely to one another for the PBR and not for the 6BES rotor, and the absence of scissors modes for the PBR. Tables of rotor frequencies for both rotor models are provided in Appendix A.

The collective modes of each rotor model generally follow a familiar pattern with a first mode (inplane rigid body) below 1 /Rev and a second mode (out of plane cantilevered bending) at around 1.1 /Rev, however, the PBR has a third mode very similar to the second but tuned at 1.25 /Rev where the 6BES does not. The PBR also has a 6^{th} mode tuned very close to the 5^{th}, with a separation of the two of around 0.2 /Rev, and the 6BES does not.

The cyclic modes of the two rotor models also generally follow an expected pattern, each with flapping modes at 1 /Rev, 1^{st} inplane modes between 1 /Rev and 2 /Rev, and secondary out of plane bending modes at around 3 /Rev. Similarly to the collective mode fanplots, the cyclic mode fanplot of the PBR shows similarly shaped modes tuned closely together and the 6BES rotor model does not. Further discussion of this result is undertaken in the modeshapes section of this chapter.

5.3 Tuning Issues of the 6BES and PBR Rotor Models

The measures taken to achieve the rotor tuning of each of the subject rotors, and the realism of the rotor component properties selected are discussed in this section.

5.3.1. 6BES Rotor Model Tuning Issues

For the 6BES rotor, the 1^{st} cyclic inplane mode, 3^{rd} cyclic out of plane mode, 2^{nd} cyclic inplane mode, 1^{st} scissors inplane mode, and 2^{nd} scissors out of plane mode drove the rotor component property selection for tuning purposes.

The 6BES blade ratio of beamwise bending stiffness to chordwise bending stiffness was set to 0.75 from 36% rotor radius to the tip to reduce the variation of the frequency of modes with blade collective pitch angle. This ratio of beam to chord stiffness is not out of the question, but it would require a specially designed, unconventional blade structural member.

The 1st cyclic inplane mode and 1st scissors inplane mode are virtually the same mode, which should be tuned above about 1.2 /Rev on the cyclic mode fanplot to avoid coupling with the flapping mode and below about 1.8 /Rev on the scissors mode fanplot to avoid driving high loads at 2 /Rev. The 17 lb tip weight in the 6BES rotor blade contributes to tuning the scissors inplane mode at 1.8 /Rev, as opposed to a higher frequency for a blade with less tip weight. The inplane mode is well separated from 1 /Rev on the cyclic mode fanplot.

The 3rd cyclic out of plane mode tuned to straddle 5 /Rev is an example of the benefit to tuning provided by the relatively high beam to chord stiffness ratio of the blade. If the blade beamwise stiffness was much lower than the chordwise stiffness, the lower blade collective pitch angles in the flight envelope would cause this mode to drop into 5 /Rev.

The 2nd cyclic inplane mode tuning is also improved by the blade stiffness similarity. The tip weight also provides better separation of this mode from 7 /Rev at the airplane mode RPM.

The 2nd scissors out of plane mode is better separated from 4 /Rev with the tip weight. The 2nd scissors out of plane mode was fine tuned, simultaneously with the cyclic 3rd out of plane and 2nd inplane modes, with reasonable changes to the inboard blade stiffness.

5.3.2. PBR Rotor Model Tuning Issues

For the PBR rotor, the 1st and 2nd cyclic inplane modes, 4th and 5th cyclic out of plane modes, and 4th collective out of plane mode were critical modes for rotor tuning.

The PBR blade ratio of beamwise bending stiffness to chordwise bending stiffness was set to 1.0 from the blade root to 50% rotor radius and to 0.75 from 50% rotor radius to the tip. The ratio of beam to chord stiffness in the inboard blade can be raised compared to the outboard blade with reasonable confidence since the thickness to chord ratio is higher inboard. The blade beam to chord stiffness ratios for the PBR blade are by no means conventional, but neither are they inconceivable. A total of 170 lb / blade of tuning weight was added to the PBR blade. The 40 lb tip weight, 70 lb midspan weight, and 60 lb tuning weight at around 80% rotor radius account for the tuning weight total.

The 1st cyclic inplane mode should be tuned above 1.2 /Rev and 2nd cyclic inplane mode should be tuned at or below 1.8 /Rev. These two modes are similarly sensitive to changes in rotor component properties. The tuning of the PBR rotor has the 1st cyclic inplane mode at 1.22 /Rev and the second cyclic inplane mode at 1.8 /Rev. A scaling factor of 0.33 applied uniformly to the PBR yoke chordwise bending stiffness, as compared to the 6BES yoke chordwise stiffness, was a property modification that contributed significantly to the acceptable tuning of the 1st and 2nd cyclic inplane modes. For a common yoke rectangular cross section, chordwise bending stiffness is a cubic function of the chordwise linear dimension of the yoke. The 67% yoke chordwise stiffness reduction of the PBR yoke would require a 31% reduction in yoke chordwise dimension. Any weight in the rotating rotor components contributes to lowering the frequencies of the 1st and 2nd cyclic inplane modes, but the 40 lb tip weight is in the most effective spanwise location for this purpose. The tuning of the 1st and 2nd cyclic inplane modes was also aided by the similarity in blade beamwise and chordwise stiffness, which reduces the distance on the fanplot spanned by these modes along the vertical axis of the fanplot.

The cyclic 4th and 5th out of plane modes and the collective 4th out of plane mode were tuned simultaneously by the 70 lb midspan weight and the 60 lb tuning weight at around 80% rotor radius. These modes alone could have been tuned with less weight, but the accompanying yoke chordwise bending stiffness reduction to tune the cyclic 1st and 2nd inplane modes would have been unreasonable.

The highest concentration of tuning weight in the PBR blade (79 lb evenly distributed from rotor radial station 317.74 in. to station 348.96 in.) was 2.53 lb/in. For tungsten tuning weight, ρ = 0.7 lb/in^3, a blade cross section in this radial range would have 3.6 in^2 of tuning weight, which does not seem unreasonable for a blade of this size.

5.3.3. Tuning Issue Comparison of PBR to 6BES Rotor

As is the case for any rotor with a large blade collective pitch angle range, both subject rotor models had better rotor frequency placement relative to forcing frequencies when blade

beamwise bending stiffnesses were increased to values closer to the blade chordwise bending stiffnesses.

The paired blade rotor required close to an order of magnitude more tuning weight than the 6BES rotor required. The presence of a second, slightly higher frequency, primary inplane bending (or lead-lag) mode drove most of this weight into the PBR blade.

Some of the rotor component properties used to tune the subject rotors would require unconventional manufacturing methods, but none of the rotor component properties can be dismissed as impossible to achieve.

5.4 Comparison of 6BES and PBR Rotor Modeshapes

The modeshapes of the first four 6BES collective and cyclic modes are compared to the modeshapes of appropriate PBR rotor modes for helicopter mode RPM and 75° blade root collective pitch angle in this section. The plots of modeshapes in this chapter are of modal displacements of the yoke and blade plotted as a contiguous curve.

5.4.1. Collective Mode Modeshape Comparison

The 6BES 1st collective modeshape is shown in Figure 5.6, and the PBR 1st collective modeshapes for LE and TE blades are shown in Figures 5.7 and 5.8, respectively. The rigid body inplane modeshapes shown in Figures 5.6 – 5.8 are virtually identical between the two rotors.

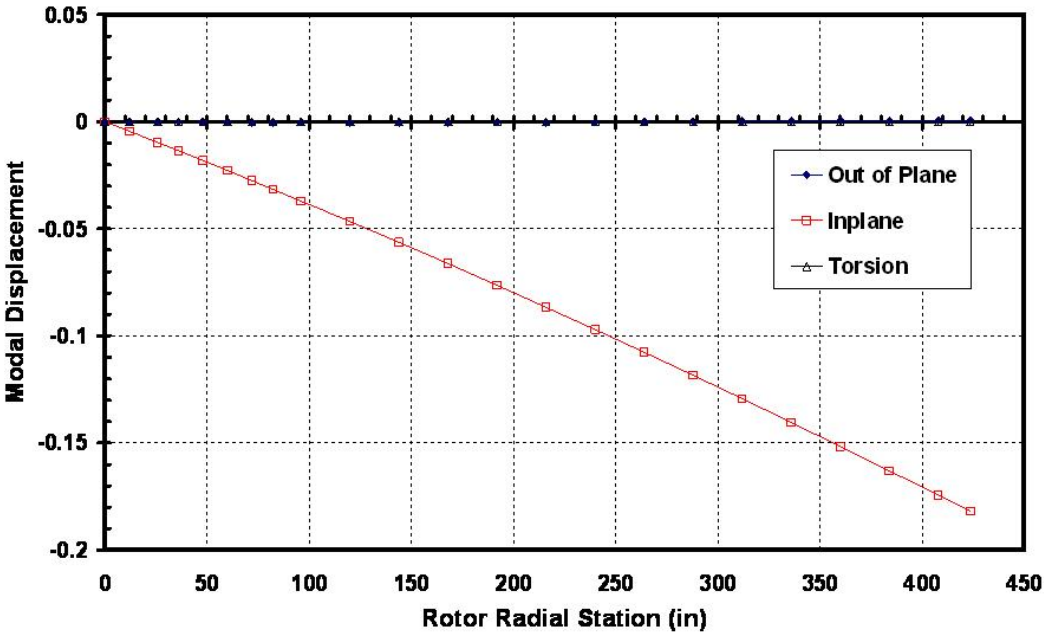

Figure 5.6 6BES 1st Collective mode modal displacement plot.

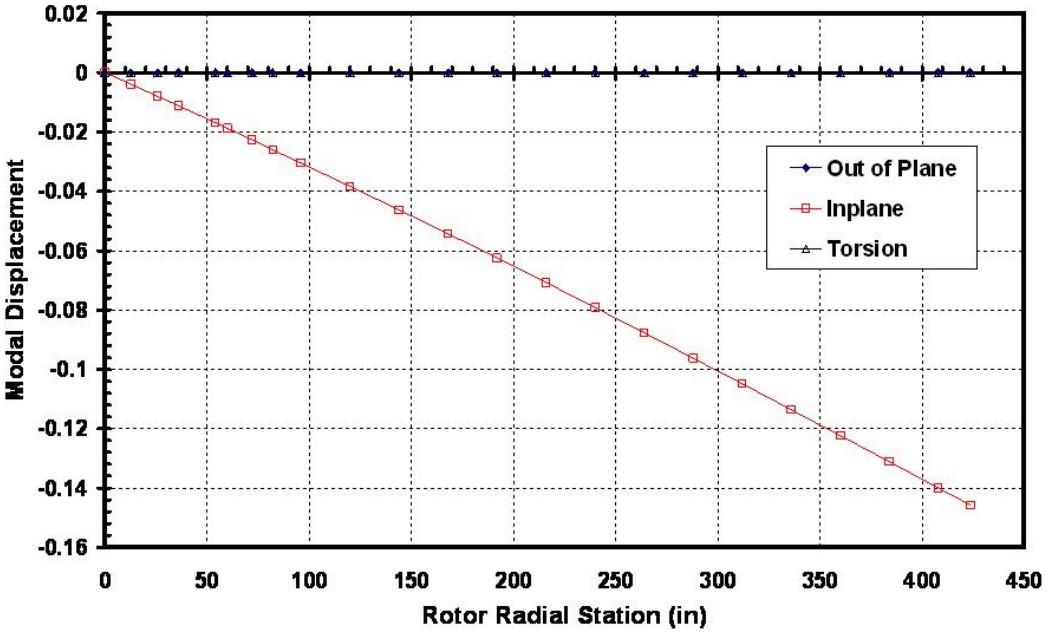

Figure 5.7 PBR LE Blade 1st Collective mode modal displacement plot.

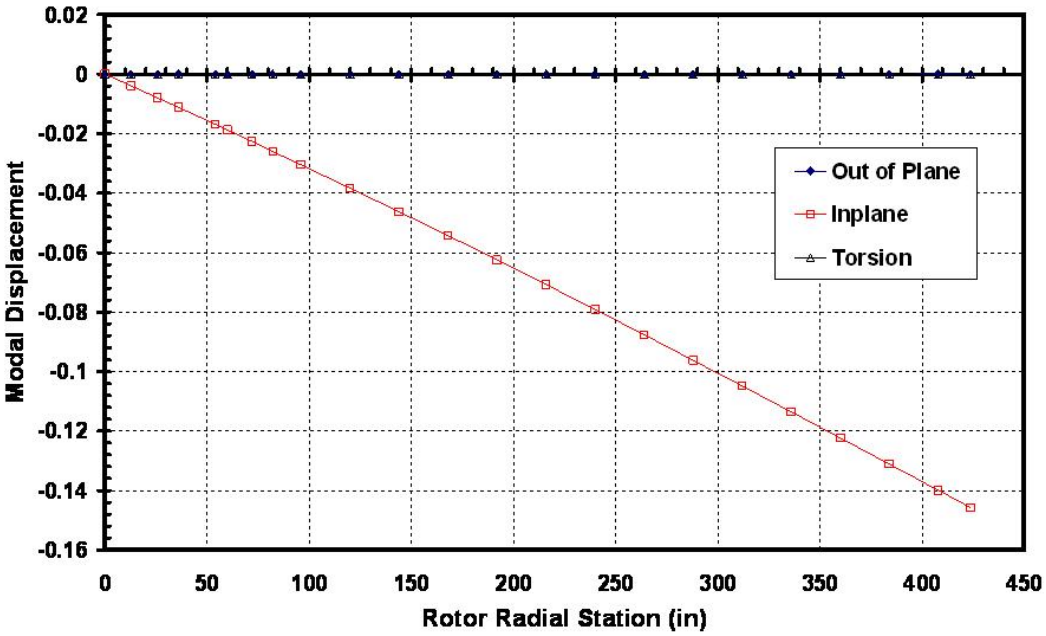

Figure 5.8 PBR TE Blade 1st Collective mode modal displacement plot.

The 6BES 2nd collective (coning) modeshape is shown in Figure 5.9, and the PBR 2nd collective modeshapes for LE and TE blades are shown in Figures 5.10 and 5.11, respectively. The coning modeshapes are very similar between the two rotors. The PBR has a mode tuned just above the coning mode with a modeshape that is similar to the coning modeshape, with more out of plane curvature in the yoke. The PBR modeshapes of this "second coning" mode are shown for LE and TE blades in Figures 5.12 and 5.13, respectively.

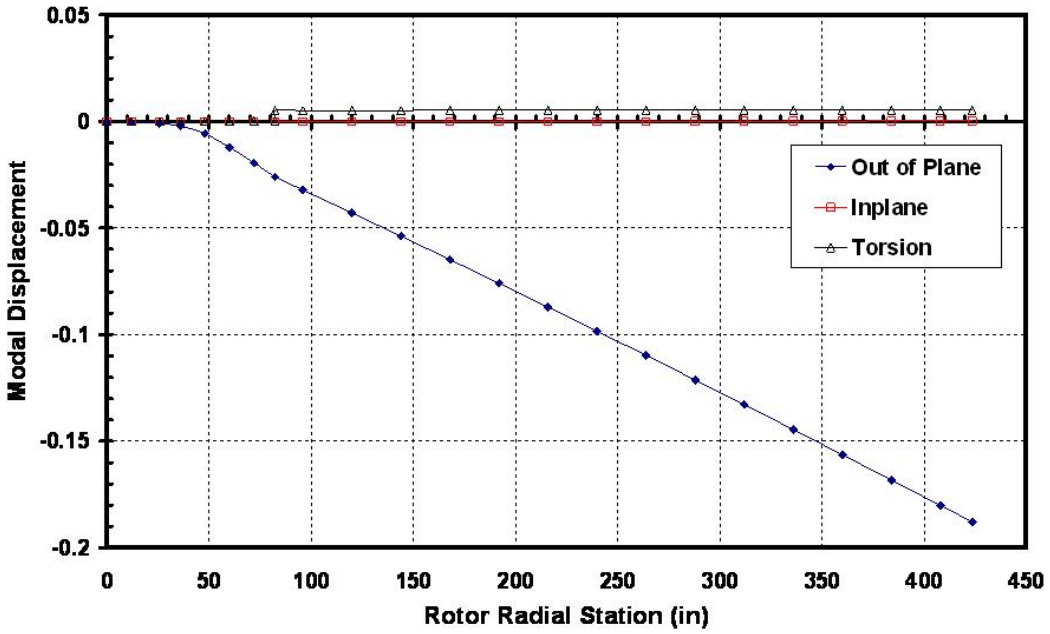

Figure 5.9 6BES Blade 2nd Collective mode modal displacement plot.

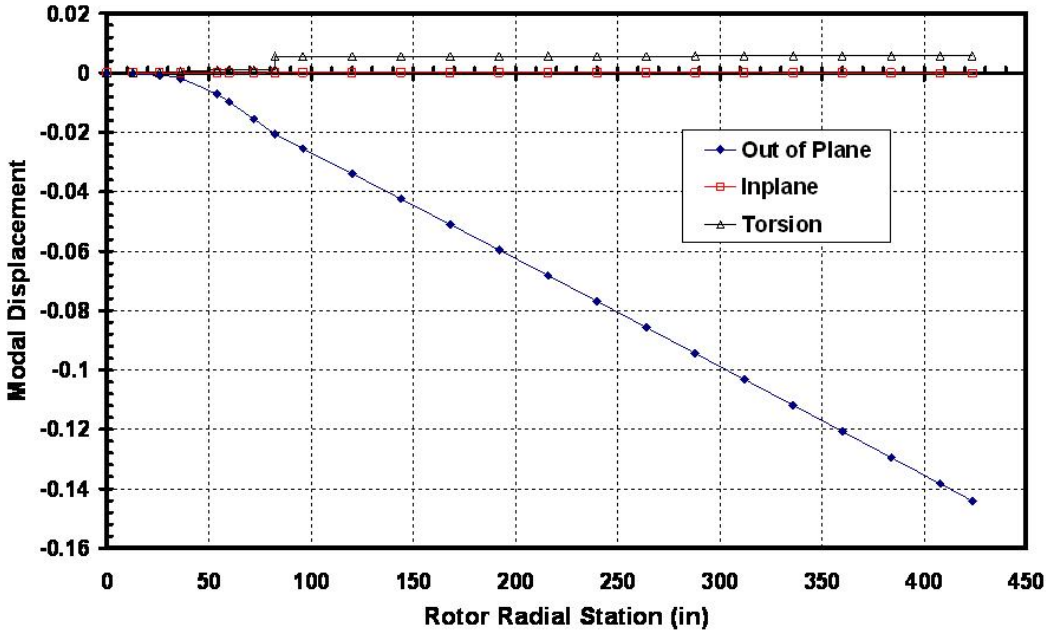

Figure 5.10 PBR LE Blade 2nd Collective mode modal displacement plot.

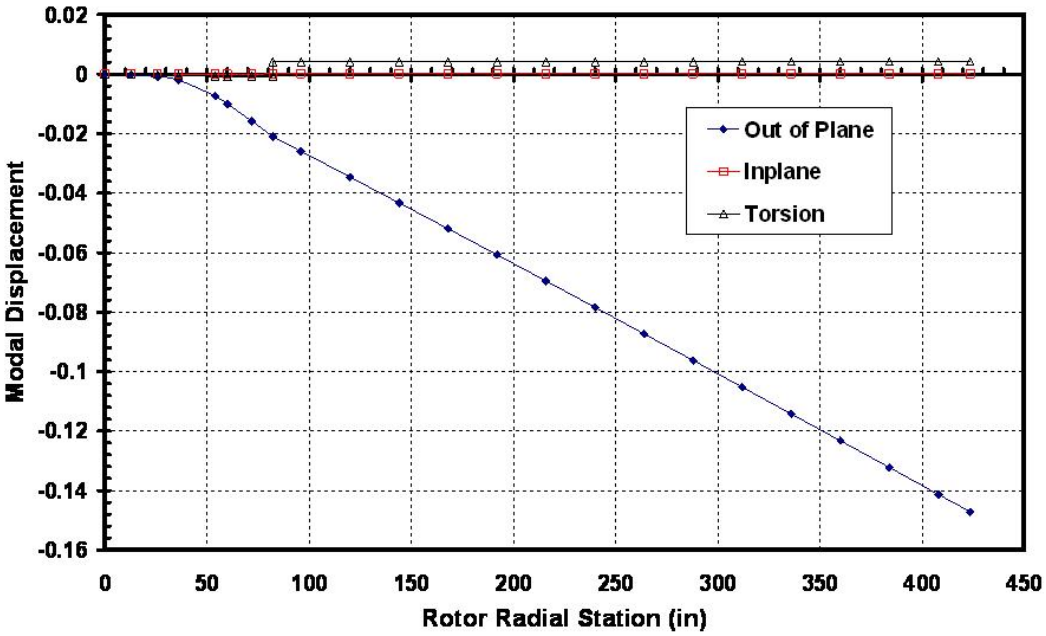

Figure 5.11 PBR TE Blade 2nd Collective mode modal displacement plot.

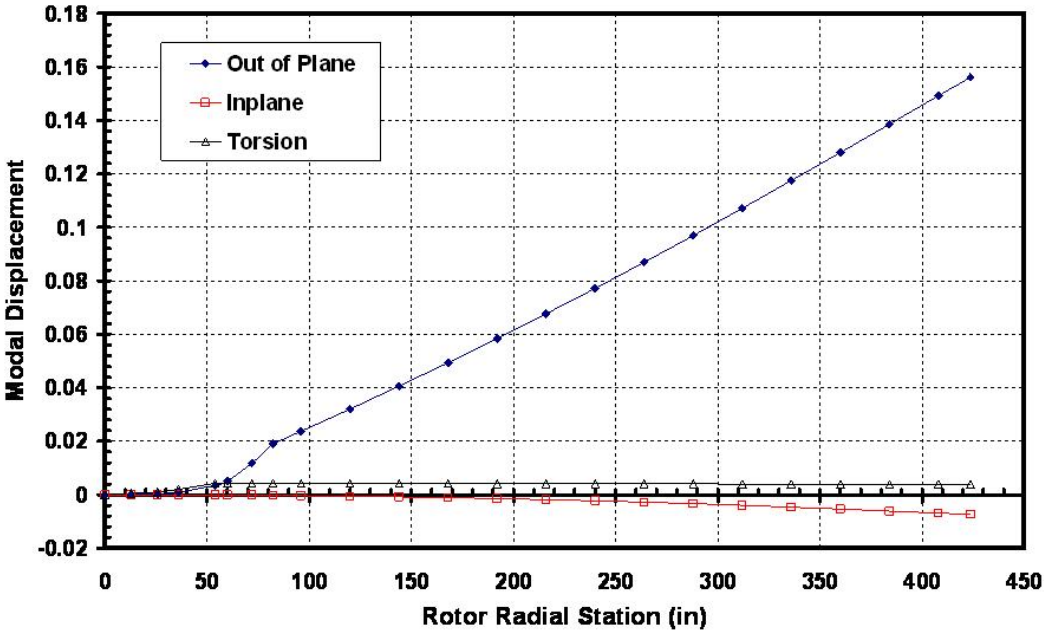

Figure 5.12 PBR LE Blade 3rd Collective mode modal displacement plot.

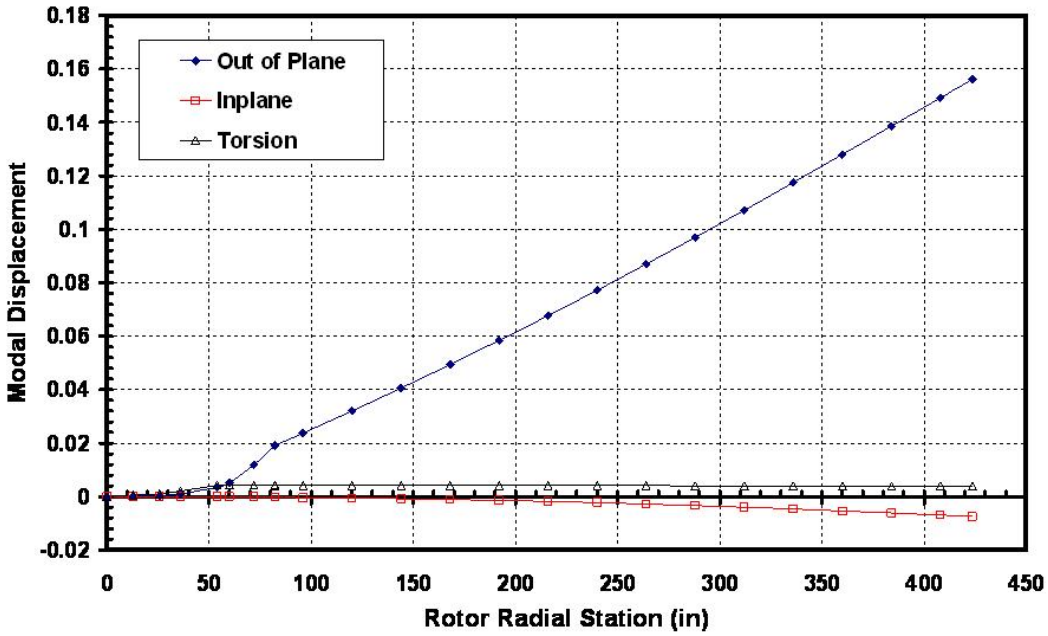

Figure 5.13 PBR TE Blade 3rd Collective mode modal displacement plot.

The 3rd 6BES collective modeshape is shown in Figure 5.14, and the comparable PBR 4th collective modeshapes for LE and TE blades are shown in Figures 5.15 and 5.16, respectively. These second collective inplane modes shown in Figures 5.14 – 5.16 are similar in shape between the two rotors.

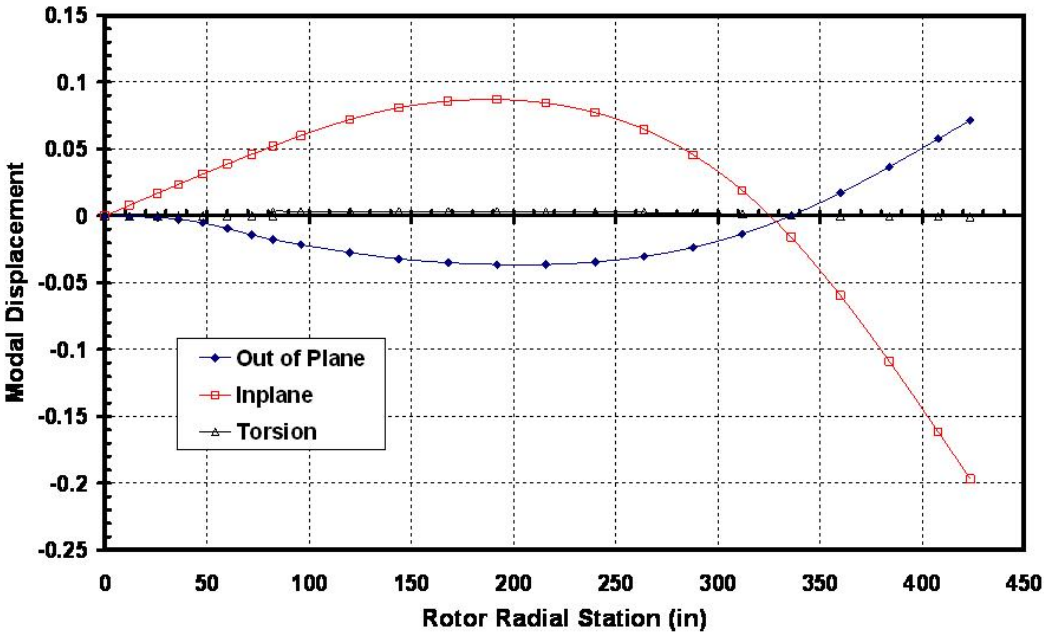

Figure 5.14 6BES Blade 3rd Collective mode modal displacement plot.

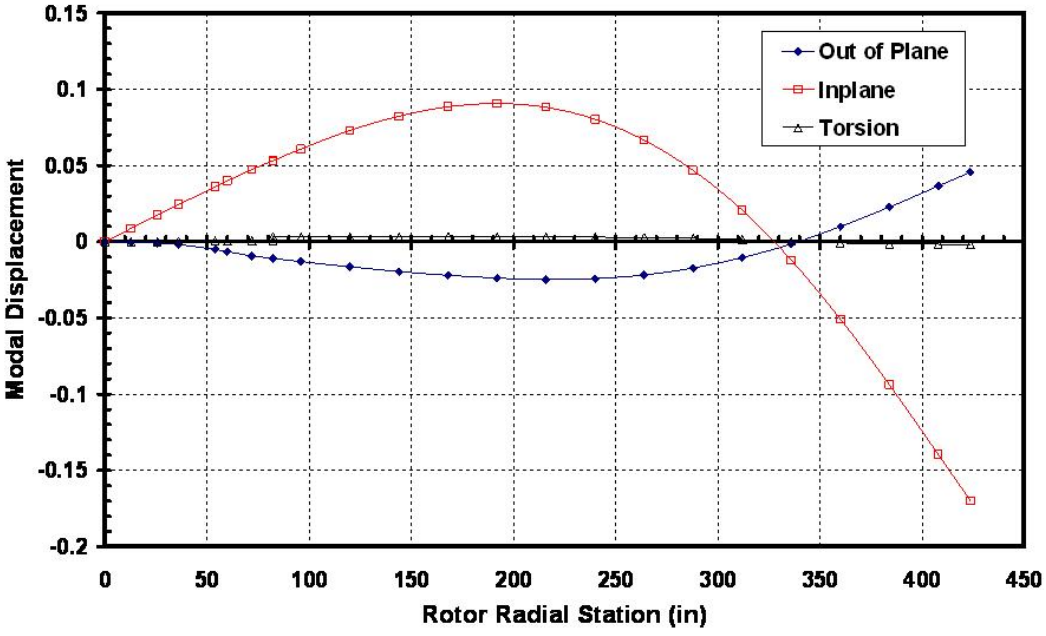

Figure 5.15 PBR LE Blade 4th Collective mode modal displacement plot.

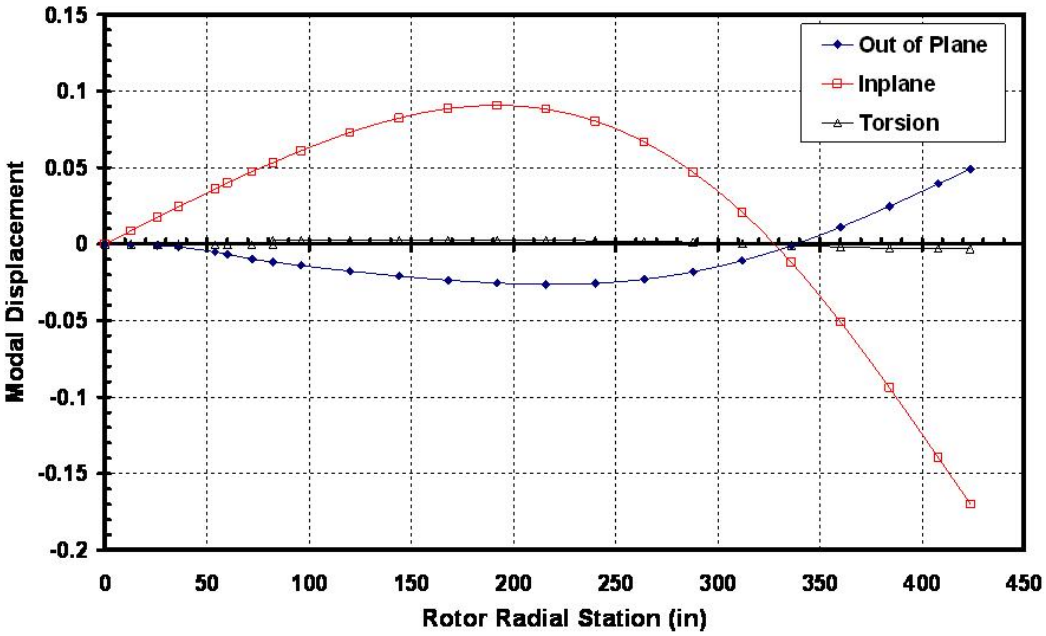

Figure 5.16 PBR TE Blade 4th Collective mode modal displacement plot.

The 4th 6BES collective modeshape is shown in Figure 5.17, and the comparable PBR 5th collective modeshapes for LE and TE blades are shown in Figures 5.18 and 5.19, respectively. The PBR rotor has a 6th collective mode that is tuned just above the 5th with a similar second out of plane bending modeshape except that the 6th PBR collective mode has more out of plane bending curvature in the yoke. The 5th PBR collective mode has the LE and trailing edge blades deflecting in-phase with one another, and the 6th collective PBR mode has the blades moving out-of-phase to one another. The 6th PBR collective modeshapes are shown in Figures 5.20 and 5.21 for LE and TE blades, respectively.

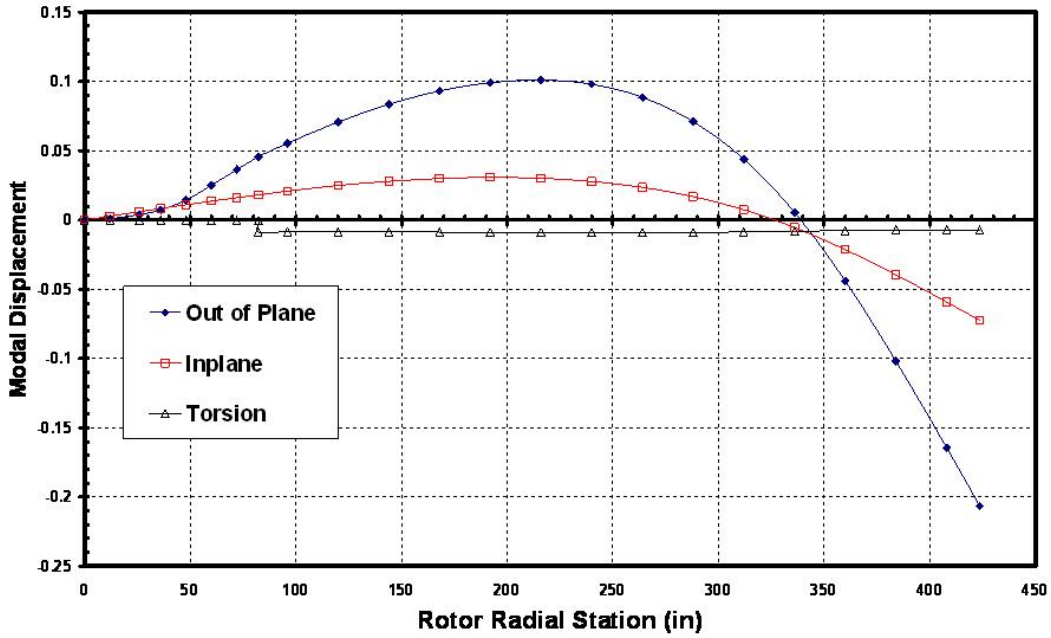

Figure 5.17 6BES Blade 4th Collective mode modal displacement plot.

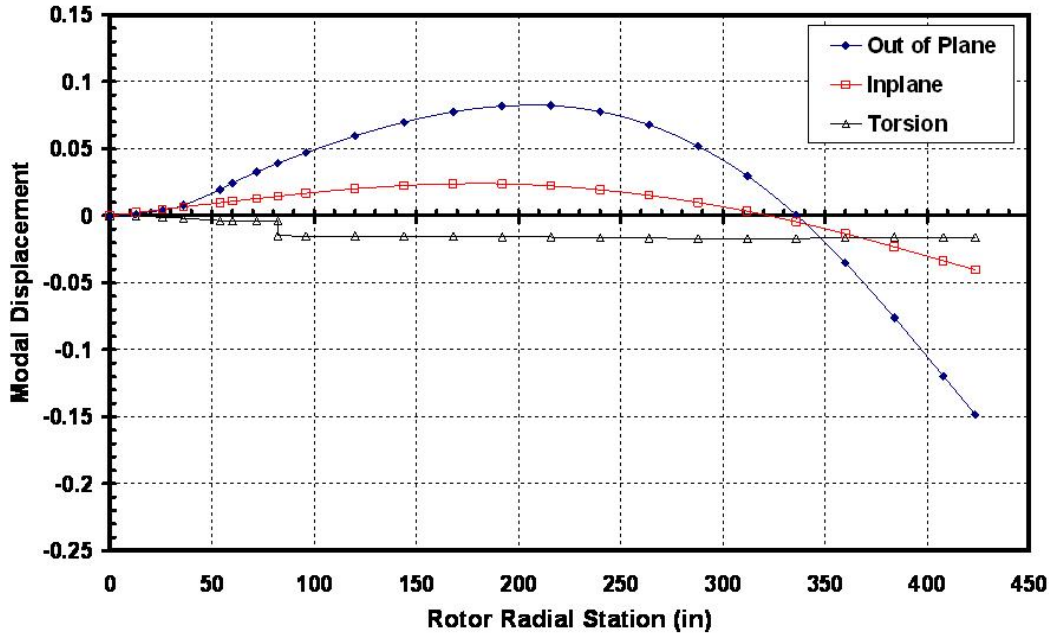

Figure 5.18 PBR LE Blade 5th Collective mode modal displacement plot.

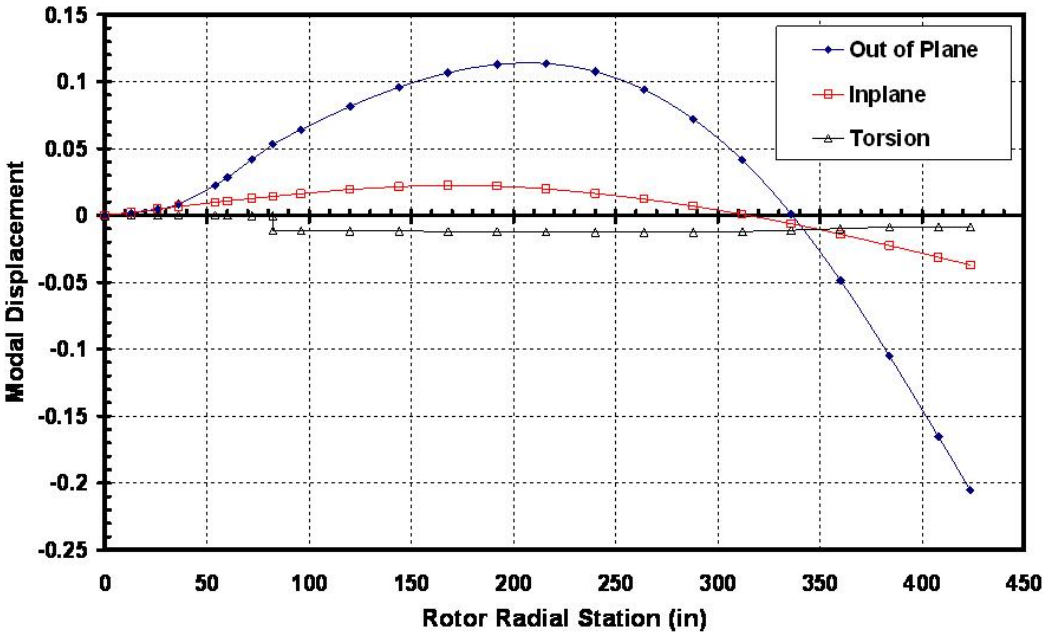

Figure 5.19 PBR TE Blade 5th Collective mode modal displacement plot.

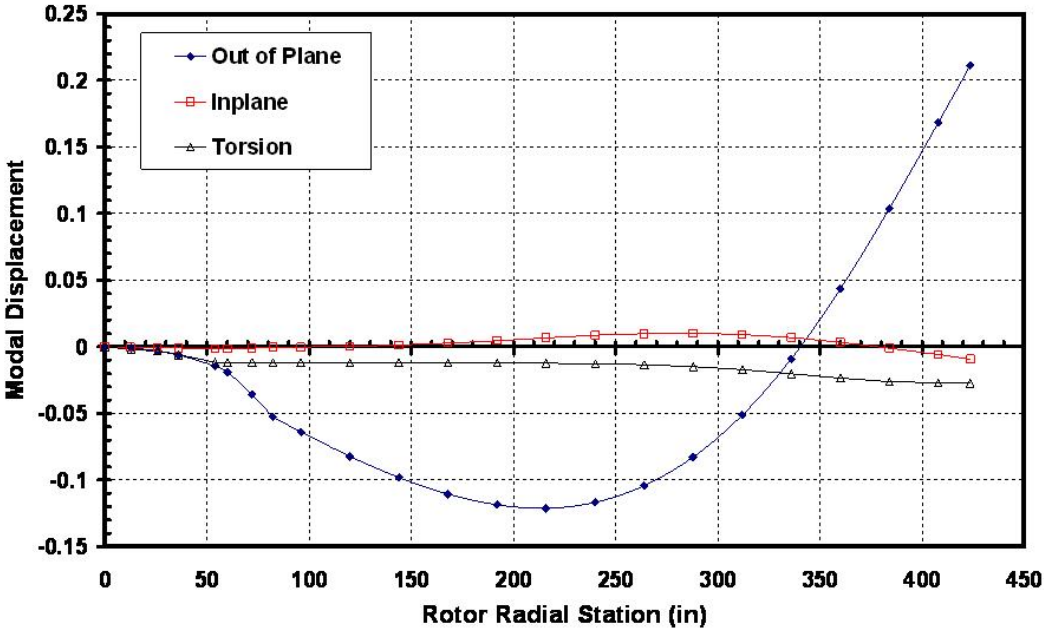

Figure 5.20 PBR LE Blade 6th Collective mode modal displacement plot.

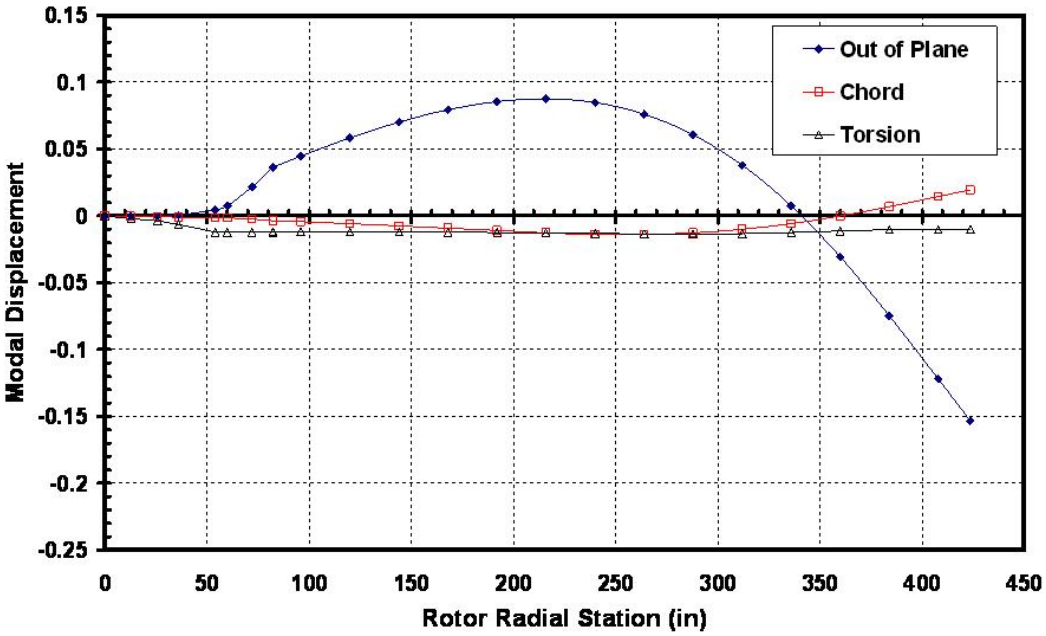

Figure 5.21 PBR TE Blade 6th Collective mode modal displacement plot.

5.4.2. Cyclic Mode Modeshape Comparison

The 6BES 1st cyclic modeshape is shown in Figure 5.22 and the PBR 1st cyclic modeshapes for LE and TE blades are shown in Figures 5.23 and 5.24 respectively. The rigid body out of plane (flapping) modeshapes are more or less identical between the two rotors. The PBR has a 2nd cyclic mode tuned 0.25 /Rev above the flapping mode that is generally similar in shape to the flapping mode except for the presence of significant out of plane bending in the yoke in the 2nd mode. In this PBR second cyclic mode, the gimbal flaps down and the blades flap up. The 2nd PBR cyclic modeshapes for LE and TE blades are shown in Figures 5.25 and 5.26, respectively.

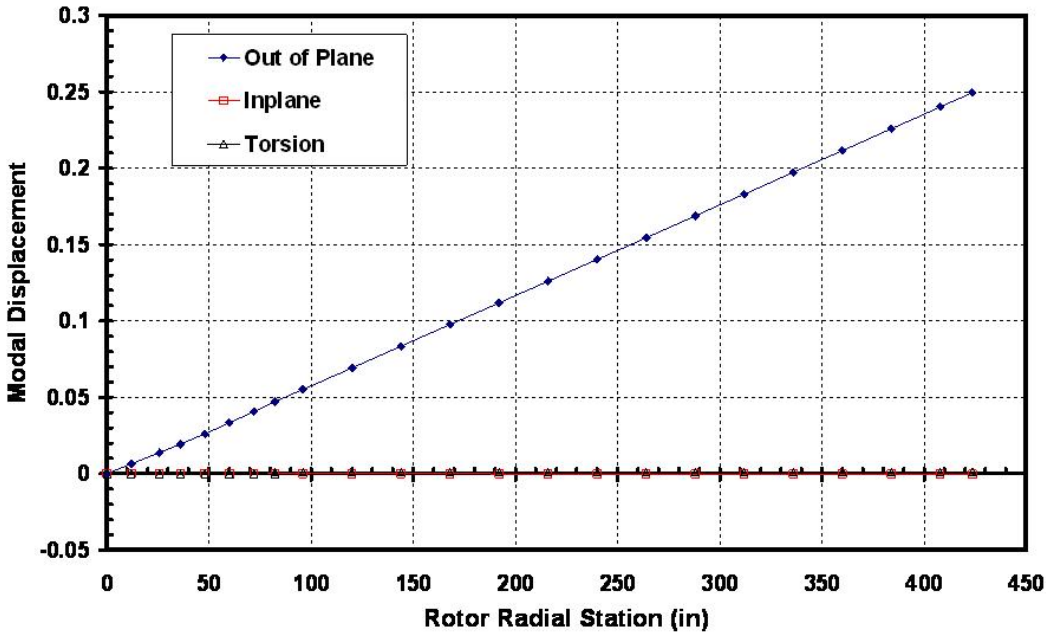

Figure 5.22 6BES 1st Cyclic mode modal displacement plot.

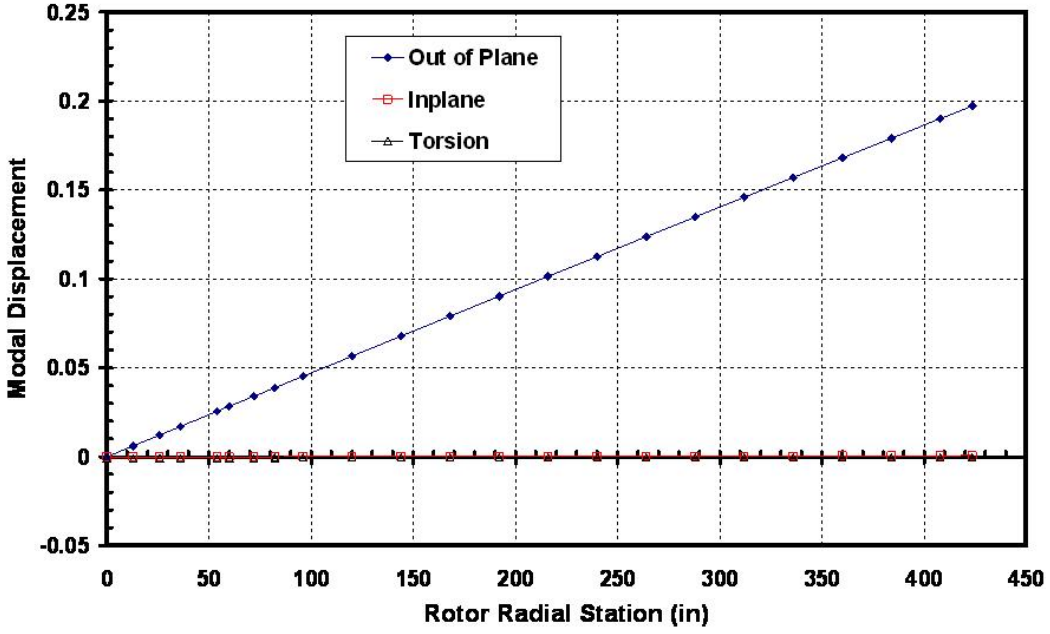

Figure 5.23 PBR LE Blade 1st Cyclic mode modal displacement plot.

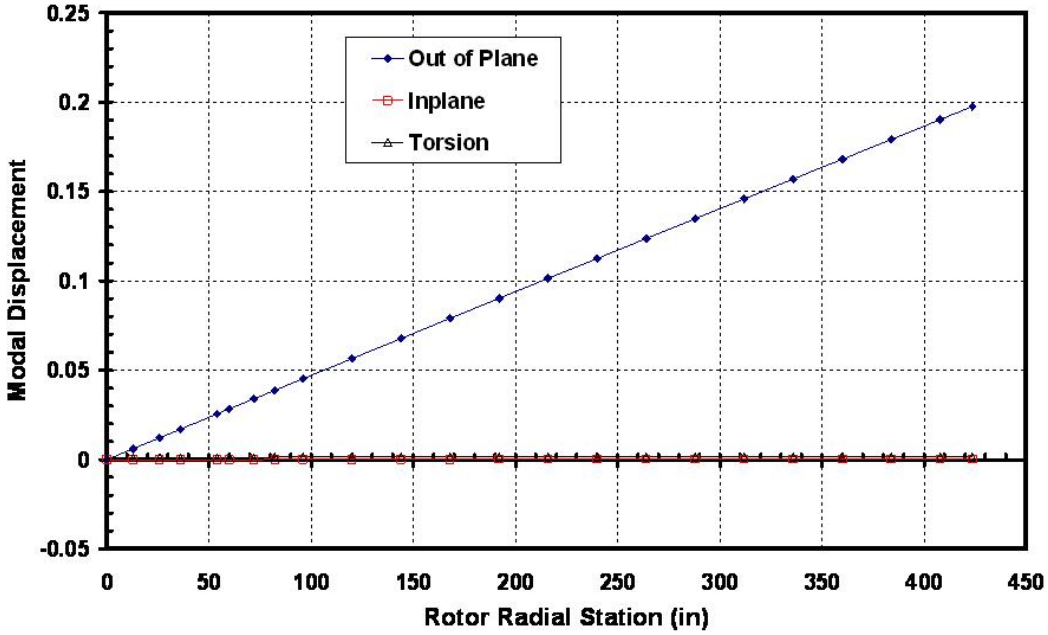

Figure 5.24 PBR TE Blade 1st Cyclic mode modal displacement plot.

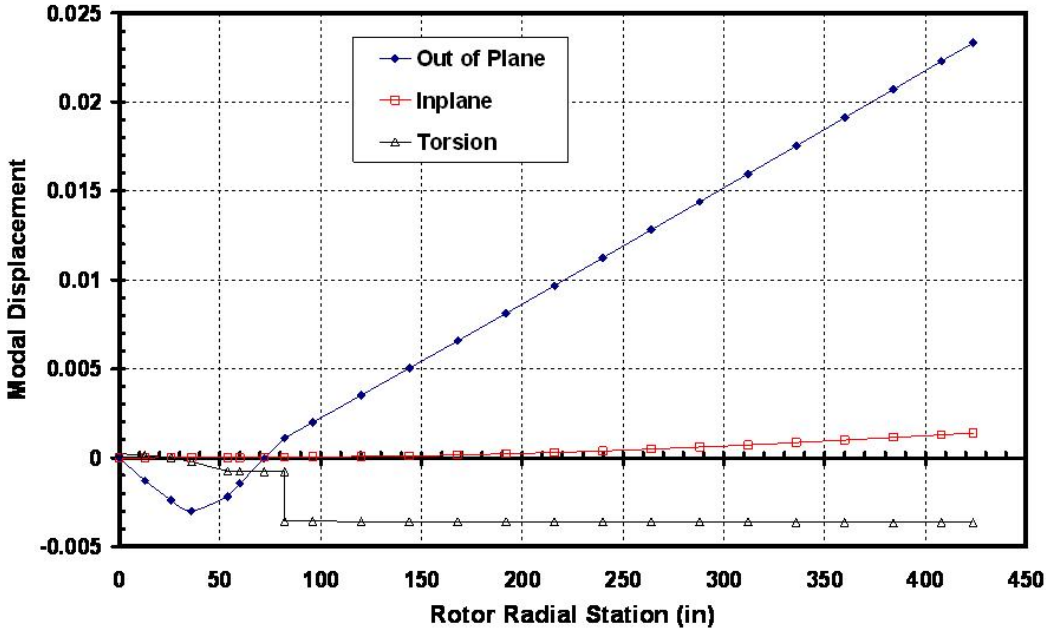

Figure 5.25 PBR LE Blade 2nd Cyclic mode modal displacement plot.

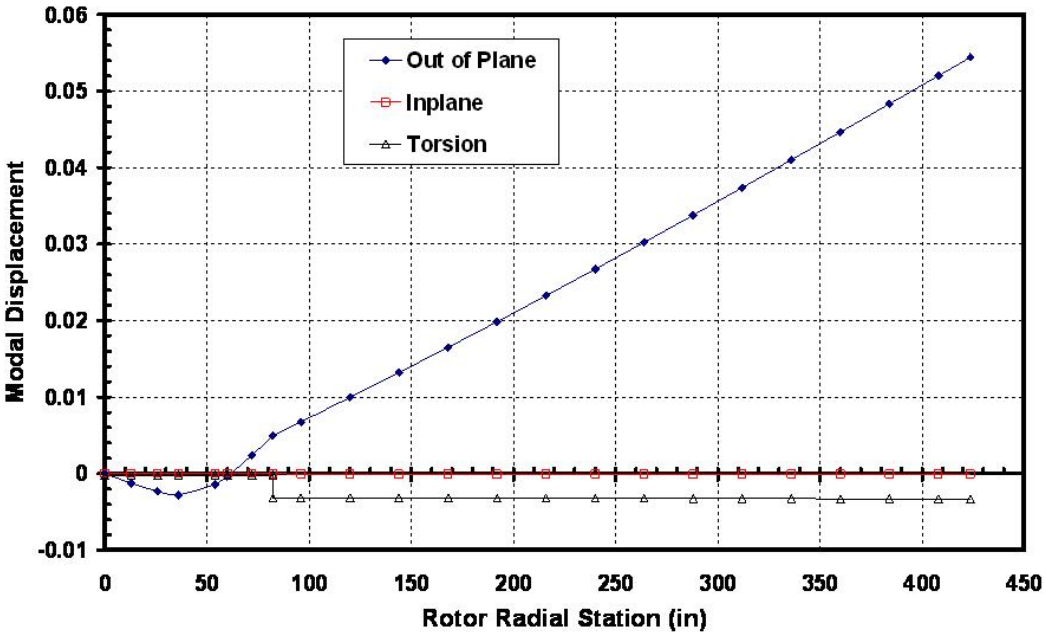

Figure 5.26 PBR TE Blade 2nd Cyclic mode modal displacement plot.

The 3rd PBR cyclic mode has a shape that is not comparable to any 6BES mode. This mode has inplane modal deflections consistent with a first cantilevered beam bending mode, and out-of-plane modal deflections of the same order of magnitude as the inplane deflections with a shape similar to the out of plane deflections in the 2nd PBR cyclic mode. Modeshapes of the PBR 3rd cyclic out of plane mode are shown in Figures 5.27 and 5.28 for LE and TE blades, respectively.

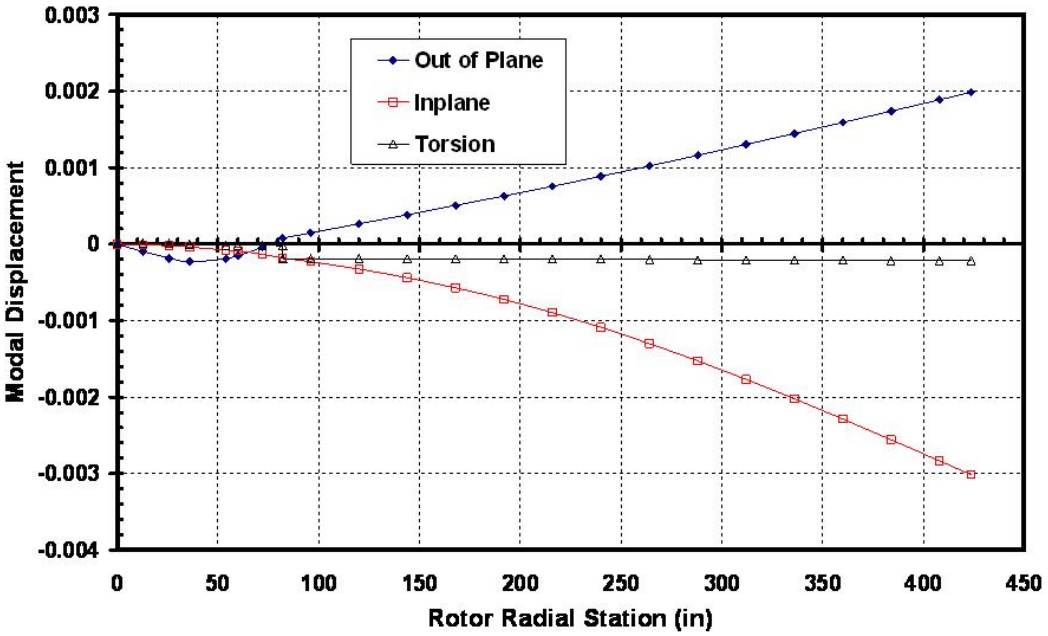

Figure 5.27 PBR LE Blade 3rd Cyclic mode modal displacement plot.

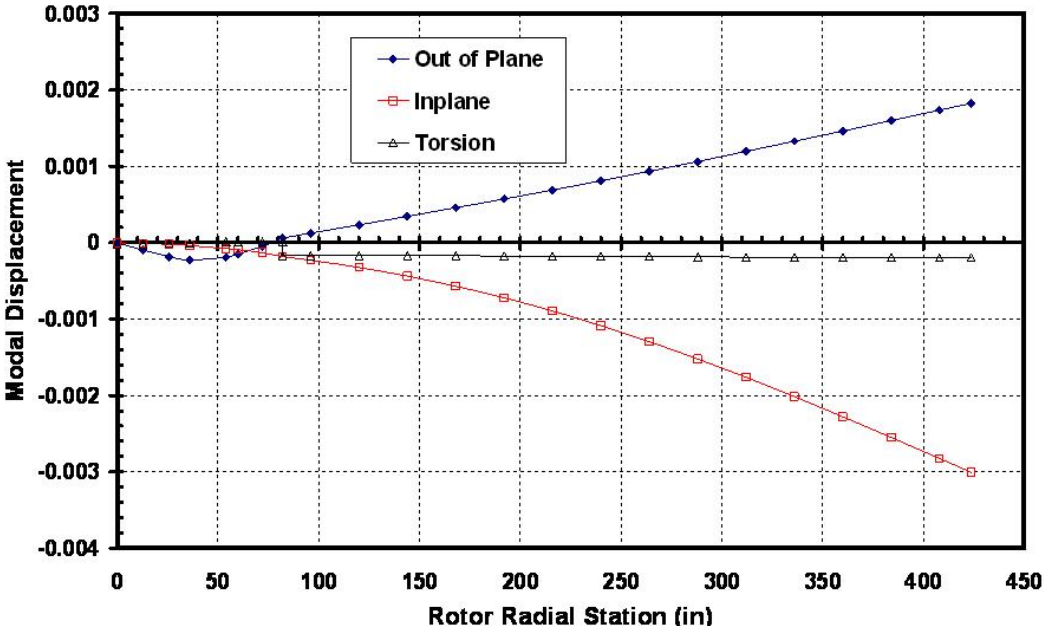

Figure 5.28 PBR TE Blade 3rd Cyclic mode modal displacement plot.

The 6BES 2nd cyclic modeshape is shown in Figure 5.29 and the comparable 4th PBR cyclic modeshapes for LE and TE blades are shown in Figures 5.30 and 5.31, respectively.

These modeshapes are similar between the two rotors, with the dominant feature being a 1st cantilevered inplane modal deflection curve. The PBR has slightly more deflection in the out of plane degree of freedom than the 6BES for this mode, and the LE and TE blades of the PBR move out-of-phase to one another.

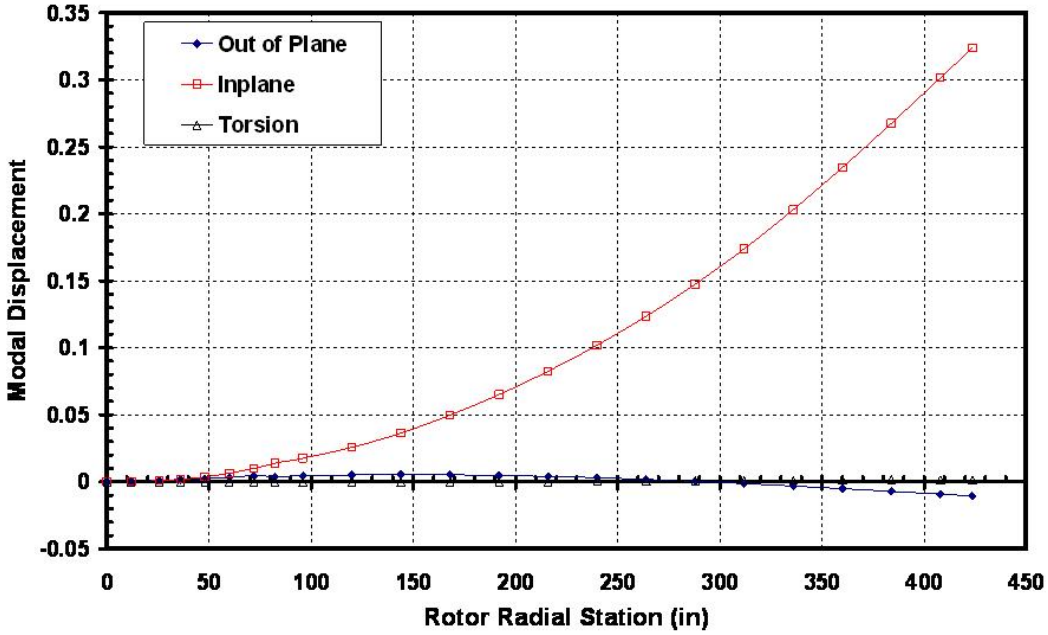

Figure 5.29 6BES 2nd Cyclic mode modal displacement plot.

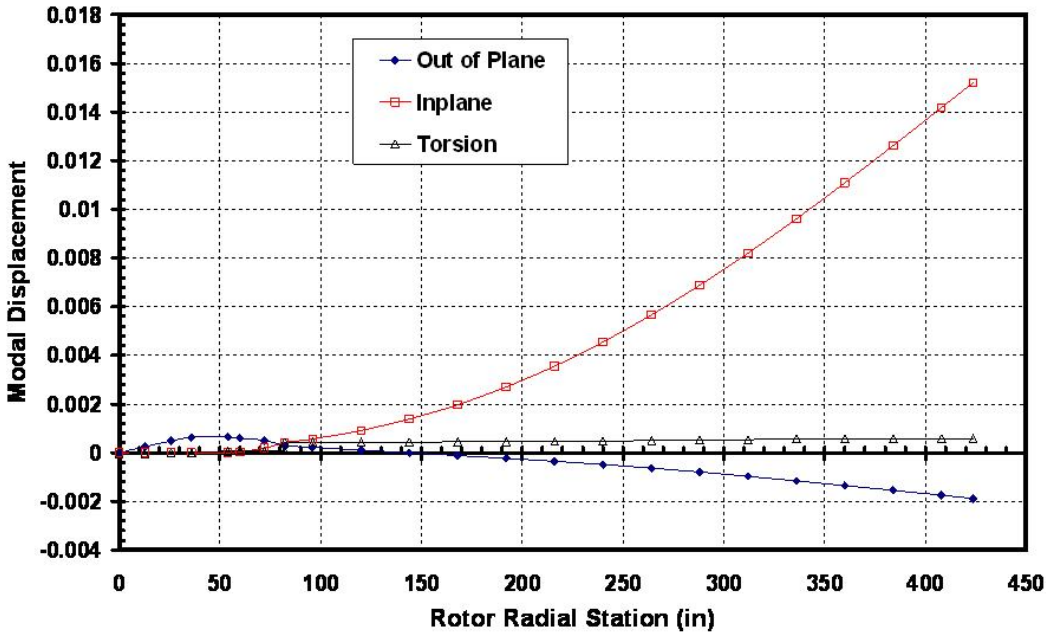

Figure 5.30 PBR LE Blade 4th Cyclic mode modal displacement plot.

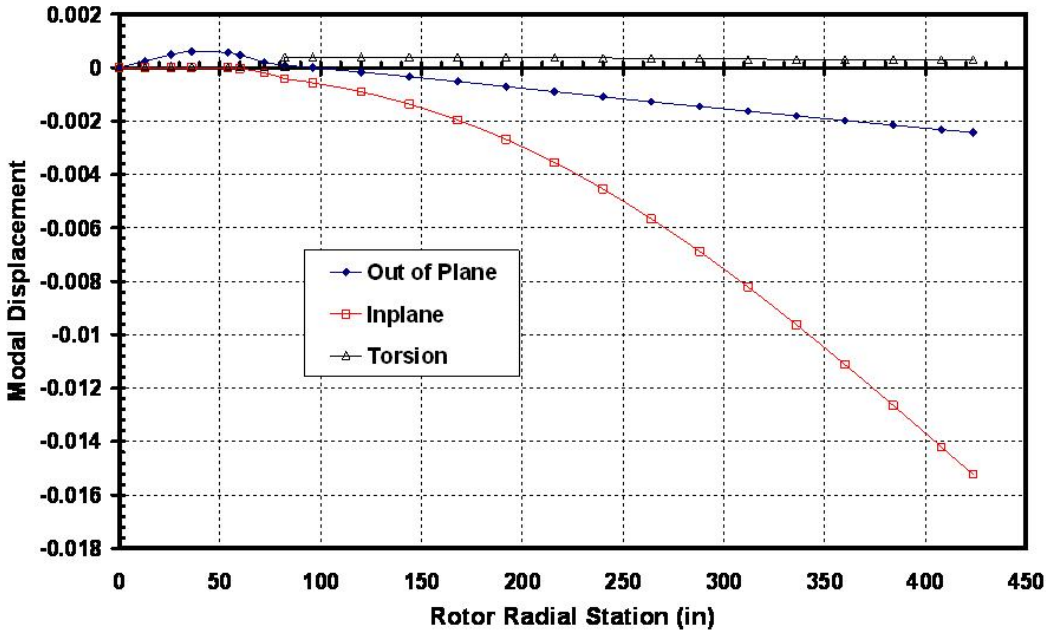

Figure 5.31 PBR TE Blade 4th Cyclic mode modal displacement plot.

The 6BES 3rd cyclic modeshape is shown in Figure 5.32 and the comparable 5th PBR cyclic modeshapes for LE and TE blades are shown in Figures 5.33 and 5.34, respectively. These modeshapes are similar between the two rotors, with out of plane gimbal slope and inboard yoke deflection in a direction opposite to primary out of plane blade bending.

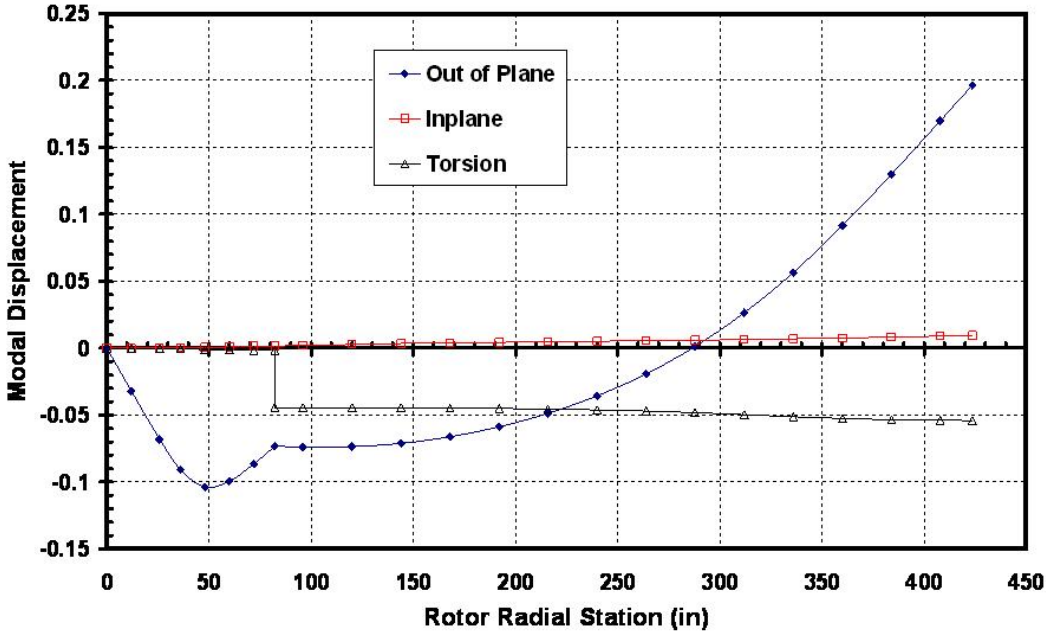

Figure 5.32 6BES 3rd Cyclic mode modal displacement plot.

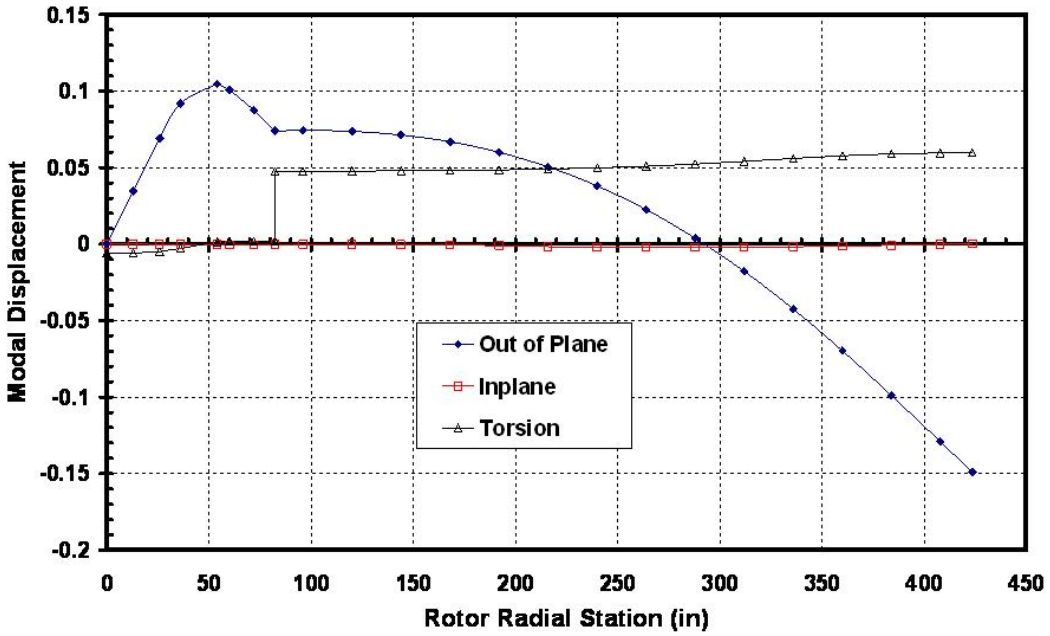

Figure 5.33 PBR LE Blade 5th Cyclic mode modal displacement plot.

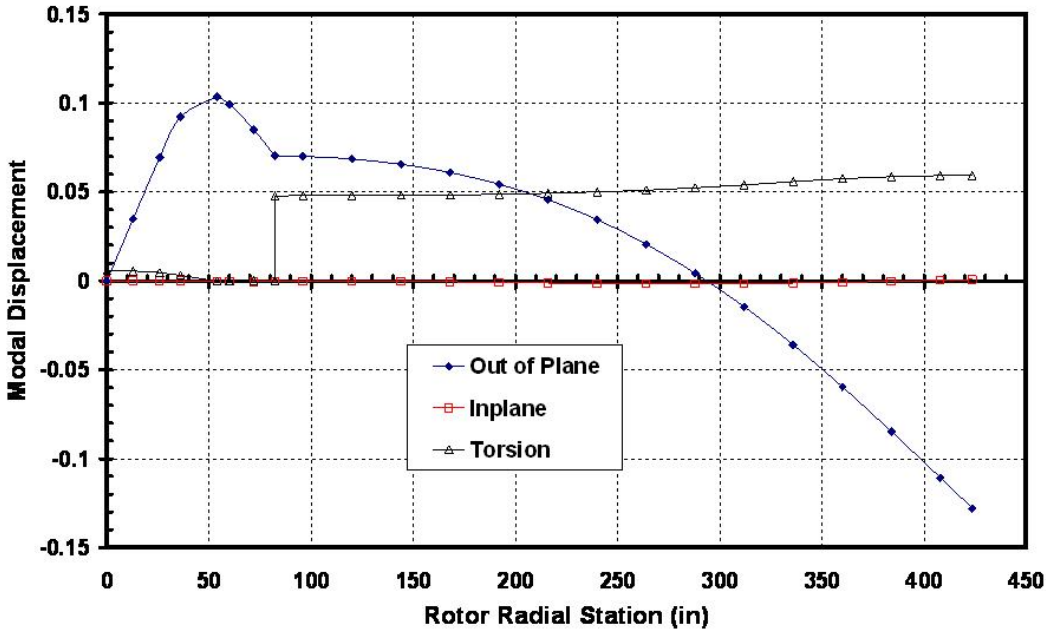

Figure 5.34 PBR TE Blade 5th Cyclic mode modal displacement plot.

The 6BES 4th cyclic modeshape is shown in Figure 5.35 and the comparable 6th PBR cyclic modeshapes are shown in Figures 5.36 and 5.37 for LE and TE blades, respectively. The PBR TE blade out of plane modal displacement amplitude is on the order of 40 times larger than for the LE blade. These modeshapes are generally similar between the two rotors, with the 6BES rotor having more yoke out of plane deflection than the PBR and a larger rigid body blade pitch deflection than the PBR. The PBR has a 7th cyclic mode tuned slightly above the 6th, with a modeshape that is similar to the 6th mode. There is more yoke out of plane deflection in the 7th mode than the 6th, making it more similar to the 6BES rotor. The PBR cyclic 7th modeshapes for LE and TE blades are shown in Figures 5.38 and 5.39, respectively.

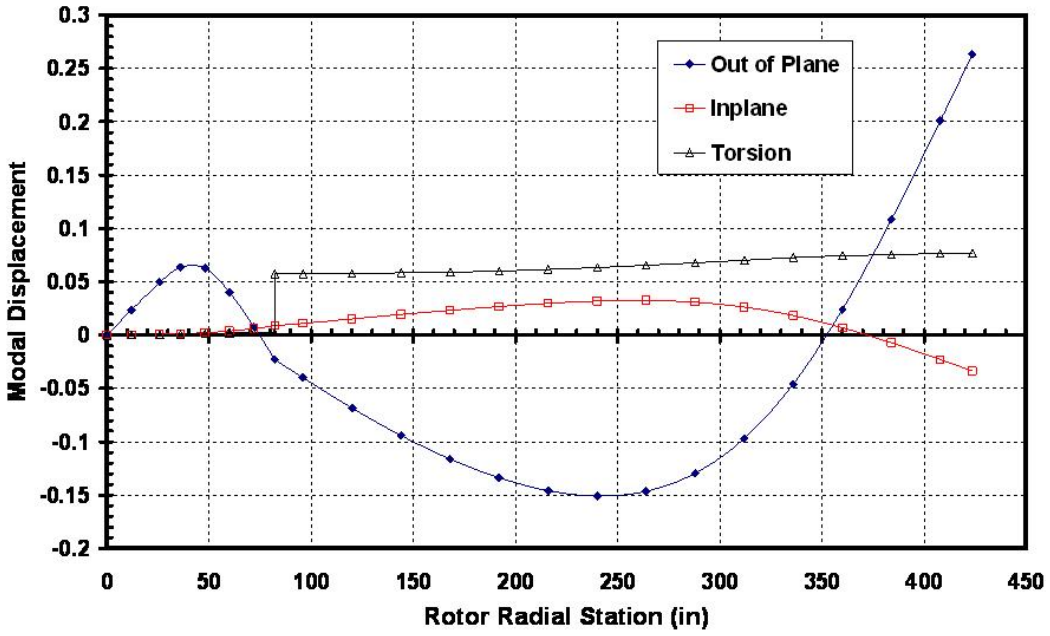

Figure 5.35 6BES 4th Cyclic mode modal displacement plot.

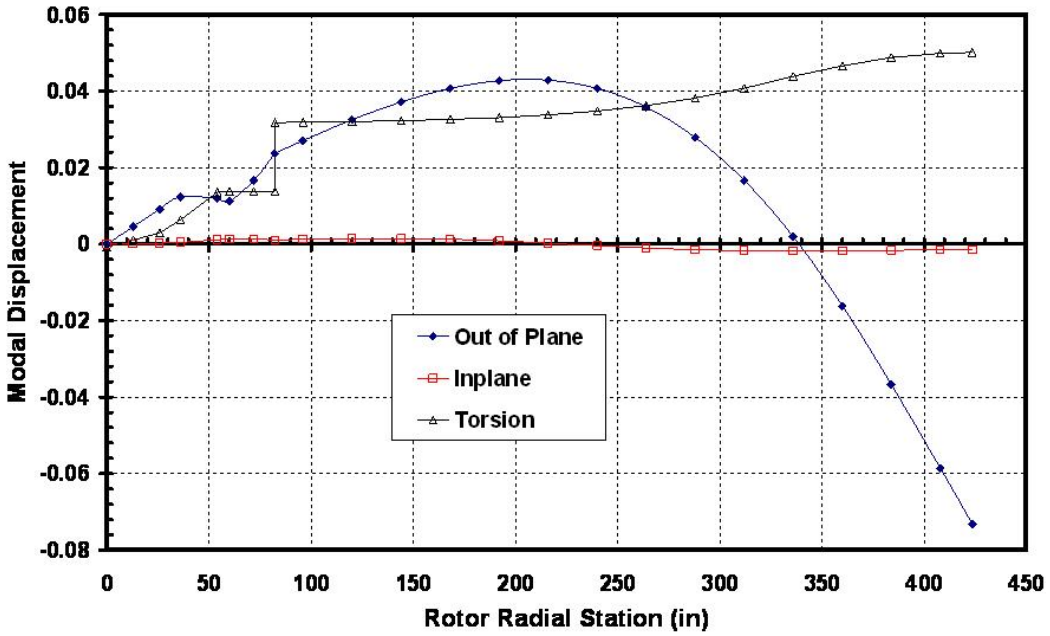

Figure 5.36 PBR LE Blade 6th Cyclic mode modal displacement plot.

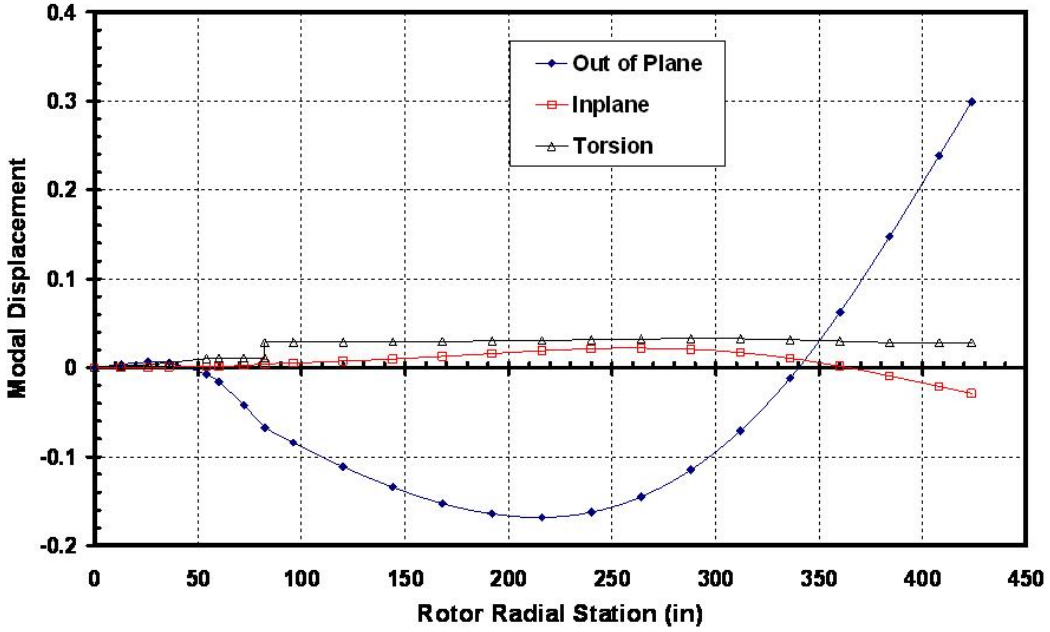

Figure 5.37 PBR TE Blade 6th Cyclic mode modal displacement plot.

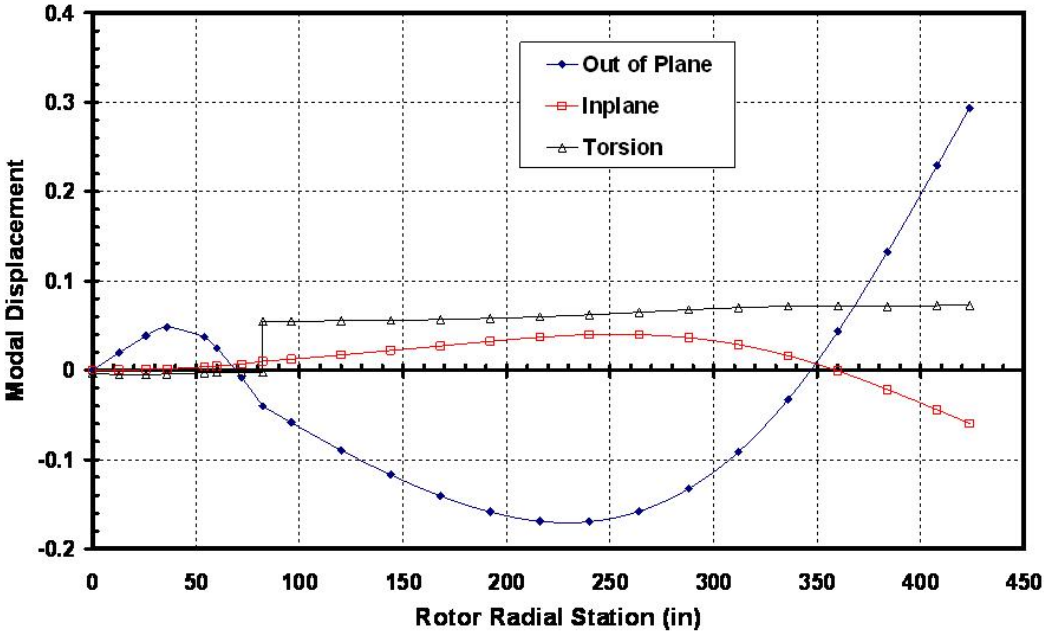

Figure 5.38 PBR LE Blade 7th Cyclic mode modal displacement plot.

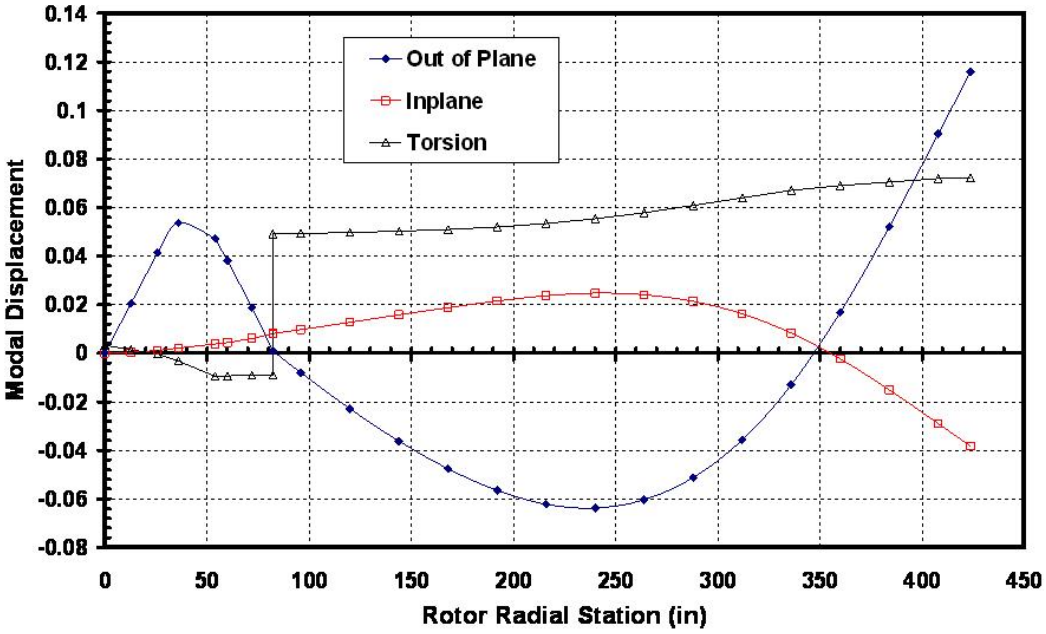

Figure 5.39 PBR TE Blade 7th Cyclic mode modal displacement plot.

5.4.3. Modeshape Comparison Summary

The modeshapes of the 6BES and PBR rotors are similar for fundamental rotor modes. The PBR has modes of similar shape tuned closely to one another, with one of the modes having a difference in yoke modal displacement from the other. The 6BES rotor modeshapes present no such phenomenon.

5.5 Comparison of PBR to 6BES Kinematic and Elastic Coupling Parameters

The kinematic and elastic coupling parameters discussed in section 1.3 are compared between the PBR and 6BES rotors for airplane mode RPM and 87.77° blade root collective pitch angle.

5.5.1. Pitch-Flap Coupling (δ_3) Comparison

The geometric δ_3 is -15° for the 6BES rotor and -5° for the PBR. Th e PBR δ_3 values calculated from flapping mode modal displacement data were calculated for the LE and TE blades separately. One set of PBR δ_3 values was calculated from modal displacements read in the global coordinate system, and another set of PBR δ_3 values was calculated from data read in the leading edge blade coordinate system (LEA) for the LE blade and in the trailing edge blade coordinate system (TEA) for the TE blade.

Geometric δ_3 and values of δ_3 calculated from Dymore modal displacement data for the PBR and the 6BES rotor are listed in Table 5.1.

Table 5.1 Geometric and Calculated Values of δ_3 For 6BES and PBR Rotor Models

	6BES Global	**PBR LE Global**	**PBR LE LEA**	**PBR TE Global**	**PBR TE TEA**
Total δ_3 (deg)	-6.08	-2.25	7.77	-2.61	-12.53
Kinematic δ_3 (deg)	-6.12	-2.29	7.82	-2.34	-12.36
Elastic δ_3 (deg)	0.037	0.045	-0.049	-0.264	-0.175
Geometric δ_3 (deg)	-15	-5	-5	-5	-5

All elastic δ_3 values were less than 2% of the total δ_3 except for the PBR TE blade δ_3 calculated in the global coordinate system, for which elastic δ_3 was 10% of the total.

The δ_3 values calculated in the global coordinate system for both rotors were roughly half of the geometric δ_3.

The PBR δ_3 value calculated for the LE blade in LEA coordinates was +10° to the same value calculated in the global coordinate system. The PBR δ_3 values calculated for the TE blade in TEA coordinates was -9.9° to the same value calculated in the global coordinate system. These offsets of δ_3 between coordinate systems nearly exactly match the offsets of the coordinate systems themselves.

Whether stability analysis would return results consistent with the PBR δ_3 values calculated in the global coordinate system or values calculated in the coordinate systems aligned with the blades is not obvious.

5.5.2. Pitch-Cone Coupling (δ_0) Comparison

PBR δ_0 values were calculated in both global and blade-local coordinates for LE and TE blades. Calculated δ_0 values for the 6BES and PBR rotor models are presented in Table 5.2.

Table 5.2 Values of Kinematic and Elastic δ_0 For 6BES and PBR Rotor Models

	6BES Global	**PBR LE Global**	**PBR LE LEA**	**PBR TE Global**	**PBR TE TEA**
Total δ_0 (ND)	0.99	0.93	1.33	1.44	1.01
Kinematic δ_0 (ND)	0.98	0.92	1.31	1.41	0.99
Elastic δ_0 (ND)	0.018	0.008	0.020	0.033	0.017

The elastic δ_0 values in Table 5.2 are in the range of 1% - 2% of the total δ_0. The PBR LE blade δ_0 is 43% more positive when measured in LEA coordinates than when measured in global coordinates. The TE blade δ_0 is 30% less positive when measured in TEA coordinates than when measured in global coordinates.

Positive δ_0, as predicted for both rotors in this study, is favorable for handling qualities. The effect of the δ_0 values predicted for these rotors on stability analysis is reserved for further study.

5.5.3. Pitch-Lag Coupling (K_{pl}) Comparison

As was done for the other two coupling parameters, paired blade rotor K_{pl} values were calculated for LE and TE blade for both local blade and global coordinates. Calculated K_{pl} values for 6BES and PBR Dymore rotor models are listed in Table 5.3.

Table 5.3 Values of Kinematic and Elastic K_{pl} For 6BES and PBR Rotor Models

	6BES Global	**PBR LE Global**	**PBR LE LEA**	**PBR TE Global**	**PBR TE TEA**
Total K_{pl} (ND)	0.153	0.160	0.167	0.161	0.157
Kinematic K_{pl} (ND)	0.04	0.01	0.01	-0.004	-0.001
Elastic K_{pl} (ND)	0.114	0.146	0.157	0.165	0.158

The elastic K_{pl} values listed in Table 5.3 range from 75% of total K_{pl} to 99% of total K_{pl}. Most, if not all, of the total pitch lag coupling takes place in the elastic blade. Comments on the effects of these values of K_{pl} on stability for this rotor are reserved for future stability analysis.

5.6 Effects of blade spacing in PBR Rotor Model

The baseline PBR rotor model presented to this point has 20° inplane separation between a pair of blades that share a yoke arm and blade pitch input mechanism. The effects of variations in blade spacing angle from 15° to 40° on rotor frequencies (at helicopter mode RPM and 75° blade root collective pitch angle) and coupling parameters (at airplane mode RPM and 87.77° blade root collective pitch angle) are presented in this section.

5.6.1. Effect of PBR Blade Spacing on Rotor Frequency

The three PBR collective modes whose frequencies changed by more than 1% compared to the 20° spacing over the range of blade spacing from 15° to 40° are plotted against blade spacing angle in Figure 5.40.

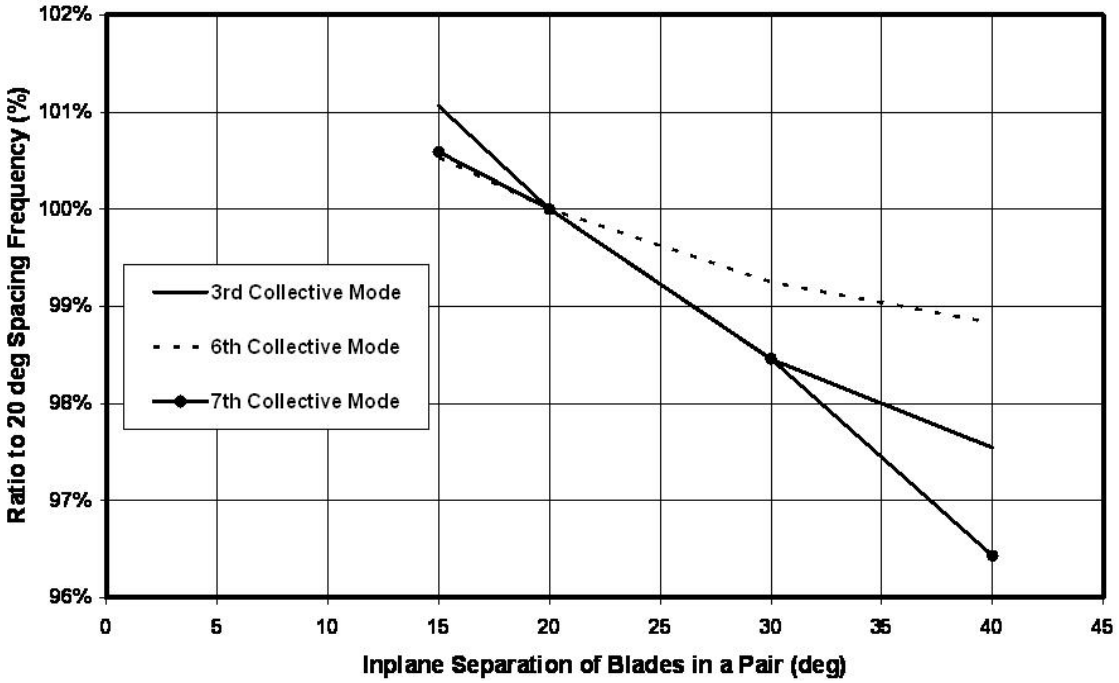

Figure 5.40 Effect of PBR blade spacing on collective modes

Consulting the PBR collective mode fanplot in Figure 5.4 and Figure 5.40, it is clear that the changes in the frequencies of PBR collective modes due to blade spacing over the range considered present no degradation in collective mode rotor tuning.

The four cyclic PBR rotor modes whose frequencies changed by more than 1% compared to the 20° spacing over the range of blade spacing angles considered are plotted versus blade spacing angle in Figure 5.41.

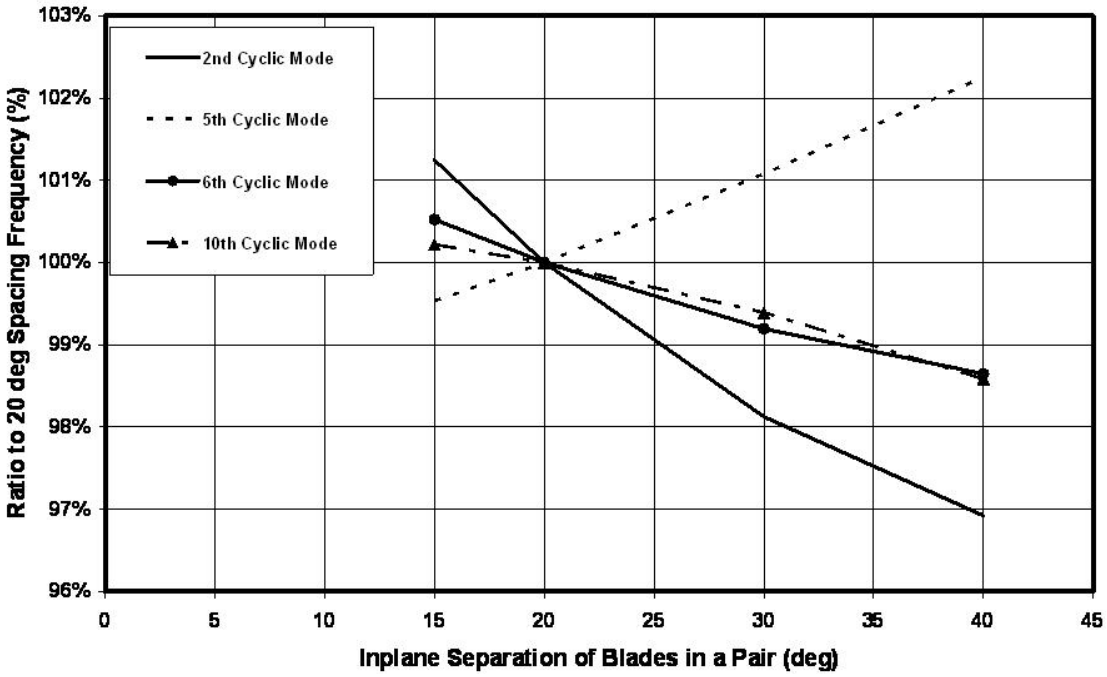

Figure 5.41 Effect of PBR blade spacing on cyclic modes

The changes in the frequencies of PBR cyclic rotor modes due to blade spacing over the range considered do not result in any unacceptable frequency placements.

5.6.2. Effect of PBR Blade Spacing on Coupling Parameters

The effect of blade spacing on PBR rotor model δ_3, do, K_{pl} for the airplane mode RPM and 87.77° blade root collective pitch angle are presented in this section.

The total δ_3 values for LE and TE blades, measured in the global coordinate system and in blade local coordinate systems, are plotted versus blade spacing angle in Figure 5.42.

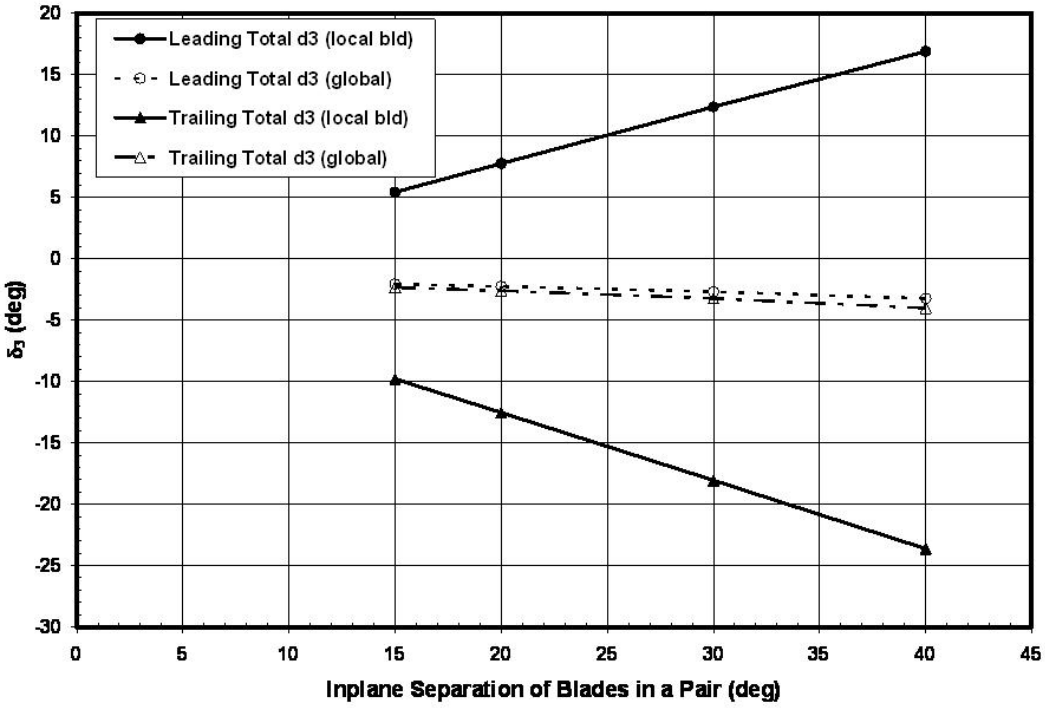

Figure 5.42 Effect of PBR blade spacing on δ_3

If the rotor has aeroelastic behavior consistent with the δ_3 values measured in local blade coordinates, larger blade spacing angles would have unacceptable values of δ_3. However, if the rotor has aeroelastic behavior consistent with the δ_3 values measured in global coordinates, blade spacing has negligible effects on δ_3.

The blade δ_0 values for LE and TE blades, measured in global and local blade coordinates, are plotted against blade spacing angle in Figure 5.43.

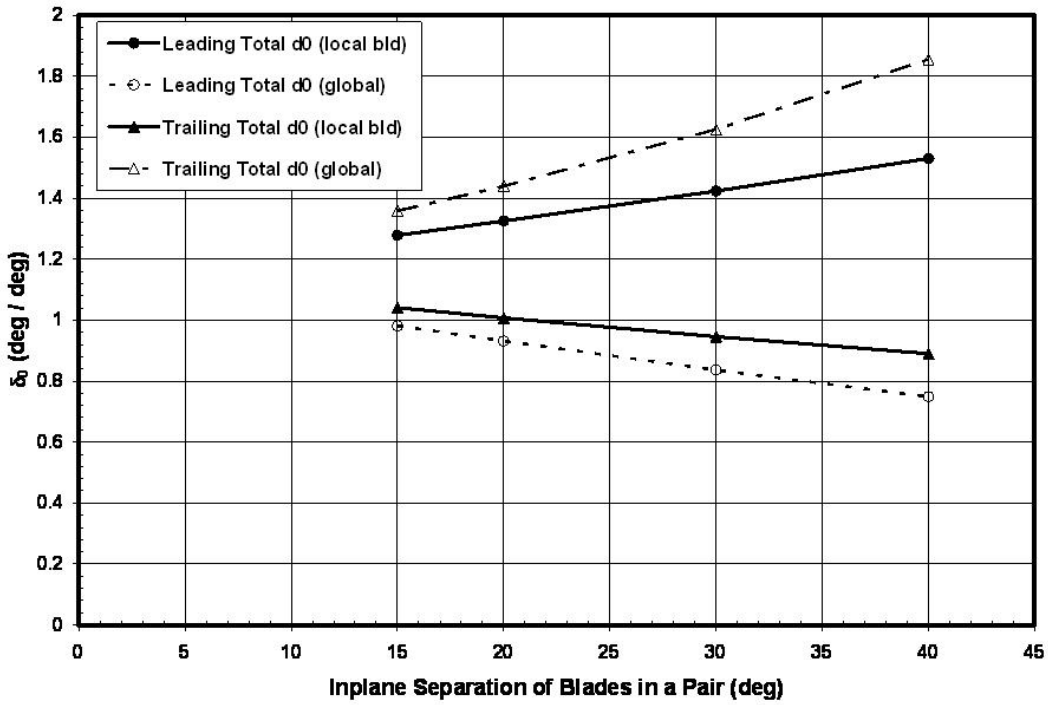

Figure 5.43 Effect of PBR blade spacing on δ_0.

For local blade coordinate values of δ_0, LE blade δ_0 increases with blade spacing angle and TE blade δ_0 decreases with blade spacing angle. These trends are reversed for δ_0 measured in global coordinates. All δ_0 values predicted in the blade spacing range considered are positive.

The total K_{pl} values for LE and TE blades, measured in local blade and global coordinates, are plotted versus blade spacing angle in Fig 5.44.

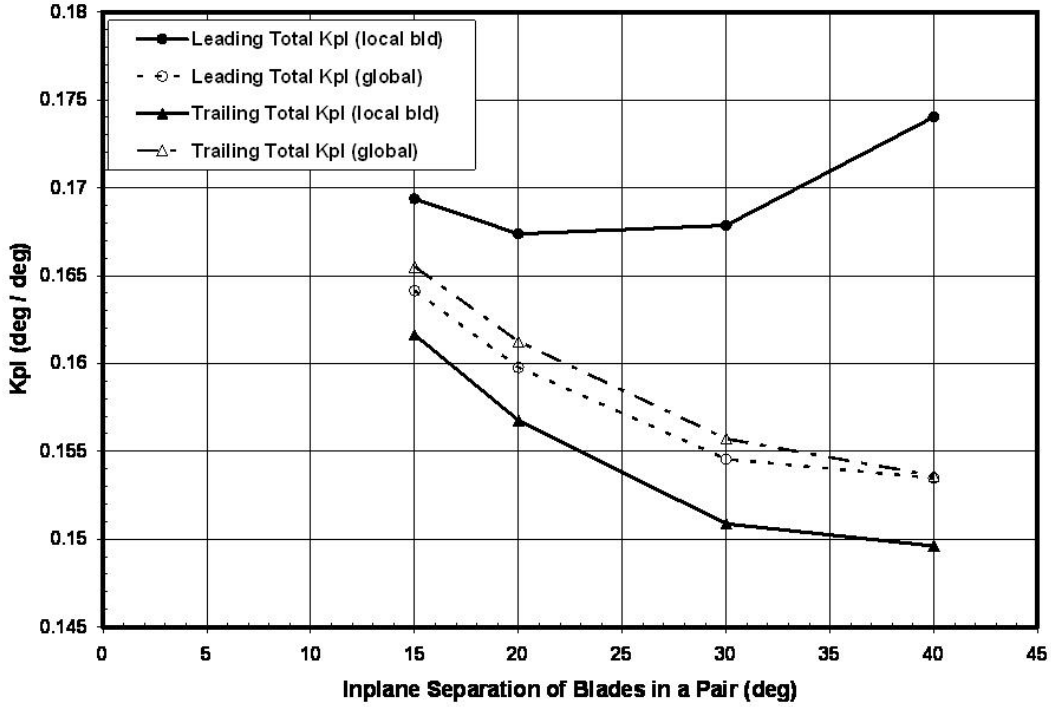

Figure 5.44 Effect of PBR blade spacing on K_{pl}.

Values of K_{pl} for both LE and TE blades in all coordinate systems considered are within 20% of the baseline value and positive over the blade spacing range considered.

5.6.3. Summary of Effects of PBR Blade Spacing

Blade spacing was found to have benign effects on rotor frequency placement for this PBR configuration over the range of spacings considered. Blade spacing had no detrimental effect on δ_0 or K_{pl}, but may cause unacceptable values of δ_3 for this pitch link location at high blade spacing angles depending on whether the rotor behaves more like δ_3 is averaged over the LE and TE blades or the δ_3 is local to each blade.

CHAPTER 6

CONCLUSIONS AND RECOMMENDATIONS

6.1 Conclusions

The purpose of the paired blade rotor design is to achieve higher than traditional tiltrotor solidity while maintaining acceptable pitch-flap coupling and satisfying control system packaging requirements. The goal of the work presented here was to determine the feasibility of the paired blade rotor for application on tiltrotor aircraft by Dymore finite element analyses of the subject rotor and a rotor of equal solidity with evenly spaced blades for comparison.

Validation of the Dymore modeling process by rotor frequency comparison to a Bell in-house code for an interim configuration of the evenly spaced rotor showed good correlation. The average magnitude of frequency differences was 0.815%, and the largest magnitude frequency difference was 3.90%.

Rotor frequency comparison showed that the paired blade rotor is tuned as well as the evenly spaced rotor, relative to the appropriate forcing frequencies, and that neither rotor is tuned poorly. The forcing frequencies per mode type differ between the two rotors, and the paired blade rotor configuration considered has no scissors modes. The paired blade rotor has modes of similar shape tuned closely together, and the evenly spaced rotor does not. This feature of the paired blade rotor increases the complexity of the tuning process compared to the evenly spaced rotor, but is not prohibitive to achieving an acceptable tuning.

The frequency placement of both rotors considered here was improved by unconventionally but not unreasonably high ratios of beamwise bending stiffness to chordwise bending stiffness in the blades. This feature reduces the range of frequencies in any mode over the large range of blade collective pitch angles considered. The paired blade rotor required 170 lb/blade of tuning weight, primarily to place the closely-tuned pair of first cantilevered inplane modes between 1.2 /Rev and 1.8 /Rev. The tuning weight in the paired blade rotor is 7.9% of

the 2,147 lb/blade total weight. The evenly spaced rotor required a total of 24 lb/blade of tuning weight, most of which was used to place the scissors 1st inplane mode sufficiently below 2 /Rev. The tuning weight in the evenly spaced rotor blade represents 1.2% of the 2,001 lb/blade total weight.

The modeshapes of the paired blade rotor and the evenly spaced rotor are similar in general. Modeshapes of the first few modes are virtually identical between the two rotor models. The paired blade rotor has several instances of two modes with similar shape tuned closely to one another. These pairs of modes differ most noticeably in the yoke displacements. For example, a cantilevered out of plane, first bending mode at 1.1 /Rev is close to a mode at 1.25 /Rev that can also be best described as cantilevered out of plane, first bending. The mode at 1.25 /Rev has more bending curvature in the yoke. The evenly spaced rotor shows no such results.

Of the three coupling parameters compared between the two rotor models, the pitch-flap coupling (δ_3) proved the most interesting. The δ_3 values calculated in the global coordinate system of both rotors were about half of the geometric δ_3. The paired blade rotor δ_3 value for the leading edge blade in a pair, calculated in a coordinate system local to the leading edge blade, was 10° more positive than the same value calculated in global coordinates. The trialing edge blade δ_3 was 9.9° more negative when calculated in local blade coordinates than when calculated in global coordinates. These differences in δ_3 from local blade to global coordinates nearly exactly match the rotations of the coordinate systems relative to one another. If stability analysis returns results consistent with the δ_3 values calculated in global coordinates, no undesirable stability characteristics are expected. However, if the stability analysis returns results consistent with the δ_3 values calculated in the local blade coordinate systems, the leading edge blade δ_3 will be problematic for stability. All calculated elastic δ_3 values were less than 2% of total δ_3.

All pitch-cone coupling parameters (δ_0) calculated for both rotors were positive. Positive δ_0 is favorable for handling qualities. The calculated elastic δ_0 values were in the range from 1% to 2% of the total δ_0.

Most or all of the pitch-lag coupling (K_{pl}) calculated for these rotors takes place in the elastic blade. The total K_{pl} values were positive for both rotors and all coordinate systems. The effect of positive K_{pl} on the overall stability of the paired blade rotor is reserved for future analysis, but previous analytical studies and test data show that positive K_{pl} is stabilizing for stiff-inplane tiltrotors.

The blade spacing angle between blades in a pair was found to have benign effects on rotor frequency placement for this paired blade rotor configuration over the range of spacings from 15° to 40°. Blade spacing over the range considered had no detrimental effect on δ_0 or K_{pl}, but may cause unacceptable values of δ_3 for this pitch link location at high blade spacing angles depending on whether stability analysis predicts rotor behavior more like δ_3 is averaged over the leading edge and trailing edge blades or the δ_3 is local to each blade. This determination is reserved for future stability analysis.

A clear and fundamental advantage of the paired blade rotor is that it meets the control system packaging requirement, and the evenly spaced rotor does not.

6.2 Recommendations

A logical next step in the process would be to incorporate aerodynamics into the models to determine loads and stability characteristics. The loads analysis would allow for checking whether the structural properties selected for the purpose of rotor tuning are sufficient to carry the loads. The stability analysis would answer questions raised in this work about an appropriate method for calculating pitch-flap coupling for a pair of rotor blades controlled by one pitch link.

APPENDIX A

PAIRED BLADE ROTOR AND EVENLY SPACED ROTOR DYMORE FREQUENCY TABLES

Table A.1 Paired Blade Rotor Collective Mode Frequencies

Mode No.	RPM	Freq (/Rev)	Freq CPM	Coll (deg)	DOF
1	157.2	0.52	81.6	67.4	IP
1	157.2	0.52	81.6	95.36	IP
1	157.2	0.52	81.6	87.77	IP
1	209.6	0.39	81.7	38	IP
1	209.6	0.39	81.9	75	IP
1	209.6	0.39	81.9	78.6	IP
2	157.2	1.09	171	87.77	OP
2	157.2	1.09	171	95.36	OP
2	157.2	1.09	171	67.4	OP
2	209.6	1.07	224	78.6	OP
2	209.6	1.07	224	75	OP
2	209.6	1.07	224	38	OP
3	157.2	1.25	196	67.4	OP
3	157.2	1.25	196	87.77	OP
3	157.2	1.25	196	95.36	OP
3	209.6	1.17	245	78.6	OP
3	209.6	1.17	245	75	OP
3	209.6	1.17	246	38	OP
4	157.2	4.65	731	95.36	IP
4	157.2	4.69	737	87.77	IP
4	157.2	4.78	752	67.4	IP
4	209.6	3.81	799	78.6	IP
4	209.6	3.82	801	75	IP
4	209.6	3.91	820	38	IP
5	157.2	5.23	822	67.4	OP
5	157.2	5.34	839	87.77	OP
5	157.2	5.37	844	95.36	OP
5	209.6	4.15	869	38	OP
5	209.6	4.26	893	75	OP
5	209.6	4.27	895	78.6	OP
6	157.2	5.42	852	67.4	OP
6	157.2	5.52	868	87.77	OP
6	157.2	5.57	876	95.36	OP
6	209.6	4.35	912	38	OP
6	209.6	4.42	927	75	OP
6	209.6	4.44	930	78.6	OP
7	157.2	8.60	1353	95.36	TORS
7	157.2	9.15	1438	87.77	TORS
7	157.2	9.42	1480	67.4	TORS
7	209.6	6.35	1331	38	IP
7	209.6	6.86	1438	78.6	TORS
7	209.6	7.14	1497	75	TORS

Table A.1 – *Continued*

8	157.2	11.05	1738	95.36	IP
8	157.2	11.16	1755	87.77	IP
8	157.2	11.40	1792	67.4	TORS
8	209.6	8.67	1818	78.6	TORS
8	209.6	8.70	1823	75	TORS
8	209.6	8.71	1825	38	TORS
9	157.2	11.49	1806	95.36	TORS
9	157.2	11.51	1809	87.77	TORS
9	157.2	11.54	1815	67.4	TORS
9	209.6	8.74	1831	78.6	TORS
9	209.6	8.77	1837	75	TORS
9	209.6	8.99	1885	38	OP
10	157.2	12.13	1906	67.4	OP
10	157.2	12.30	1934	87.77	OP
10	157.2	12.35	1942	95.36	OP
10	209.6	9.14	1917	38	IP
10	209.6	9.38	1966	75	OP
10	209.6	9.40	1971	78.6	OP
11	157.2	12.78	2009	67.4	TORS
11	157.2	12.92	2031	95.36	TORS
11	157.2	12.94	2034	87.77	TORS
11	209.6	9.71	2035	38	TORS
11	209.6	9.83	2060	78.6	TORS
11	209.6	9.85	2064	75	TORS
12	157.2	13.48	2119	95.36	TORS
12	157.2	13.51	2125	67.4	TORS
12	157.2	13.52	2126	87.77	TORS
12	209.6	9.94	2084	38	TORS
12	209.6	10.23	2144	78.6	TORS
12	209.6	10.32	2163	75	TORS

Table A.2 Paired Blade Rotor Cyclic Mode Frequencies

Mode No.	RPM	Freq (/Rev)	Freq CPM	Coll (deg)	DOF
1	157.2	0.99	156.1	95.36	OP
1	157.2	0.99	156.1	87.77	OP
1	157.2	0.99	156.1	67.4	OP
1	209.6	0.99	207.0	78.6	OP
1	209.6	0.99	207.0	75	OP
1	209.6	0.99	207.0	38	OP
2	157.2	1.24	194	67.4	OP
2	157.2	1.24	194	87.77	OP
2	157.2	1.24	194	95.36	OP
2	209.6	1.16	244	78.6	OP
2	209.6	1.16	244	75	OP
2	209.6	1.16	244	38	OP
3	157.2	1.54	243	95.36	IP
3	157.2	1.55	244	87.77	IP
3	157.2	1.57	246	67.4	IP
3	209.6	1.22	255	78.6	IP
3	209.6	1.22	255	75	IP
3	209.6	1.22	257	38	IP
4	157.2	1.77	278	95.36	IP
4	157.2	1.78	280	87.77	IP
4	157.2	1.80	283	67.4	IP
4	209.6	1.41	296	78.6	IP
4	209.6	1.42	297	75	IP
4	209.6	1.43	299	38	IP
5	157.2	3.30	519	95.36	OP
5	157.2	3.34	526	87.77	OP
5	157.2	3.36	527	67.4	OP
5	209.6	2.87	601	38	OP
5	209.6	2.93	614	78.6	OP
5	209.6	2.93	615	75	OP
6	157.2	5.37	844	67.4	OP
6	157.2	5.46	859	87.77	OP
6	157.2	5.48	861	95.36	OP
6	209.6	4.28	898	38	OP
6	209.6	4.38	919	75	OP
6	209.6	4.39	920	78.6	OP
7	157.2	5.81	913	67.4	OP
7	157.2	5.86	921	95.36	OP
7	157.2	5.87	923	87.77	OP
7	209.6	4.57	957	38	OP
7	209.6	4.74	993	78.6	OP
7	209.6	4.75	995	75	OP

Table A.2 – *Continued*

8	157.2	6.68	1051	95.36	IP
8	157.2	6.77	1064	87.77	IP
8	157.2	6.91	1087	67.4	IP
8	209.6	5.36	1124	78.6	IP
8	209.6	5.38	1128	75	IP
8	209.6	5.46	1145	38	IP
9	157.2	7.72	1213	95.36	IP
9	157.2	7.83	1230	87.77	IP
9	157.2	8.04	1264	67.4	IP
9	209.6	6.19	1297	78.6	IP
9	209.6	6.21	1303	75	IP
9	209.6	6.35	1331	38	IP
10	157.2	10.19	1602	95.36	TORS
10	157.2	10.42	1638	87.77	TORS
10	157.2	10.51	1652	67.4	TORS
10	209.6	7.60	1592	38	TORS
10	209.6	7.86	1647	78.6	TORS
10	209.6	8.04	1685	75	TORS
11	157.2	11.49	1807	95.36	TORS
11	157.2	11.51	1809	87.77	TORS
11	157.2	11.52	1811	67.4	TORS
11	209.6	8.72	1828	78.6	TORS
11	209.6	8.72	1828	38	TORS
11	209.6	8.72	1829	75	TORS
12	157.2	12.60	1980	67.4	TORS
12	157.2	12.68	1993	95.36	TORS
12	157.2	12.69	1996	87.77	TORS
12	209.6	9.49	1989	38	TORS
12	209.6	9.64	2020	78.6	TORS
12	209.6	9.66	2025	75	TORS

Table A.3 Six Blade Even Spacing Rotor Collective Mode Frequencies

Mode No.	RPM	Freq (/Rev)	Freq CPM	Coll (deg)	DOF
1	157.2	0.63	99.6	95.36	IP
1	157.2	0.63	99.7	87.77	IP
1	157.2	0.64	100.0	67.4	IP
1	209.6	0.48	100.3	78.6	IP
1	209.6	0.48	100.4	75	IP
1	209.6	0.48	100.5	38	IP
2	157.2	1.13	177	87.77	OP
2	157.2	1.13	177	95.36	OP
2	157.2	1.13	177	67.4	OP
2	209.6	1.10	230	78.6	OP
2	209.6	1.10	230	75	OP
2	209.6	1.10	230	38	OP
3	157.2	4.05	637	95.36	IP
3	157.2	4.09	643	87.77	IP
3	157.2	4.21	663	67.4	IP
3	209.6	3.34	701	78.6	IP
3	209.6	3.36	705	75	IP
3	209.6	3.57	748	38	IP
4	157.2	4.76	748	67.4	OP
4	157.2	4.89	769	87.77	OP
4	157.2	4.93	776	95.36	OP
4	209.6	3.69	772	38	OP
4	209.6	3.89	816	75	OP
4	209.6	3.91	820	78.6	OP
5	157.2	9.36	1471	95.36	TORS
5	157.2	9.87	1552	87.77	TORS
5	157.2	10.14	1594	67.4	TORS
5	209.6	7.12	1493	38	TORS
5	209.6	7.45	1561	78.6	TORS
5	209.6	7.66	1606	75	TORS
6	157.2	10.42	1638	95.36	IP
6	157.2	10.54	1657	87.77	IP
6	157.2	10.82	1701	67.4	IP
6	209.6	8.26	1731	78.6	IP
6	209.6	8.31	1742	75	IP
6	209.6	8.65	1813	38	OP
7	157.2	12.12	1906	67.4	OP
7	157.2	12.30	1934	87.77	OP
7	157.2	12.35	1941	95.36	OP
7	209.6	9.07	1901	38	IP
7	209.6	9.39	1968	75	OP
7	209.6	9.41	1973	78.6	OP

Table A.3 – *Continued*

8	157.2	13.37	2103	95.36	TORS
8	157.2	13.75	2161	87.77	TORS
8	157.2	13.95	2192	67.4	TORS
8	209.6	10.01	2099	38	TORS
8	209.6	10.37	2173	78.6	TORS
8	209.6	10.59	2220	75	TORS

Table A.4 Six Blade Even Spacing Rotor Cyclic Mode Frequencies

Mode No.	RPM	Freq (/Rev)	Freq CPM	Coll (deg)	DOF
1	157.2	1.02	159.6	95.36	OP
1	157.2	1.02	159.6	87.77	OP
1	157.2	1.02	159.7	67.4	OP
1	209.6	1.01	211.4	78.6	OP
1	209.6	1.01	211.4	75	OP
1	209.6	1.01	211.4	38	OP
2	157.2	1.72	270	95.36	IP
2	157.2	1.74	273	87.77	IP
2	157.2	1.80	283	67.4	IP
2	209.6	1.38	290	78.6	IP
2	209.6	1.39	292	75	IP
2	209.6	1.45	304	38	IP
3	157.2	3.12	491	95.36	OP
3	157.2	3.16	496	67.4	OP
3	157.2	3.16	497	87.77	OP
3	209.6	2.68	562	38	OP
3	209.6	2.76	578	75	OP
3	209.6	2.76	578	78.6	OP
4	157.2	5.28	831	67.4	OP
4	157.2	5.32	837	95.36	OP
4	157.2	5.35	841	87.77	OP
4	209.6	4.19	878	38	OP
4	209.6	4.37	916	78.6	OP
4	209.6	4.38	917	75	OP
5	157.2	6.49	1021	95.36	OP
5	157.2	6.57	1033	87.77	IP
5	157.2	6.72	1056	67.4	IP
5	209.6	5.21	1091	78.6	IP
5	209.6	5.22	1095	75	IP
5	209.6	5.31	1113	38	IP
6	157.2	10.76	1692	95.36	TORS
6	157.2	10.92	1716	87.77	TORS
6	157.2	10.95	1721	67.4	TORS
6	209.6	8.04	1686	38	TORS

Table A.4 – *Continued*

6	209.6	8.23	1724	78.6	TORS
6	209.6	8.34	1749	75	TORS
7	157.2	12.47	1960	67.4	TORS
7	157.2	12.69	1996	87.77	TORS
7	157.2	12.77	2007	95.36	TORS
7	209.6	9.37	1964	38	TORS
7	209.6	9.64	2022	75	TORS
7	209.6	9.64	2022	78.6	TORS
8	157.2	13.93	2190	95.36	TORS
8	157.2	14.22	2235	87.77	TORS
8	157.2	14.61	2297	67.4	IP
8	209.6	11.00	2306	78.6	IP
8	209.6	11.09	2324	75	IP
8	209.6	11.39	2387	38	IP

Table A.5 Six Blade Even Spacing Rotor Scissors Mode Frequencies

Mode No.	RPM	Freq (/Rev)	Freq CPM	Coll (deg)	DOF
1	157.2	1.13	177.1	87.77	OP
1	157.2	1.13	177.1	95.36	OP
1	157.2	1.13	177.1	67.4	OP
1	209.6	1.10	230.0	78.6	OP
1	209.6	1.10	230.1	75	OP
1	209.6	1.10	230.2	38	OP
2	157.2	1.72	270	95.36	IP
2	157.2	1.74	274	87.77	IP
2	157.2	1.80	283	67.4	IP
2	209.6	1.39	290	78.6	IP
2	209.6	1.39	292	75	IP
2	209.6	1.45	304	38	IP
3	157.2	4.64	729	67.4	OP
3	157.2	4.80	755	87.77	OP
3	157.2	4.87	766	95.36	OP
3	209.6	3.68	772	38	OP
3	209.6	3.83	802	75	OP
3	209.6	3.85	806	78.6	OP
4	157.2	6.49	1020	95.36	IP
4	157.2	6.56	1031	87.77	IP
4	157.2	6.71	1055	67.4	IP
4	209.6	5.20	1089	78.6	IP
4	209.6	5.21	1093	75	IP
4	209.6	5.31	1113	38	IP
5	157.2	9.36	1471	95.36	TORS
5	157.2	9.89	1555	87.77	TORS

Table A.5 – *Continued*

5	157.2	10.17	1598	67.4	TORS
5	209.6	7.12	1493	38	TORS
5	209.6	7.46	1563	78.6	TORS
5	209.6	7.68	1610	75	TORS
6	157.2	11.50	1808	67.4	OP
6	157.2	11.90	1871	87.77	OP
6	157.2	12.10	1902	95.36	OP
6	209.6	8.65	1814	38	OP
6	209.6	8.99	1885	75	OP
6	209.6	9.04	1894	78.6	OP
7	157.2	13.17	2070	95.36	TORS
7	157.2	13.50	2123	87.77	TORS
7	157.2	13.82	2172	67.4	TORS
7	209.6	10.01	2099	38	TORS
7	209.6	10.26	2151	78.6	TORS
7	209.6	10.47	2195	75	TORS
8	157.2	13.93	2190	95.36	TORS
8	157.2	14.23	2237	87.77	TORS
8	157.2	14.62	2298	67.4	IP
8	209.6	11.00	2306	78.6	IP
8	209.6	11.09	2325	75	IP
8	209.6	11.39	2387	38	IP

REFERENCES

[1] Gaffey, Troy. “The Effect of Positive Pitch-Flap Coupling (Negative δ_3) on Rotor Blade Motion Stability and Flapping.” *Journal of The American Helicopter Society* 2 (1969): 49-67.

[2] Moore, Michael J. and others. “High Speed Tiltrotors: Dynamics Methodology.” American Helicopter Society 49th Annual Forum, St. Louis, Missouri, May 1993.

[3] Johnson, Wayne. *Helicopter Theory*. New York: Dover, 1980.

[4] Nixon, Mark W. and others. “Aeroelastic Tailoring for Stability Augmentation and Performance Enhancements of Tiltrotor Aircraft.” American Helicopter Society 55th Annual Forum, Montreal, Quebec, Canada, May 1999.

[5] Piatak, David J. and others. “A Wind-Tunnel Parametric Investigation of Tiltrotor Whirl-Flutter Stability Boundaries.” American Helicopter Society 57th Annual Forum, Washington, DC, May 2001.

[6] Bauchau, Olivier. “FlexMb.” Available from http://www.ae.gatech.edu/people/obauchau/flexmb/FlexMb.pdf. Internet; accessed 23 April 2009

[7] Bauchau, Olivier. “Dymore 2.0 User’s Manual.” Available from http://www.ae.gatech.edu/people/obauchau/Dwnld/dymore20/DymoreManual.pdf. Internet; accessed 5 January 2008.

[8] Bauchau, Olivier. “Dymore.” Available from http://www.ae.gatech.edu/people/obauchau/dymore.pdf. Internet; accessed 3 March 2009.

[9] Bramwell, A.R.S., George Done, and David Balmford. *Bramwell’s Helicopter Dynamics.* 2nd ed. Reston: Butterworth, 2001.

BIOGRAPHICAL INFORMATION

Orion Braziel earned a BS in aerospace engineering from the University of Texas at Arlington in 2002. Orion began working toward a MS in aerospace engineering at the University of Texas at Arlington and was hired into the rotor dynamics group at Bell Helicopter in the fall of 2004.